Dynamics of Rad51 during homologous recombination in living yeast

Siyu Liu

PSL UNIVERSITÉ PARIS

THÈSE DE DOCTORAT
DE L'UNIVERSITÉ PSL

Préparée à UMR3664 Institut Curie CNRS/Equipe Taddei

Dynamics of Rad51 during homologous recombination in living yeast

Dynamique de Rad51 lors de la recombinaison homologue chez la levure vivante

Soutenue par

Siyu LIU

Le 30/11/2022

Ecole doctorale n° 515

Complexité Du Vivant

Spécialité

Biologie

Composition du jury :

Olivier ESPELI DR, Collège de France	*Président*
Eric COIC DR, CEA.	*Rapporteur*
Josée GUIROUILH-BARBAT CR, Institut Cochin	*Rapportrice*
Pauline DUPAIGNE CR, Goustave Roussy	*Examinatrice*
Judith MINE-HATTAB CR, Institut Curie	*Directrice de thèse*
Angela TADDEI DR, Institut Curie	*Directrice de thèse*

institutCurie

ACKNOWLEDGEMENTS

In this section, I would like to express my sincere gratitude to people who were part of my Ph.D. experience during the last four years.

First and foremost, I wish to thank my supervisor, **Angela Taddei,** who provided me an opportunity to join her team and for her guidance, support, and encouragement during my Ph.D. I majored in engineering; it used to be a challenge for me to do a thesis in biology because of my lack of biological knowledge. Angela has been very patient in instructing me on how to think genetically and develop critical thinking on everything. She was so open-minded that I dared to propose some fanciful ideas and didn't afraid of making mistakes; I enjoyed the weekly discussion during these years.

I sincerely thank another supervisor, **Judith Mine-Hattab**, who proposed this project and invited me to join in after my M2 internship. She has been energetic and inspiring since my training, helping me with microscopy and image analysis. It is an exciting experience to do super-resolution microscopy with her. By encouraging me to continue studying as a Ph.D. student in the group, I extended my expertise and widened my ways of an interdisciplinary approach to solving biophysical problems.

Then I would like to thank my thesis committee throughout these years, **Eric Coic, Xiaohu Song,** and **Florian Mueller**, for offering me helpful advice from different views.

During these years in the lab, dozens of people have helped and supported me immensely. **Marie Villemeur** helped me a lot with strain construction in the first year of my Ph.D. **Myriam Ruault**, as a master in yeast and genetics, offered me lots of helpful advice. Besides, she helped me to solve mechanical problems of microscopy. **Isabelle Loiodice**, for teaching me how to do ChiP-Seq and reminding me of the precautions in the lab. I also would like to thank the other two Ph.D. students on our team, **Manuela Baquero Perez** and **Gertjan Laenen**, for all the fun, discussions, great talks, and delicious food we shared after work and for organizing those fancy activities on Friday night. **Caroline Audouin** and **Marie Khuoy**, two particularly helpful people from the administration of our unit thanks to you, I can survive in Paris with my limited French. You helped me deal with insurance, residency, and tax documents. All of you enriched my Ph.D. life, and I had a great time in and outside the lab.

Next, I would be grateful to all the members of my thesis jury, who kindly accepted my invitation to review and helped to improve my thesis.

Finally, I cannot forget my family members in China. Especially my mother, **Xi Yang**, and my father, **Zhiwen Liu**, cannot attend my thesis defense because of COVID. However, they still supported me unconditionally every day for these four years, regardless of the distance.

ABSTRACT

DNA is the major carrier of genetic information in prokaryotic and eukaryotic cells and its integrity is vital for the survival of cells. However, DNA is under pressure of damages caused by both exogenous and endogenous factors. Double strand break (DSB) is one of the most toxic DNA damages and even one unrepaired DSB is lethal to cells. Cells have evolved several pathways to repair DSBs, including non-homologous end joining (NHEJ), and homologous recombination (HR). HR is an error free repair pathway that uses an intact homologous sequence as a template to repair the damage. This involves identifying the homologous sequence among the mega bases of the genome and in the nuclear volume of eukaryotic cells. At the molecular level, DNA sampling and strand invasion of the homologous dsDNA is achieved by a nucleoprotein filament (NPF), formed by the recombinase, RecA in bacteria and Rad51 in eukaryotes, coating ssDNA. This mechanism has been extensively studied *in vitro* and *in vivo* through genetic and molecular approaches at the level of cell populations, but its dynamics could not be studied in living cells due to lack of functional fluorescent version of Rad51. Thus**, how broken DNA can find a homologous sequence in the volume of the nucleus and among the megabases of DNA remains mysterious.**

Thanks to structural insights from our collaborator Raphael Guerois (I2BC, CEA, France), we developed and characterized the first functional, internally tagged version of a recombinase in the yeast *S. cerevisiae*. Following the induction of unique DSB, we observe for the first time in living cells, Rad51 forming micrometer long filaments spanning across the whole nucleus and contacting the donor sequence. As predicted from genetic and *in vitro* data, their formation requires the recombinase loader Rad52 and the formation of long stretch of ssDNA. Furthermore, emerging filaments adopt a variety of shapes, not reported *in vitro* and modulated by Rad51 ancillary factors, shedding new light on the function of these factors in living cells.

In contrast to what has been reported for RecA filaments in bacteria, Rad51 filaments show a surprisingly dynamic behavior: with frequent compaction events followed by re-extension providing opportunities for the NPF to be projected into a different nuclear area, and thus explore new genomic regions. Biophysical modeling of the homology search process by our collaborator Leonid Mirny (MIT, USA) reveals that these cycles of compaction/extension constitute a very robust strategy for a unique identity to find its target in the nuclear space.

In summary, **this work reveals a radically different mechanisms for genome- and nucleus-wide homology search than the prevailing models** of broken ends seeking the homologous sequence as a

compact focus. Instead, we show that of homology sampling units dynamically stretch across the nucleus and undergo cycles of compaction/extension allowing a rapid and robust exploration of the nuclear volume.

Given the importance of Homologous recombination for genome stability, and the conservation of this mechanism across evolution, our findings bear broad implications for genome maintenance in other species

Finally, the capacity to monitor the dynamics of Rad51 in living cells opens new avenues to screen genetic factors and small molecules impacting on HR regulation with strong implications for both our understanding of HR regulation and medical applications.

Summary

FIGURE LIST: INTRODUCTION

FIGURE LIST: RESULTS

Section A

Section B

ABREVATIONS

Alt-NHEJ	alternative non-homologous end joining
ATR	ataxia telangiectasia and Rad3 related
ATM	ataxia telangiectasia mutated
AP	apurinic/apyrimidinic
BER	base excision repair pathway
BIR	break-induced replication
CIN	chromosomal instability
DSB	double strand break
dHJ	double Holliday junction
FRET	forster resonance energy transfer
FL	fluorescence
GCRs	gross chromosomal rearrangements
HU	hydroxyurea
HR	homologous recombination
HJ	holliday junction
IEG	immediate early gene
IR	ionizing radiation
ICL	inter-stand crosslink
LLPS	liquid-liquid phase separations
LOH	loss of heterozygosity
MIN	minisatellite instability
MMR	mismatch repair
MSD	mean square displacement
NE	nuclear envelope
NER	nucleotide excision repair
NHEJ	non-homologous end joining
NPC	nuclear pore complex
NPF	nucleoprotein filament
PALM	photo activable localization mic roscopy
RAG1	recombination activating gene1
RIF	radiation induced foci
ROS	reactive oxygen species
RPA	replication protein A
SDSA	synthesis-dependent strand annealing
SPB	spindle pole body
SR	super resolution
SSA	single strand annealing
SSBR	single strand break repair
STORM	stochastic optical reconstruction microscopy
TADs	topologically associating domains
TEM	transmission electron microscopy
TLS	translesions DNA synthesis

I. INTRODUCTION

PREFACE

DNA is the major carrier of genetic information in prokaryotic and eukaryotic cells, and its integrity is vital for the survival of cells. Despite its importance, DNA is under the pressure of damage caused by both exogenous and endogenous factors. Double strand break (DSB) is one of the most toxic DNA damages, and even one unrepaired DSB is lethal to cells. There are many ways to repair DSB, including non-homologous end joining (NHEJ), alternative non-homologous end joining (Alt-NHEJ), and homologous recombination (HR). HR occurs primarily in S-G2 phase cells and uses an undamaged homologous DNA sequence as a template for copying the missing information. A common source for the duplex DNA donor is the undamaged sister chromatid; however, homologous sequences on either the homolog or on a different chromosome can be used as a template to perform inter-homolog recombination or ectopic recombination respectively. HR with the sister chromatid is an error-free pathway. However, inter-homologue and ectopic recombination can induce a loss of heterozygosity or result in gross chromosomal rearrangements, including duplications, deletions, and translocations.

The homology search is performed by nucleofilaments formed by the association of the recombinase (Rad51 in eukaryote, RecA in bacteria) coating ssDNA formed on DSB flanking sequences. My PhD project focuses on the dynamics of the eukaryotic recombinase Rad51 during HR in living yeast (Godin et al. 2016; San Filippo et al. 2008; Petukhova et al. 1998).

Yeast has a light genome and 6000 genes non-randomly distributed in 16 chromosomes (Botstein et al. 1997, Mager et al. 2005, Mewes et al.1997). To study the dynamics of Rad51 in living yeast, I will present the related background knowledge in the introduction.

1, The first part would be a general review of the genome instability and DNA repair. Yeast and mammalian cells have different genome organizations, but both face genome instability. Here, the primary source of genome instability and DNA damage are listed along with the repair pathways.

2. In the second part, I will focus only on the DSB and HR among all the damages and pathways. HR in yeast and mammalian cells will be compared to help us understand why we chose yeast to study HR.

3. In the third part, after briefly introducing the significant repair proteins in HR, I will discuss the function of the key HR player, Rad51, its structures and features during homology search and pairing in yeast.

4. Then, I will discuss the dark side of HR. The Rad51 filament is a double-edged sword that can faithfully repair DSB but can also have deleterious effects leading to genome instability or cell death if not adequately controlled. Therefore, major negative and positive regulators of Rad51 filaments during HR are detailed in this part. I will present their functions, relationships, and mechanisms.
5. Finally, based on the review above, I will discuss how HR takes places in the nuclear space, including the localization of repair proteins, the chromatin dynamics upon DSB and the homology search in the nuclear space.

1 Genome instability and DNA repair

1.1 Genome organization

Containing a whole set of genetic information, the genome has been intensively studied in different organisms, notably with the genome sequencing project. During biological processes, proteins interact with folded chromatin rather than linear DNA, so it is critical to understand the spatial genome organization. DNA is not randomly positioned inside the nucleus. Indeed, the genome is highly organized, from the chromosome level to the position of individual genes (Lanctot et al. 2007; Takizawa et al. 2008), and it varies significantly between prokaryotes and eukaryotes. Furthermore, the 3D organization of the genome sometimes imposes physical constraints that have consequences on cellular activities. The importance of spatial organization is especially obvious for HR, which requires physical contact between the damaged DNA and the homologous donor sequence, which needs to be identified amongst megabases of DNA distributed in the nuclear space. Therefore, grasping the basic spatial genome organization is essential for studying HR.

Taking bacteria as an example, their genomes vary in size by at least an order of magnitude, and there could be considerable variations in genome size within a bacterial species (Herdman 1985). Unlike eukaryotes, the bacterial genome forms a circular chromosome with extrachromosomal elements such as plasmids and phages (Lederberg 1998). With little non-coding or intervening sequences, most parts of bacterial genomes are functional protein-coding regions (Mira et al. 2001), which is why, in most cases, their gene number scales linearly with genome size (Bobay and Howard 2017). The bacterial genomes are very dynamic, folding into loops on the order of 10kbp in size and dividing into independent domains on the order of 1Mbp (Lioy et al. 2018). The chromosomes of bacteria interact intimately with many cellular processes offering a major driving force for genome structure and organization (Rocha 2008). In *E. coli*, it has been revealed through fluorescent microscopy that the chromosomal segments organize into two macrodomains, the Ori domain (on the centromere-like site *migS*) and the Ter domain (on the replication terminus). The domains are possibly involved in processes dedicated to managing chromosome condensation and dynamics (Espeli and Boccard 2006). The Ter region manages the bacterial chromosome through a MatP/*matS* site-specific organization system during the cell cycle (Mercier et al. 2008).

On the other side, the eukaryote genome is more complex and is separated from other organelles by a double-membrane called the nuclear envelope (NE), which delimitates the nucleus inside the genetic material that is hierarchically packaged. This complex genome organization includes

multiscale structural units of chromosome territories, compartments, topologically associating domains (TADs) and chromatin loops (Zheng and Xie 2019). DNA wrapped around histones forms chromatin fibres with a 3D structure necessary for many biological processes, like transcription, DNA replication, cell division and meiosis (Hug et al. 2018; Gorkin et al. 2014; Beagrie et al. 2017). Therefore, the 3D structures are robust as well as flexible enough to be dynamic and frequently change (Dixon et al. 2015). Chromatin has distinct structural domains acting as different functional units of the genome (Bonev and Cavalli 2016) and defects in the higher-order chromatin organization can lead to development abnormalities and human diseases (Lupianez et al. 2016). Since we use budding yeast as a model for this study, it is necessary to introduce the genome organization in yeast further.

The budding yeast *S. Cerevisiae* is a eukaryote organism which contains a 13 mb sized genetic material divided into 16 chromosomes inside a 1µm radius nucleus (Miné-Hattab and Taddei 2019). Compared with other eukaryotes, the yeast genome is very compact with fewer non-coding and repetitive sequences (except for the *rDNA*). The key structural elements are the nuclear envelope (NE), the nuclear pore complex (NPC) and the nucleolus. The spindle pole body (SPB) is embedded in the nuclear envelope and nucleates intranuclear microtubules and mitotic spindle (Taddei and Gasser 2012). In exponentially growing cells, *Saccharomyces cerevisiae* presents a Rabl-like organization in which all the centromeres remain attached to the SPB through short microtubules during interphase, while telomeres are located close to the nuclear periphery (Miné-Hattab and Taddei 2019) (Figure 1). Opposite to the centromeres is the nucleolus formed around the ribosomal DNA (*rDNA*) repeats located on chromosome XII. Although the global architecture of the genome is relatively stable during interphase, local movements with amplitudes reaching 1 µm within 10 seconds have been reported using live cell imaging (Heun et al.2001; Miné-Hattab et al. 2012).

Furthermore, nuclear organization is regulated by the physiological state of the cells, as illustrated in long lived quiescent cells, in which telomeres cluster into a unique, large focus in the center of the nucleus (Guidi et al. 2015). The nuclear organization is involved in regulating genome functions by forming distinct regions with different molecular compositions where unrelated molecules are excluded, but specific factors are concentrated (Leger et al. 1999). These domains named sub-compartments, include nucleolus, silencing, replication, and repair foci (Mine-Hattab and Taddei 2019) (Figure1).

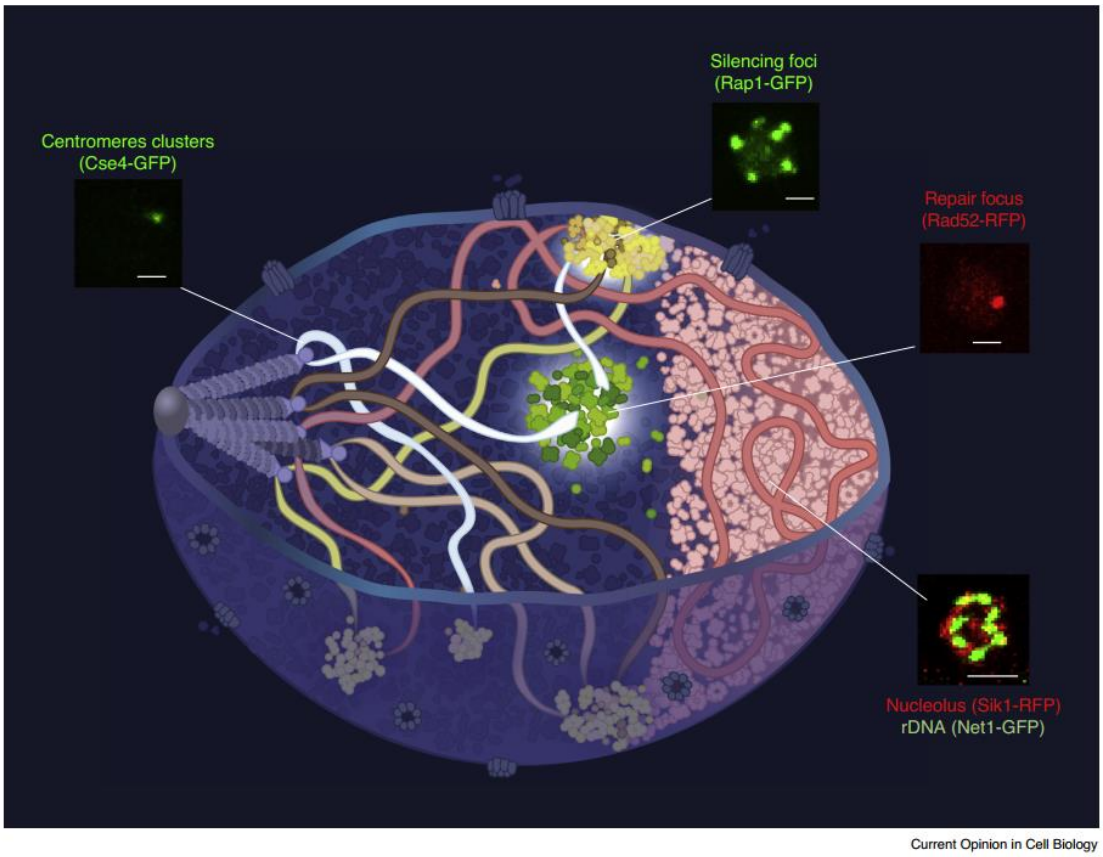

Figure 1 Illustration of a yeast nucleus in G1.

Five of the 16 chromosomes are represented following the Rabl-like configuration. Chromosomes size ranges from 229 kb to 2.8 Mb. Microscopy images illustrate some of the membrane-less compartments. Rad52-RFP (Mine-Hattab et al., unpublished), Rap1-GFP and Net1-GFP/Sik1-RFP (courtesy of Myriam Ruault). Scale-bars are 1 mm. (Illustrator: Olga Markova). (Mine-Hattab and Taddei 2019).

Nucleolus. The nucleolus plays a major in nuclear spatial organization (Saez-Vasquez and Oliver 2010). Initiated by production of ribosomal RNA (rRNA), the formation of nucleolus is a self-organized process (Trumtel et al. 2000; Misteli, 2001). The nucleolus is a very dense sub-compartment occupying around 30% of the nuclear volume, which offers space for *rDNA* and ribosome proteins to form pre-ribosomes. Apart from ribo-biogenesis, the nucleolus is also related to cell cycle progression through the sequestration of the Cdc14 phosphotase (Shou et al.1999; Kobayashi et al.2011), the regulation of the SUMO system and the telomerase activity in yeast (Ouenzar et al.2017; Sydorskyy et al. 2010).

Silencing foci (Telomere foci). In haploid yeast strain, 32 telomeres associate to form several unequal clusters (Taddei et al. 2010), which recruit the silent regulation factors Sir2, Sir3 and Sir4 to form the SIR complex (Palladino et al. 1993). The silencing foci are very dynamic and can be affected by the amount of Sir3 just like the nuclear distribution of telomere clusters (Hoze et al. 2013; Ruault et al.

2011; Ruault et al. 2021). Telomere clustering is also affected by the metabolic state of the cell, the telomeres form hyperclusters and re-organize the genome in long-lived quiescent cells after carbon source exhaustion (Guidi et al. 2015).

Repair foci. After a double strand break (DSB) occurs, repair proteins relocalize from a diffuse distribution inside the nucleus to a highly concentrated sub-compartment at the damaged site called repair “focus" (Lisby et al. 2004). During HR, multi-protein complexes can form mega-Dalton protein complexes containing 500-2000 proteins (Lisby et al. 2004), reaching a 50 times greater protein concentration than the rest of the nucleus (Bordelet and Dubrana 2019). In addition, it has been shown that cells containing two DSBs make a single repair focus most of the time, implying that there must be a movement of the broken chromosomes to the “repair centers” (Lisby et al. 2003). Similarly, after irradiation in human cells, multiple DSBs rapidly cluster into repair centers called radiation induced foci (RIF) (Neumaier et al. 2012). The repair foci are highly mobile, allowing them to explore with the broken chromatin a nuclear volume up to 10 times larger than without damage (Dion et al. 2012).

1.2 Genome instability

Genome integrity and faithful genome propagation are essential during cell proliferation. Error-free DNA replication with DNA-damage sensing and repair mechanisms ensure the integrity during replication, preventing mutations and chromosome rearrangements. These events are a major source of genome instability which can contribute to evolution at the molecular level and generate genetic variation. The learning behaviours cause widespread DSB formation in both neuronal and glial cells (Stott et al. 2021). These DSBs play an adaptive role in the central nervous system through impairing long-term memory and altering immediate early gene (IEG) expression (Weber Boutros et al. 2022). However, they can also be harmful to the cell and organism (Aguilera et al. 2008). The generated genome instability triggers pathological disorders such as premature aging, cancer predisposition and human-inherited diseases (Vijg et al. 2013). For our yeast model, genetic instability is generally associated with aging. The loss of heterozygosity increases as diploid yeast mother cells age (McMurray et al. 2003).

Genomic instability can be divided into different classes, including base substitutions, micro-insertions, micro-deletions, chromosomal instability (CIN), Micro- and minisatellite instability (MIN) caused by mismatch repair (MMR) or HR (Draviam et al. 2004, Friedberg et al. 2005). The primary cause for mutations is replication errors and repair impairment. The HR-mediated events can result in gross chromosomal rearrangements (GCRs), such as translocations, duplications, inversions, or deletions, generated by DNA breaks. The accumulation of these DNA damages can lead to cancer such as UV-induced skin tumors (Sinha et al.2002) and cancerogenic chemicals (Wolfe et al. 1987).

1.3 DNA damage and repair pathways

DNA can be damaged by either endogenous or exogenous factors. Exogenous DNA damage is caused by physical, chemical, or biological genotoxic agents, while endogenous DNA damage arises from hydrolysis, oxidation, alkylation, and DNA metabolism. The mismatch of DNA bases can be caused by the reactive oxygen species (ROS) and nitrogen species (NOS). Frequently, it can stem from errors during normal or aberrant DNA metabolism, including replication and repair (Hakem et al. 2008). The mismatched nucleotides are formed in heteroduplex DNA during recombination because of the unidentical donors and acceptors (Spies and Fishel et al.2015). Moreover, it is important to know that there are programmed DNA damages involved in various physiological pathways such as meiosis, the V(D)J recombination and Class-Switch Recombination in mammals and the mating type switch in budding yeast (Oster et al. 2020). Although endogenous factors may be more frequent and/or more extensive than exogenous factors, both factors exert genotoxic action on DNA with the same mechanism (Chakarov et al. 2014). Different types of DNA damages are classified based on the structure and site, including base modifications and loss, DNA-DNA intra-strand and inter-strand crosslinks, DNA-proteins crosslinks, single strand, and DSB (Moustacchi et al. 2000). Among them, DSBs are extremely dangerous and lethal to cells if they remain unrepaired.

Mutations arise as a consequence of DNA damage tolerance. The translesion DNA synthesis (TLS) polymerases are capable of bypassing DNA damage in the template DNA strand so replication can progress (Friedberg et al. 2005). These damages can persist in the genome and be important origins of evolution (Friedberg et al. 2005). However, the cells undergoing enormous genomic insult might choose to initiate programmed cell death to protect their population from severe consequences (Friedberg et al. 2003). Except for the cases mentioned previously, DNA damages are usually arrested by checkpoint activation and will be repaired by different pathways. Considering their essential functions, it is unsurprising that repair genes are highly conserved, making the repair processes fairly similar from bacteria to humans. *RAD51* and *BRCA2* genes are essential in mammals, which makes the obtenation of KO cells difficult (Zhang et al. 2021). This is why it is convenient to use bacteria and yeast as powerful tools to unravel these repair mechanisms (Moustacchi et al. 2000).

DNA repair pathways can be divided into error-free and error-prone repair pathways, and we will briefly describe several of these conserved pathways together with their targeted damages (Figure 2).

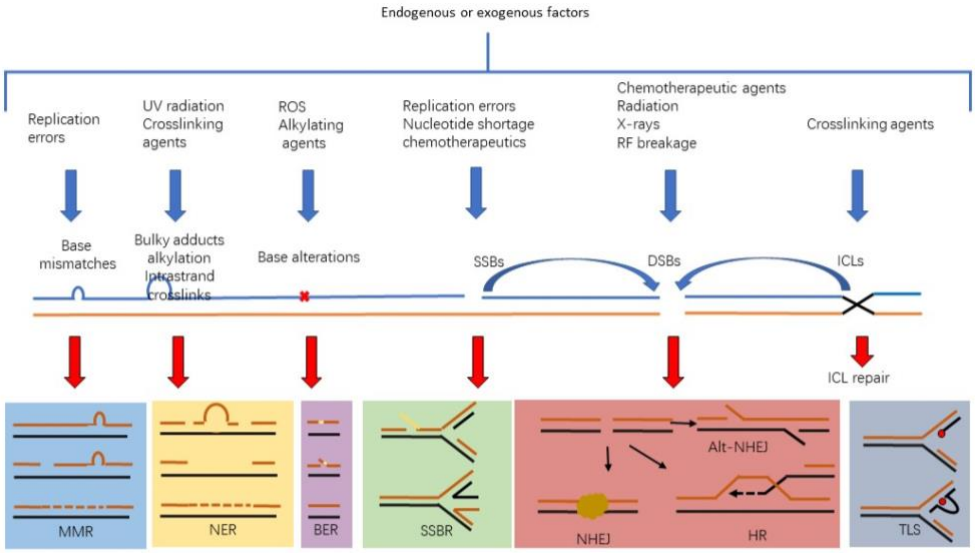

Figure 2 DNA damage source, types, and repair pathways

(Adapted from Razqallah et al.2008)

Mismatch repair (MMR). During DNA replication, base mismatches can occur and result in point mutations in the place of the mismatched base. This process involves a complex interplay of MMR-specific proteins with the replication and/or recombination machinery. The complex is activated by binding mismatch-recognition factors, Mutα and Mutβ, on substrates that contain mismatched bases and insertion/deletion loops. The nicked strand will then be replaced by newly synthesized DNA (Fishel and Lee 2016).

The base excision repair (BER). Base alteration arises from ROS-induced DNA damage or base alkylation, which can also be converted into point mutation and cause replication stress. DNA glycosylases will first excise the altered base, then apurinic/apyrimidinic (AP) endonuclease will cleave adjected phosphodiester bond and form a nick in the DNA strand. The AP site containing strand is either displaced by DNA synthesis or selectively cut out (Dianov et al. 2013).

The nucleotide excision repair (NER). UV radiation or DNA intra-strand crosslinks result in larger lesions, which further induce double helix distortion or transcription blockage. Then NER-associated proteins are recruited and generate a gap, by dual incision, that will be filled by DNA polymerase for ligation (Marteijn et al. 2014).

DNA single strand break repair (SSBR). It arises either during other repair processes like NER and BER, or oxidative DNA damage. SSBs are not very toxic lesions but can still block transcription when occurring in an active transcription region. If they remain unrepaired, SSBSs can convert into extremely toxic DNA DSBs. SSBs are recognized by the replication fork pausing and the recruitment of other essential factors for lesion repair (Caldecott et al. 2008).

DNA double break (DSB) repair. DSBs are the most toxic of DNA lesions and can be repaired by multiple pathways, including HR, NHEJ, alt-NHEJ and MMEJ. These pathways will be further discussed in the following parts.

DNA inter-stand crosslink (ICL) repair. Certain compounds can covalently link two DNA strands together and form ICLs. They are a dead-end substrate for NER because the crosslinker alters both strands. Usually, in the S phase, ICL lesions would collide with replication forks which would complicate the repair as it would trigger several other DNA repair pathways such as NER, HR and TLS (Deans et al. 2011).

2 Homologous recombination and double-strand break repair

2.1 DNA double-strand breaks and their sources

DNA damage, including base lesions, cross-links, and single strand breaks (SSBs), is repaired frequently with 10^5 lesions per cell daily (Hoeijmakers 2009). DNA double strand breaks (DSBs), in which two complementary DNA strands are broken spontaneously, are less frequent but extremely dangerous (Mehta and Haber 2014). If unrepaired, DSBs lead to gross chromosomal aberrations, extensive genome instability, genomic rearrangements and/or cell death (So et al. 2017). A single DSB can be potentially lethal to the cell (Weiffenbach and Haber 1981).

All these types of DNA damage can arise from endogenous metabolic reactions and replication stress or exogenous sources like radiation and chemotherapeutics. The common exogenous DNA damaging agents are chemotherapeutic drugs and ionizing radiation (IR). Chemotherapeutic drugs include DNA-alkylating agents, cross-linking agents and radiomimetic compounds that can result in other DNA damages (Chen and Stubbe 2005; Wyrobek et al. 2005). For example, the topoisomerase inhibitors, camptothecin and etoposide, can induce SSBs and DSBs, respectively (Koster et al. 2007). On the other hand, IR leads to extensive base damage and creates DNA SSBs by attacking the sugar-phosphate backbone (Ward et al. 1994; Thompson et al. 2012). Under high doses of IR, DSBs are generated when two SSBs happened in the complementary DNA strands within one helical return, with a ratio of 10:1 (Milligan et al. 1995, Ma et al. 2012). Similarly, DNA damage induced by UV radiation is dependent on its wavelength. Thus, UVC radiation (10-280nm) induces more DSBs and a lower survival rate than UVA (320-400nm) (Santos et al. 2013). The broken DNA ends produced by IR usually show phosphoglycolates and terminal nucleotides, being considered "dirty" ends that cannot be ligated to "clean" ends generated by endonucleases (Weinfeld and Soderlind 1991).

Besides exogenous factors, DSBs can also be caused by endogenous sources, especially during replication. The frequency of spontaneous DSBs can be estimated by counting the viability of cells upon inhibition of DSBs repair pathways or by monitoring the damaged-induced foci by immunofluorescence. During gene transcription, the topoisomerase II (TOP2) can induce DSBs, which are partially repaired by tyrosyl-DNA phosphodiesterase 2 (TDP2) dependent NHEJ (Gomez-Herreros et al. 2017). The kinetics of TOP2-induced DSBs is decided by chromatin structure and transcriptional activity (Canela et al. 2019). In yeast, the mortality rate in homologous recombination (HR) deficient cell is around 12% per cell division, suggesting a similar 12% of DSBs that requires HR to be repaired

(Ozenberger and Roeder 1991; Coïc et al. 2008; Claussin et al. 2017). The formation of spontaneous recombination foci has also been used to estimate DSBs in living yeast, although it might underestimate the number of DSBs since multiple DSBs can only form one repair focus (Lisby et al. 2003). Likewise, it was shown in human cells that around 1% of SSBs are converted to 50 DSBs per cell per cycle and that the spontaneous rate per base pair is around 2×10^8 per cell cycle (Vilenchik and Knudson 2003).

The majority of spontaneous DSBs come from DNA replication and transcription (Syeda et al. 2014). Through unwinding and annealing of a newly synthesized strand, stalled replication forks form a Holliday junction, which will be cleaved by nucleases or HJ resolvases, such as Mus81-Mm4 or Yen1, to lead to a one-ended chromosome break (Wyatt and West 2014). In addition, during transcription, RNA: DNA hybrids can stop replication fork and form R-loops or three-strand nucleic acid structures, which can sometimes result in R-loops-mediated DSBs formation and the activation of the DNA damage response (DDR) (Groh and Gromak 2014; Sordet et al. 2009). In human cells, the activation of the ataxia telangiectasia and Rad3-related (ATR-CHK1) pathway requires the MUS81 endonuclease to face R loop accumulation. ATR protects the genome from R loops by suppressing transcription replication collisions, promoting replication fork recovery and enforcing a G2/M cell-cycle arrest (Matos et al.2020). Besides DNA replication, chromosome segregation defects led to chromatin disruption and DSBs formation (Hoffelder et al. 2004; Samoshkin et al. 2009; Janssen et al. 2011; Quevedo et al. 2012).

Despite being the most deleterious DNA lesions, DSBs can also occur under physiological conditions and benefit development and survival. They include developmentally programmed DSBs, such as the ones involved in extensive genome rearrangements in the ciliate Paramecium (Baudry et al. 2009, Kapusta et al. 2011), VDJ recombination in mammals (Soulas-Sprauel et al. 2007) and the programmed switching of mating-type genes in yeast (Haber et al. 2012).

In mammals, the V(D)J recombination is initiated by the recombination activating gene1 and 2 (RAG1 and RAG2) proteins that induce DSBs. Indeed, RAG1 and RAG2 bind and cleave genomic DNA at recombination signal sequences that lie adjacent to antigen receptor gene segments where they generate DSBs. V(D)J recombination assembles antigen receptor genes as well as T-cells receptor genes in the appropriate cell lineage and developmental order (Schatz et al. 2011). This process is crucial for the generation of different receptor repertoires during lymphocyte development (Bassing et al. 2002).

In budding and fission yeast, mating-type switch begins with a targeted DSB at the mating type locus that is repaired by the opposite mating-type alleles through HR (Arcangioli et al. 2000; Klar et al. 2007). The site-specific endonuclease, homothallic (HO), generates a DSB with 4-bp, 3'-OH overhanging ends, specifically in the budding yeast *Saccharomyces cerevisiae* (Haber et al.2012). Another specialized endonuclease in budding yeast is the mitochondrial enzyme *I-SceI* (Colleaux et al. 1988). Both enzymes are commonly used as DSB-inducible systems for understanding DSB repair.

2.2 DSBs repair pathways

Based on the availability of a homology sequence, DSBs repair pathways can be classified into three classes: homologous recombination (HR), non-homologous end-joining (NHEJ) and alternative repair pathways, like alternative non-homologous end-joining (alt-NHEJ) also known as microhomology-mediated end joining (MMEJ) (Figure3). They can induce non-programmed genome rearrangements and genome instability if DSB repair is not properly regulated (So et al. 2017).

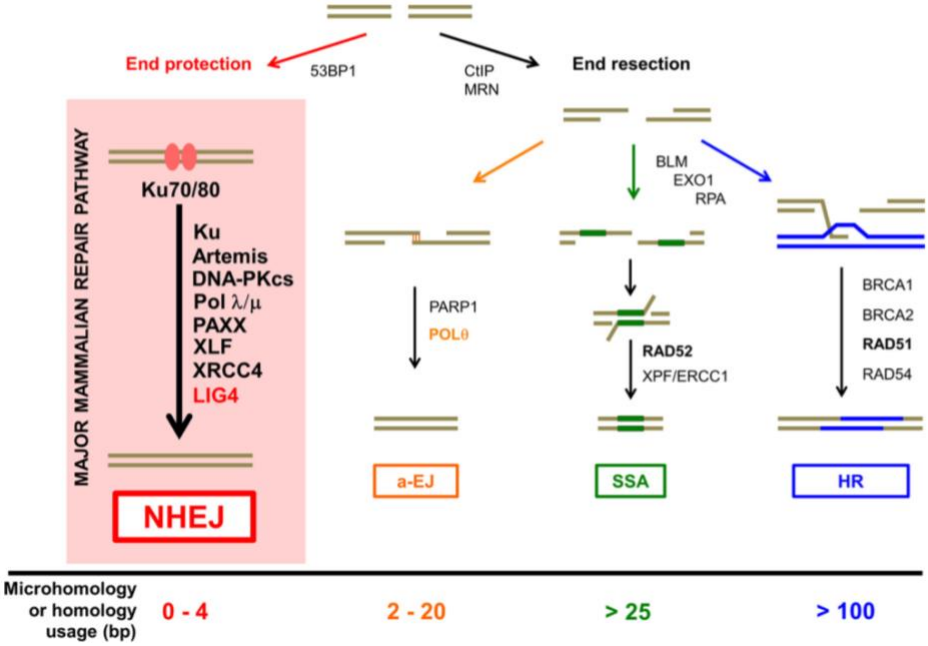

Figure 3 DSB repair pathways.

DNA double-strand breaks (DSBs) can be repaired by NHEJ, alternative end-joining (a-EJ), single-strand annealing (SSA), or homologous recombination (HR). Pathway choice and pathways other than NHEJ are discussed in other Minireviews in this thematic series. The name NHEJ originally arose to distinguish it from repair that requires extensive DNA homology (i.e., HR and SSA). Lengths of terminal microhomology (MH) between 1 and 4 bp are common in NHEJ. a-EJ is also called microhomology-mediated end joining (MMEJ) or Pol-mediated end joining (TMEJ). The major difference in the pathways is the requirement for significant DNA end resection. The p53-binding protein 1 (53BP1) is a chromatin remodeler and a positive regulator for NHEJ. Although ArtemisDNA-PKcs can carry out some nucleolytic resection (typically 20 nt), the NHEJ pathway does not require extensive end resection, and the ends are protected from deeper resection by the binding of the Ku heterodimer (Ku70–80) to the DNA ends. By contrast, the C-terminal binding protein-interacting protein (CtIP) and the MRN (MRE11 (meiotic recombination 11)RAD50NBS1 (Nijmegen breakage syndrome protein 1)) complexes are involved in extensive 5 to 3 resection of regions of the duplex, and this generates stretches of ssDNA at DNA ends for a-EJ, SSA, and HR. SSA typically requires 25 bp of microhomology, whereas the requirement for a-EJ is typically 20 bp. Poly(ADP-ribose) polymerase 1 (PARP1) and Pol are important for a-EJ. Bloom syndrome RecQ-like helicase (BLM) and exonuclease 1 (EXO1) account for additional resection, and replication protein A (RPA) binds to ssDNA to promote the SSA and HR pathways. RAD52 anneal small lengths of homologous sequence in the SSA pathway. XPF-ERCC1 cuts the remaining 3 nonhomologous ssDNA prior to ligation by DNA ligase 1. By contrast, RAD51-mediated strand exchange with its association with BRCA1, BRCA2, and RAD54 is essential for facilitating the HR pathway. (Nicolas et al. 2017)

Non-homologous end joining (NHEJ). NHEJ is an error-prone pathway in which two DSB ends are

joined by apposition, processing, and ligation. NHEJ can repair DSBs throughout the whole cell cycle and process nearly all DSBs outside S and G2 phases, *i.e*. DSBs that are away from the replication fork (Nicolas et.al 2018).

NHEJ is an iterative process and requires the same central set of proteins in both yeast and mammalian cells: yKu70/80 (KU70/80), Dnl4/Lif1 (DNL4) and the MRX complex (MRN complex) (Aylon et al. 2004). In yeast, the yKu70/yKu80 complex is located at the telomeres but can relocalize at the DNA ends after DSB induction (Martin et al. 1999). NHEJ is rarely error-free since it requires the MRX to do end processing, degradation, or polymerization, before ligation (Chen et al.2001, Connelly et al.2002). However, end processing is not required when the DSB ends are compatible and have 3'hydroxyl and 5' phosphate. After end processing and resynthesis by DNA polymerases, the Dnl4-Lif1 complex is recruited, ligating the broken chromosomal ends. In mammalian cells, the DNA end-binding protein kinases, KU70 and KU80, are recruited and activate the catalytic subunit of the DNA-dependent protein kinase (DNA-PKcs) by stabilizing its interaction with DNA ends (Karran 2000). Both DNA-PKcs and Ku complexes are necessary for NHEJ, although DNA-PKcs-deficient cells show a milder phenotype in DSB survival than KU-deficient cells (Smith et al. 1999). Finally, NHEJ is completed by the DNA ligase IV/XRCC4 complex (Frank et al. 1998, Barne et al. 1998) (Figure 4).
The described Ku-dependent NHEJ is also referred to as canonical NHEJ (C-NHEJ). However, when end-joining involves small homology (less than ~20 bp), it is referred to as MMEJ (Kishore et al. 2013), which does not require Ku or DNA ligase IV.

Alternative-NHEJ (alt-NHEJ). Alt-NHEJ is also related to chromosome abnormalities such as deletions, translocations, inversions, and other complex rearrangements (Chen et al.2008, Yu et al.2003, Weinstock et al.2007, Welcker et al.2000). Although it is similar to the C-NHEJ, alt-NHEJ is independent of KU, XRCC4 and DNA-PKcs and it starts by the resection of broken DNA ends via the MRN complex (Burma et al.2006, Guirouilh-Barbat et al.2004). The most distinguishing feature of alt-NHEJ is the alignment of a short and limited microhomologous sequence, around 5-25 bp, before the ligation. After DNA resection, the microhomology sequence would be annealed by the crucial enzyme DNA Polymerase Polθ in mammalians (Polδ and Pol4 in yeast) (Seol et al. 2018). Polθ would also catalyze the extension of the annealed strands to form flap structures which will be cleaved subsequently (McVey et al.2008). After DNA end processing, the strands in alt-NHEJ are ligated by XRCC1 and DNA ligase III in most eukaryotes or Ligase I and IV in yeast (Bennardo et al.2008).

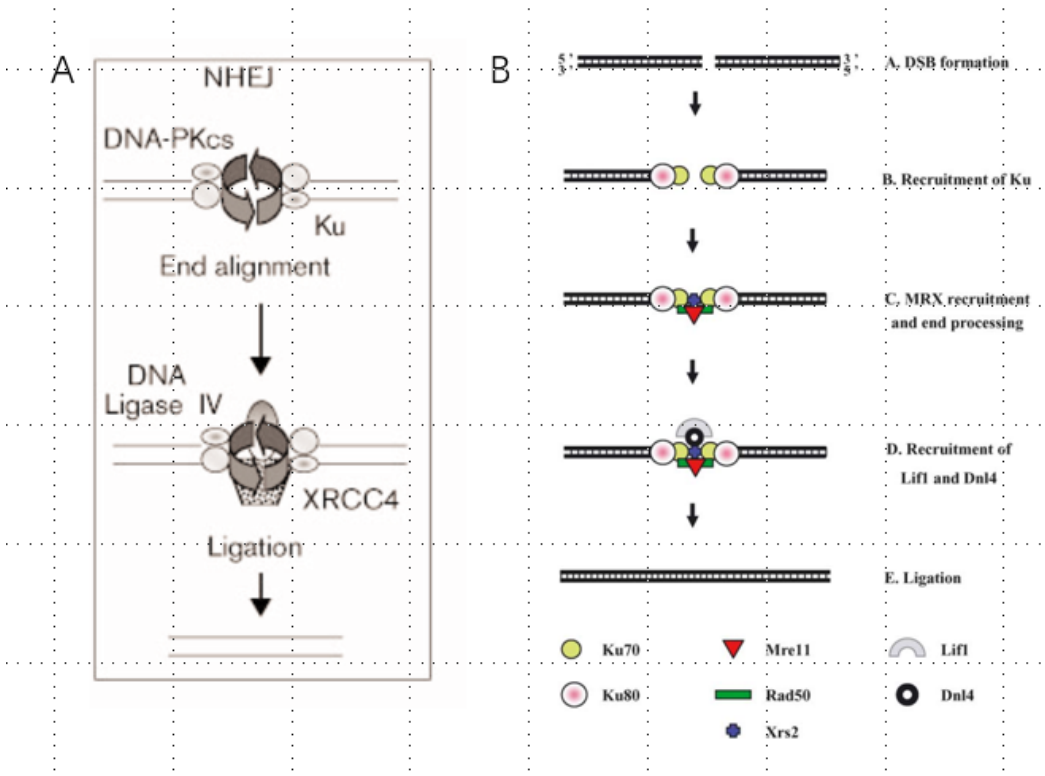

Figure 4 Mechanism of Non-homologous end joining

A, NHEJ in mammalian cells. The termini of a DNA DSB introduced by ionising radiation or other means are bound either by the Ku heterodimer/DNA-PKcs complex or by hRad52. In the NHEJ rejoining pathway, repair is completed by DNA ligase IV and XRCC4. (Karran 2000) B. A detailed description of the mechanism of non-homologous endjoining. Since the order of recruitment is still unsolved, steps (B) and (C) could be reversed. Following DSB creation (A), the yKu heterodimer is recruited to the broken ends (B) The Mre11/Rad50/Xrs2 (MRX) complex is then recruited (C) Both complexes may play roles in holding the broken ends together and participate in end-processing. The Lif1/Dnl4 complex is then recruited (D). The MRX and Lif1/Dnl4 complexes promote activity of Lif1/Dnl4, resulting in ligation of the broken ends (E) (Aylon et al 2004)

Homologous Recombination (HR). HR is an accurate DSB repair pathway; it uses a homology sequence of more than 100bp to repair the damaged DNA ends, and it mainly occurs in the S phase or G2 phase (Shahar et al. 2012, Shibata et al.2011). We will discuss HR, as well as its alternative pathways, in detail in the next chapter.

2.3 Homologous recombination

Homologous recombination (HR)is critical in meiosis for chromosomal pairing, as well as in mitosis for repairing DNA lesions such as DSBs. By promoting accurate repair of DSBs, HR is indispensable for maintaining genome integrity and avoiding human cancers (San Filippo et al. 2008). In addition, HR is an efficient bypass pathway for telomere maintenance in yeast, the Anopheles gambiae mosquito, immortalized human cell lines and tumours (Dunham et al. 2000; Lundbald et al. 2002; Sobinoff et al. 2020).

The linear relationship linking homology length with HR efficiency was initially used in bacteria to define MEPS: minimal efficiency processing segment. The proposed interpretation was that any segment of DNA contains an overlapping series of MEPS that is proportional to the size of the segment, provided that the segment is longer than the MEPS, thus explaining the linear relationship between substrate size and the recombination rate observed above this threshold (Shen et al, 1986). The MEPS has been determined to be between 132 and 232 bp of perfect shared sequence identity between recombining homologs in cultured mouse cells (Waldman and Liskay 1998); between 337 and 456 bp in humans for efficient meiotic homologous recombination (Reiter et al. 1998). Although yeast cells can process homologous recombination with a 30bp sequence (Hua et al. 1997), the exchange rate is approximately linear above 250bp, with a sharp decline below this threshold (Jin-Robertson et al. 1993).

Notably, the factors involved in HR are named differently between yeast and human cells. Table 1 lists the most crucial HR factors in yeast and human cells according to their correlations on functions during HR, which will be discussed in the following chapters.

HR can be divided into three stages: pre-synapsis, synapsis, and post-synapsis, as shown in Figure 5.

Pre-synapsis.

In the first stage, HR is initiated by the recruitment of the MRX complex to the broken DNA ends (Krejci et al. 2012). CtIP activates the endonuclease activity of Mre11 nicking dsDNA (Cejka et al. 2010) and provides substrates for Mre11 3’-5’ exonuclease activity. After the initial short-range resection (100-300nt), long-range resection is mediated by the combined action of Exo1 and Dna2/ Sgs1 (Zhu et al. 2008; Nimonkar et al. 2011, Ceika 2015). Long ssDNA is formed after resection and bound by RPA to prevent possible endonucleolytic degradation. A sufficient amount of DNA-bound RPA is required to activate kinases, ataxia telangiectasia and Rad3 related (ATR) and ataxia telangiectasia

mutated (ATM) that trigger RPA phosphorylation, checkpoint activation and cell cycle arrest, which is the last step of presynapsis (Liu et al. 2012).

Synapsis.

In the next step, Rad52 removes RPA and loads Rad51 on the ssDNA to form a nucleofilament. The Rad51 nucleofilament has the capacity to search for homologous sequences throughout the entire genome and, if available, locate a region of homology and then promote strand invasion into the homologous duplex DNA (Carver and Zhang et al. 2021). The search for a homologous dsDNA across the genome is considered a key step of homologous recombination. Both homology search and strand invasion are stimulated by Rad52, Rad55/Rad57, Rdh54 and Rad54 proteins (Krejci et al. 2012). Rad55-Rad57 are Rad51 paralogs that protect the stiff Rad51 filament from negative regulators like the Srs2 helicase (Liu et al. 2011).

The Shu complex is also involved in the decision between HR and error-prone repair by inhibiting the disassembly reaction of Srs2 (Bernstein et al. 2011). It is a heterotetramer formed by the SWIM domain-containing protein, Shu2, and the Rad51 paralogs, Csm2, Psy3 and Shu1, which promotes the Rad51 filament formation in vitro (Sasanuma et al.2013). The Psy3-Csm2 constitutes a core sub-complex with DNA- binding activity and stabilizes the Rad51-ssDNA independtly of nucleotide cofactor (Sasanuma et al.2013). In contrast to HR genes deleting components of the SHU complex does not lead to increased sensitivity to DSB-inducing agents. However, SHU complex mutants are primarily sensitive to the alkylating agent MMS (Shor et al. 2005).

With the support of Rad54, the Rad51 filaments search for the donor sequence and invade the homologous sequence to form a displacement D-loop (Krejci et al. 2012). Once the homology is found, the nucleofilament associates with the homologous dsDNA forming a stable synapsis (Heyer et al. 2006). Then, the extensive strand exchange occurs between the nucleofilament and the dsDNA template within the synapsis, ultimately restoring the genetic information disrupted at the DSB. The 3’ DNA end is extended by the DNA polymerase and PCNA while the RAD54 motor protein clears Rad51 from the D-loop intermediate, for the following transition from DNA strand invasion to DNA synthesis (Heyer et al. 2006).

Post-synapsis.

Finally, in post-synapsis, there are three HR sub-pathways with specific enzymatic requirements (BLM, FANCM, GEN1, EME1) in mammalian cells, synthesis-dependent strand annealing (SDSA), break-induced replication (BIR) and DSB repair (DSBR) (Heyer et al.2007; Krogh et al.2004; San Filippo et al. 2008), as shown in Figure 5. SDSA arises from the extended D-loop intermediate disruption and is the

preferred DSB repair pathway in mitotic cells. The extended ssDNA stretch anneals with the second DNA strand to promote accurate DSB repair without crossover (Sung and Klein 2006; Heyer et al. 2010; Li et al. 2019). BIR differs from the classical HR by partially assembly of the replication machinery after the initial D-loop formation step and results in DNA replication along the entire length of the chromosome. BIR occurs mostly when there is only one DNA end such as when replication forks are broken or when a DSB is induced near the end of a chromosome. In addition, BIR is important in telomerase-independent telomere elongation (McEachern and Haber 2006). BIR can result in several consequences, such as non-reciprocal translocations, loss of heterozygosity (LOH) and genome duplication (Costantino et al. 2014).

DSBR subpathway occurs in undisrupted D-loop intermediate after the formation of double Holliday junction (dHJ), which involves the capture of the second end, suggesting the inherent mechanistic bias towards SDSA (Wu et al. 2008). The dHJs can be resolved by endonucleases into crossover or non-crossover products. The crossover is often linked to chromosomal rearrangements (Heyer et al. 2010). Alternatively, dHJs can also be dissolved by a complex mechanism involving a RecQ-like DNA motor protein (Sgs1/BLM), topoisomerase 3, and cofactors. The outcome would be a non-crossover genetically, avoiding the potential for rearrangements associated with crossovers (Bussen et al. 2007; Bizard and Hickson 2014).

BIR, SDSA, and the DSBR lead to the repair of a DSB but are associated with different genetic consequences. Since the loss-of-heterozygosity and potential genomic rearrangements caused by BIR and DSBR, the SDSA has proven to be the favoured sub-pathway (Heyer et al. 2010). Furthermore, the SDSA outcompetes BIR in budding yeast because BIR is a much slower process (Heyer et al. 2010).

Besides these three subpathways, single strand annealing (SSA) is an alternative DSB repair pathway in which resection occurs but the downstream mechanism for HR is perturbed. The ssDNA sequences generated by resection can be annealed by RAD52 protein (Shinohara et al. 1998). After annealing, the ERCC1-XPF nuclease cleaves 3’ flap structures; gaps are filled by DNA synthesis, and DNA ends are ligated. This latter induces DNA loss, making SSA an error-prone pathway. Compared to MMEJ, SSA not only requires extensive homology length but also involves different proteins (Bhargava et al. 2016).

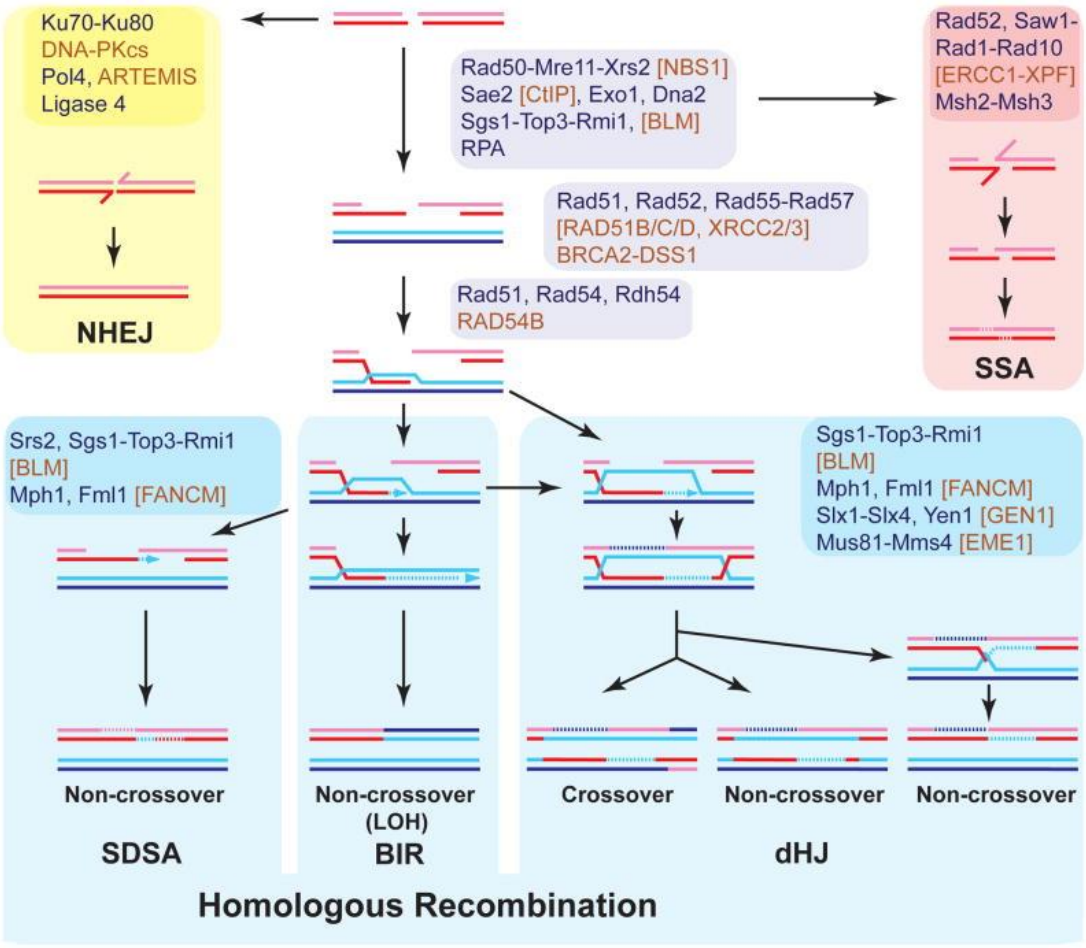

Figure 5 Scheme for homologous recombination.

Protein names refer to the budding yeast *S. cerevisiae* (black). Where different in human names (brown) are given in brackets. For proteins without yeast homolog brackets for human proteins are omitted. Broken lines indicate new DNA synthesis and stretches of hDNA that upon MMR can lead to gene conversion. (Heyer et al. 2010)

HR is a dedicated process regulated by many different factors, and yeast is a very functional model to test the hypotheses that are proposed to explain its mechanisms. Most of DNA repair mechanisms that we know in eukaryotes come from studies in budding yeast. Yeast has many advantages as a model organism. Genetic and biochemical analyses have characterized many mutants in metabolic pathways and cellular components. Generating these mutants in yeast affects their growth and thus, allows characterizing their phenotypes (Aylon et al. 2004). In addition, yeast forms four spores attached together during meiosis, which favouring micromanipulation and obtaining genetic information. As mentioned before, yeast prefers using HR rather than NHEJ, and yeast HO or *I-SceI* endonucleases led to targeted inducible DSB systems, which are often used in repair studies. Therefore, during my PhD, the budding yeast *Saccharomyces cerevisiae* was used to study HR. In the following parts, I will mainly focus on HR regulators in yeast.

	Human	*S. cerevisiae*	Function
Positive regulators	**RAD51**	**Rad51**	Homology search and DNA strand invasion
	RAD52		Recombination mediator, SSA
	BRCA2	**Rad52**	Recombination mediator
	RAD51B-RAD51C RAD51D-XRCC2 RAD51C-XRCC3 Psy3=RAD51D Shu2=SWS1 Shu1=XRCC2 Csm2=not identified	**Rad55-Rad57 Shu1-Psy3-Shu2-Csm2**	Rad51 paralogs, Recombination mediator. Stabilize the filament.
			Rad51 paralogs. Regulation of Srs2 activity, stabilization Rad51 filament.
		Rad59	ssDNA annealing, Rad51 filament stability
	RAD54	**Rad54**	ATP-dependent dsDNA translocase, stabilization of Rad51 filament
	RAD54B	**Rdh54/Tid1**	ATP-dependent dsDNA translocase, stabilization of Dmc1 filament
		Tid4/Uls1	SUMO-dependent ubiquitin ligase, stabilization of Rad51 filament
	RAD51AP1		Stabilization of D-loop formation
	SW15-MEI5	**Mei5-Sae3**	Mediator activity. Meiosis specific.
	MND1-HOP2	**Mnd1-Hop2**	Stabilization of Rad51- and Dmc-presynaptic filaments Meiosis specific.
Negative regulators	**PARI**	**Srs2**	Helicase activity, disruption of Rad51 presynaptic filament, promotes SDSA
		Hed1	Inhibition of Rad54 recruitment to Rad51 presynaptic filament. Meiosis specific.
	FANCM	**Mph1**	Helicase and branch migration activity, dissociation of D-loops formed by Rad51, Promotes SDSA
	BLM	**Sgs1**	RecQ-like DNA helicase, multiple roles in HR and DNA replication (resolution dHJ)
	RTEL1		ATP-dependent DNA helicase, inhibition of D-loop formation, promoting SDSA
	RPA	**RPA**	Binding to resected ssDNA ends (competition with Rad51)

Table 1 Repair proteins in human and yeast, grey for meiosis specific. Adapted from Krejci et al.2012.

3 The key player of HR

3.1 Rad51, the key player of HR

As the major eukaryotic homologous recombinase, Rad51 is highly conserved among organisms. The ScRad51 is 59% identical to human and mouse RAD51 and 30% identical to its bacterial homologue in *E. Coli*, RecA (Baumann and Stephan 1998). The structure of hRAD51 and ScRAD51 are similar. As the sequences of RAD51 protein family shown in Figure 6, the ScRAD51 has a block of around 50 amino acids in the N-terminally part that is absent in PfRAD51, HsRAD51, and hRAD51. ScRAD51 acts as a dominant-negative allele in mammalian cells by interacting with endogenous mRAD51 (Lambert et al.2000). ScRad51 shares some functionality with RecA and can catalyze a variety of ATP-dependent DNA pairing reactions (Liu et al. 2004). The *rad51* mutants, highly sensitive to DNA-damaging agents like MMS, show defects in mitotic and meiotic recombination in yeast (San Filippo et al. 2008).

Structure of Rad51 and its homologues

The crystal structures for Rad51 and RecA filament are presented in Figure 7A. The ScRad51 has three domains: The N-terminal (amino acids 1-154), the central (amino acids 155-374), and the C-terminal domain (amino acids 375-400) (Andrej and Chovanec 2004), and mutations that affect the bindings of ScRad51 to ScRad52, ScRad54, and ScRad55 are referred in Figure 6. The central domain of Rad51 is an ATPase domain that shows sequence similarity to ATPase domains found in helicases and involves DNA binding. ATP hydrolysis involves the dissociation of Rad51 from DNA during HR. The C- and N-terminal domains of the hRad51 and ScRad51 proteins are inverted, compared to the domains harbouring similar functions in the RecA protein. The sequence of the ScRad51 N-terminal that may interact with duplex DNA and is a critical factor for filament formation (Conway et al. 2004) is homologous to the RecA C-terminal domain. A flexible “linker” segment between the amino-terminal and core domains of Rad51 is an interface for oligomerization in human cells (David et al. 2003).

In vitro, Rad51 and RecA can form various structures (rings, filaments, and aggregates of filaments) independently of DNA (Selman et al. 2004).

Rad51 nucleoprotein filament

Rad51 is undoubtedly the central player of homologous recombination. Like RecA in *E. coli*, it forms a right-handed helix on ssDNA or dsDNA (Figure 7B). The polymerization of Rad51 on DNA forms a nucleoprotein filament (NPF) whose function is to undertake the process of homology search and to catalyze the exchange of strands between the ssDNA and homologous dsDNA substrates (Ogawa et al.1993). Then, the broken ends align with the homologous sequence and form a duplex which is further processed by other enzymes in a succession of steps, ultimately leading to the repair of the break (Conway et al. 2004).

The Rad51 monomers can polymerize in both directions on the ssDNA. Generally, they prefer the 3' to 5' direction, which is not the case for the RecA protein that polymerizes in the opposite direction. The kinetics of Rad51 polymerization strongly depends on its concentration: it has been shown *in vitro* that hRad51 polymerization is highly cooperative at low concentrations, challenging to start nucleation but has fast and smooth elongation and less cooperative at high concentrations (Mine-Hattab et al. 2007). Consequently, Rad51 NPFs formed at low concentrations are more continuous, while NPFs formed at high concentrations exhibit several discontinuities because filament growth is the limiting step. Thus, the concentration of Rad51 proteins is a crucial parameter for the structure of the NPFs, underlying the importance of working in living cells with endogenous Rad51 concentration.

	Number of monomers per helix	Pitch	Stretch factor	Angle of subcoil
RecA	6.2	91 Å	1.44	19.3
scRad51	-	94Å	1.47	18.9
UvsX	-	95Å	1.56	19.3
hRad51	6.4	99Å	1.56	18.6
RadA	6.6	105Å	1.56	18.3

The detailed structure of RecA/Rad51 NPFs has been intensively studied through electronic microscopy (Figure 7C). Rad51-DNA NPFs harbour ~18-19 bases or base pairs of DNAs and ~6 protein monomers per helical turn. Its pitch is close to 100 A, with an axial rise of 5.2-5.5 A per base or base pair (Ogawa et al.1993). The Rad51 and RecA filaments can be markedly flexible, and their pitch varies in response to ligands and within different segments of a single filament (Kinebuchi et al.2004). A

comparison between RecA, UvsX, hRad51, scRad51 and RadA NPFs is listed in Table 2. Though the RecA and Rad51 sequences are only 33% identical, the structures of their filaments are very similar. The conservation of structures through different organisms suggests that it plays an important role during HR.

Table 2 Conparison of different recombinant protein nucleofilament in different species, RecA (E Coli), scRad51(Yeast), UvsX (Bacterial T4), hRad51(human), and RadA (Spider). These data are from Egelman (Egelman et al,2001).

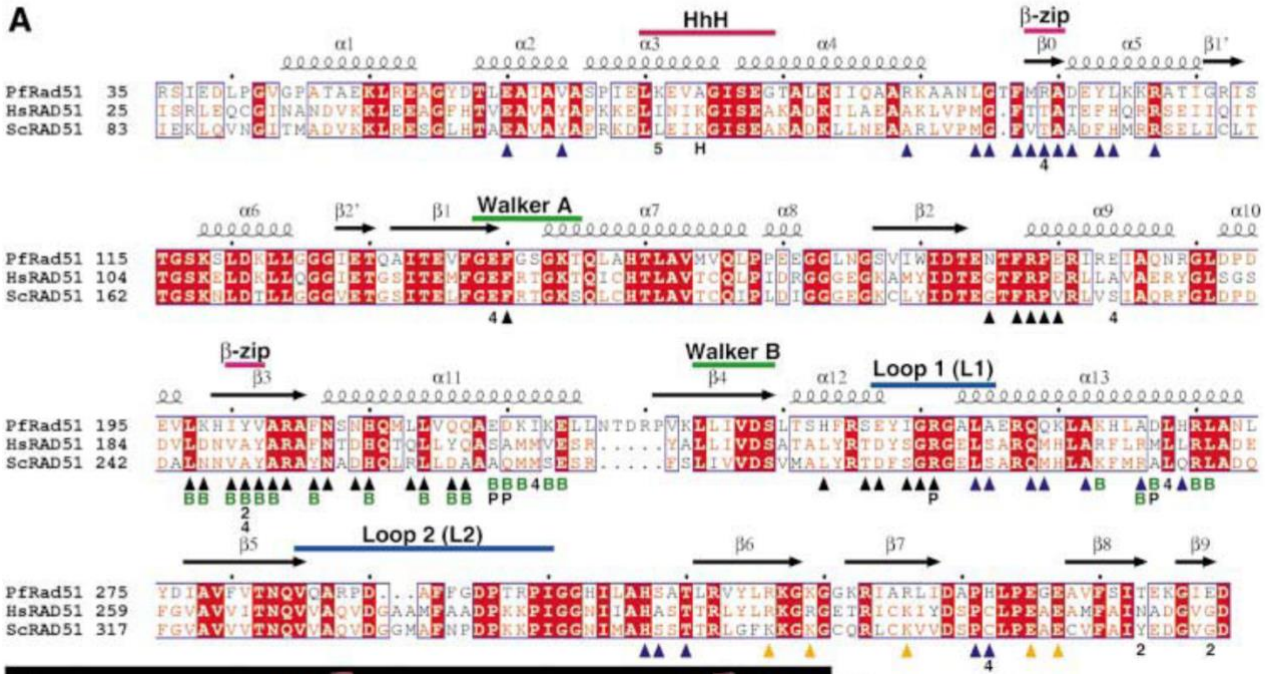

Figure 6 Sequence of RAD51 protein family

Aligment of RAD51 homologs from *P.furiosus* (PfRAD51), *H.sapiens* (HsRAD51) and *S.cerevisiae* (ScRAD51). P and H under the sequence refer to PfRad51 and HsRad51 key residues, while 2,4 and 5 refer to ScRad51 mutations that influence binding to ScRAD52, ScRAD54 or ScRAD55, respectively (Shin et al. 2003).

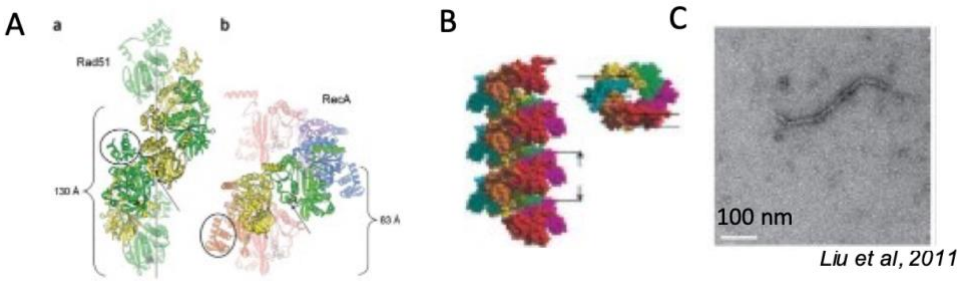

Figure 7 Structure of Rad51 and Rad51 nucleofilament

A. Crystal structure of Rad51 and RecA (**a**) The Rad51 filament found in these crystals has a helical pitch of 130 Å and is composed of two crystallographically independent monomers (yellow and green) that alternate to form a filament with exact three-fold but only approximate six-fold screw symmetry. A sulfate (black spheres) mimics the binding of phosphate in the ATPase site, which is nestled directly at the interface between two protomers (arrow). One of the N-terminal domains that line the upper surface of the filament is circled. (**b**) The filament formed in RecA crystals has a helical pitch of ~83 Å and is shown with each crystallographically equivalent monomer colored differently. The C-terminal domains (circled) line the lower surface of the filament (Convey et al. 2004). B. Right helix structure of Rad51 filaments C. EM images of Rad51 filament in budding yeast (Liu et al.2011)

Molecular mechanism of Rad51 during HR

Rad51 can load on ssDNA as well as dsDNA *in vitro*; however, only Rad51 NPF formed on ssDNA can catalyze DNA joint formation (Sung and Robberson, 1995), which is consistent with the notion that the recruitment of Rad51 initiates HR on ssDNA through replacing RPA (San Filippo et al.2008). RAD51 can control the selection of DSB repair pathways: gene conversion, SSA or alternative end-joining in human cells. Silencing RAD51 or BRCA2 can stimulate both SSA and A-EJ. Through occupying ssDNA, Rad51 protects genome integrity from non-conservative DSB repair (SSA and A-EJ) *in vitro* (So et al. 2022).

Each Rad51 monomer extends ssDNA and dsDNA by a factor of 1.5 per base compared to B-DNA; the Rad51 polymerization on dsDNA is a powerful mechanism for chromatin remodelling (Dupaigne et al. 2008). In addition, Rad51 also acts on the topology of dsDNA by unwinding dsDNA by 15 degrees per base pair *in vitro* (Bertucat et al. 1998). The changes induced by Rad51 on DNA affect not only the damaged DNA but also the dsDNA sequences that interact with the filament during the homology search process. The minor groove of the DNA is more open and accessible for homology search (Bertucat et al. 1998). Indeed, during homology search, the tested dsDNA is locally stretched and unwound (Cai et al. 2001; Wu et al. 1983), adopting the structure imposed by the NPF within the synapsis. It has been shown that when the sequence tested is heterologous, it is also unwounded and stretched during the transient formation of a synapsis (Rould et al. 1992).

The Rad51 nucleofilament is also very rigid, as shown by the measurement of its persistence length. This measure is commonly used to quantify the bending stiffness of a polymer; it is equal to the length over which correlations in the direction of the tangent are lost. For example, if the persistence length of a polymer was 500nm, we would observe a significant change in the polymer orientation every 500nm on average. Small persistence lengths correspond to soft polymers, while high persistence lengths correspond to stiff ones. The persistence length of naked dsDNA is estimated at 50 nm at pH 7.5 in TE buffer, corresponding to ~ 150 base pairs, while the persistence length for Rad51-dsDNA filament is ~300nm (Lee et al. 2013). The ssDNA is much softer, with a persistence length estimated at 1.5 to 3 nm through single-molecule FRET measurement on 10-70 nucleotides and strongly varies with the ionic conditions (Murphy et al.2004). Table 3 lists the persistence length of Dmc1, Rad51 and RecA ssDNA filaments; they were obtained from structures examined by transmission electron microscopy (TEM) after negative staining with 1% uranyl acetate. Dmc1 and Rad51 are both required

for meiotic recombination. They have overlapping and unidentical roles, but Dmc1 only works during meiosis in germ lines, which their distinct mismatch tolerance might cause during HR (Xu et al. 2021). Dmc1 forms octameric rings or helical filaments on DNA and prefers direct repair between homologous non-sister chromatids (Schwacha et al. 1997). The differences in the meiotic function of Rad51 and Dmc1 might come from the accessory proteins that could cause intrinsic differences in filament structure (Sean et al. 2008, table 3).

	Dmc1 filaments	Rad51 filaments	RecA filaments
Sample size	36	34	38
Mean persistence length (λ)	507	543	464
Standard error	45.2	45.3	42.2

Table 3 Persistence lengths of Dmc1, RecA and Rad51 filaments (Sean et al. 2008)

The ATPase domain of Rad51 and ATP might be involved in the loading process of Rad51. Rad51's ability to bind DNA is rapidly inactivated when incubated at 30-37 degrees but is stabilized by the presence of ATP and Mg^{2+}. AMP-P-N-P lacks this property, while WDP protects partially but only at 5-10 times higher concentrations than ATP (Namsaraev et al. 1998). Two mutants, Rad51-K191A (RAD51-K133A in mammals) and Rad51-K191R (RAD51-K133R in mammals) in yeast, have been used to study the effects of ATP and ATP hydrolysis on Rad51-ssDNA binding. The Rad51-K191A mutant, substituting the conserved 191 lysine residue with alanine, cannot bind DNA and has no ATPase activity. In contrast, the Rad51-K191R mutant which the lysine residue is substituted with an arginine, is capable of DNA binding but not ATP hydrolysis. In *vivo*, the rad51-K191A mutant confers a null phenotype, whereas the rad51-K191R mutant is partially functional for repair and recombination (Fung et al. 2006). ATP hydrolysis is not essential for DNA binding but is related to filament stabilization. Both rad51-K133A and rad51-K133R are deficient for foci formation after IR, suggesting ATPase activity is necessary for DNA binding in mammals (So et al. 2022). The hRAD51 nucleofilament points out more 'open' WT filament conformation in contrast to relatively 'closed' K133R and K133A mutant filaments, manifested by dramatic changes of the helical pitch and representing dynamic features of nucleofilament (Špírek et al. 2018). It is worthwhile to notice that the hRad51 interacts with Mg2+ during DNA binding, but it is not necessary for yeast (Namsaraev et al. 1998). In addition, it was

shown that Rad51 requires ATP hydrolysis for dissociation in the post-synapsis stage (Short et al.2016). During pairing, the dsDNA needs to be at least 8-nt for stable binding with the Rad51 presynaptic complex (Ragunathan et al,2012, Qi et al.2015). Longer sequences are less common but result in a higher probability of finding the correct target during a homology search. Prentiss and colleagues (Yang et al. 2015) identified a binding intermediate in which two adjacent bases from the successive triplets have flipped open and paired with the presynaptic ssDNA. This work proposes a length-based recognition mechanism that Rad51 interrogates with at least 8-nt dsDNA during homologous pairing for a robust kinetic selection.

Functions of Rad51 beyond the HR

As the primary catalyst of HR, Rad51 has been widely regarded as a guardian of genome stability. Moreover, novel roles of Rad51 have been identified in recent studies, specifically the interplay of Rad51 on DNA replication and maintenance of genomic stability (Wassing and Esashi 2020).

The importance of Rad51 varies between different species. Deleting Rad51 in yeast confers high sensitivity to γ-irradiation but is not otherwise detrimental to cell viability (Symington et al. 2002) and induces a slower growth rate than WT. RAD51 is essential for cell viability in vertebrates and, RAD51 null mutation leads to embryonic lethality in mice (Tsuzuki et al. 1996; Sonoda et al.1998).

Rad51 is required to sustain cell viability under the tetraploidization of budding yeast in which the replication-associated DNA damage is increased (Storchova et al. 2006). Importantly, the one-ended DSBs generated by fork breakage cannot be faithfully repaired *via* NHEJ (Wassing and Esashi 2020), suggesting the importance of Rad51-mediated repair. The BIR is mediated by Rad51 but also occurs in the absence of Rad51 (Anand et al. 2013).

Rad51 promotes fork reversal, a process in which stalled replication forks are reversed and remodelled into a 'chicken-foot' structure, which protects the replication fork from breakage and contributes to genomic stability (Zellweger et al. 2015). On the other hand, the fork reversal provides the entry point for nucleolytic DNA degradation at stalled forks, which can promote genome instability (Kolinjivadi et al. 2017). To conclude, Rad51 acts as a double-edged sword to genome stability; its bias depends on the nature and the severity of the genotoxic stress, the regulation of Rad51 activity and the surrounding DNA sequence (Wassing and Esashi 2020).

Replication fork arrest can be caused by endogenous lesions or genotoxic agents such as hydroxyurea (HU), UV light, ionizing irradiation and MMS (Pardo et al. 2017). Besides the lesions, the replication may be under stress at difficult-to- replicate regions, like common fragile sites, telomeres and

centromeres (Wassing and Esashi 2020). Rad51 is then recruited at the stalled fork, which is required for DNA damage tolerance in yeast (Gonzalez-Prieto et al. 2013).

The RAD51 haploinsufficiency causes congenital mirror movements (CMM) in humans, characterised by involuntary movements of one side of the body that mirror intentional movements on the opposite side (Depienne et al. 2012). Genetic analyses have revealed that the actual mirroring was characteristic of individuals in a family with a *RAD51* mutation (Franz et al. 2015). A subtype of Fanconi anemia, a hereditary disease featuring hypersensitivity chromosomal instability, bone marrow failure and a strong predisposition to cancer, is also associated with a dominant-negative mutation of *RAD51* (Ameziane et al.2015).

3.2 Other key players of HR

Genetic screens performed to identify mutants with altered recombination rates, lower survival rates in response to DNA-damaging agents, unfunctional sporulation and decreased spore viability, have identified more than 30 genes involved in recombination. The RAD52 epistasis group genes [RAD50, RAD51, RAD52, RAD54, RAD55, RAD57, RAD59, RDH54(TID1), MRE11(RAD58) and XRS2] play direct roles in HR (Krogh et al. 2004). Here we discuss the key factors involved in homologous recombination. Among them, Rad51 regulators will be detailed in the next chapter, the major players during pre-synapsis and post-synapsis, MRX and Mus81-Mms4 nuclease, and player for Rad51-independent recombination, Dmc1, Rad59, Rad52 and BRCA2, will be reviewed below.

MRX (Mre11, Rad50, Xrx2) complex initiates DSB. HR requires the nucleolytic processing of DNA ends to form invasive 3' ssDNA tails. In yeast, the ssDNA ends flanking a DSB can reach a size of hundreds to thousands of nucleotides long. *Rad50, mre11 and xrs2* null mutants are extremely sensitive to DNA damage agents (Symington et al.2016; Gobbini et al.2016). Unresected meiotic DSBs accumulate in *rad50* mutants (Sun et al. 1991), suggesting that MRX has a common role in both meiotic and mitotic DSBs. Structural and functional homologues of the Mre11/Rad50 complex exist in other organisms (Aravind et al. 1999), like the SbcC/SbcD complex in *E. coli* which also contribute to ATP-independent ssDNA endonuclease activities (Connelly et al. 1997). The nucleolytic function of Mre11 includes 1, 3'-5' exonuclease activity on blunt and 3' recessed ends; 2, endonuclease activity on circular and linear ssDNA; 3, endonuclease cleavage of hairpin ends and 3' ssDNA overhanging during the single-/double- stranded transition (Krogh et al. 2004). Rad50 dimer creates a DNA-binding interface for ATP-stimulated DNA binding (Moncalian et al. 2004). Mre11 binds at the base of the protruding antiparallel coiled-coil region (region linking two parts of the composite ATPase domain) and near the Rad50 DNA-binding interface (Hopfner et al. 2002). Xrs2, another complex component, is found only in eukaryotes and interacts with Mre11 directly (Johzuka and Ogawa 1995). The MRX complex initiates the G1, G2 and intra S-phase checkpoint in response to DNA damage, and Xrs2 is part of the damage signal (D'Amours and Jackson 2001; Grenon et al. 2006; Clerici et al. 2004).

Rad52 and BRCA2 mediators of Rad51. Rad52 is not only involved in Rad51-dependent recombination, but it also plays a role in the single-strand annealing (SSA) pathway together Rad59 and independently of Rad51 in yeast. In the absence of Rad52, *S. cerevisiae* is defective for gene conversion, SSA and recombination (Rattray and Symington, 1994). Both yeast and human Rad52 are multimeric and form ring structures (Ranatunga et al.2001). They preferentially bind ssDNA and

promote the annealing of the complementary DNA sequences with or without RPA (Mortensen et al.1996). Surprisingly, the *RAD52* gene knockout is only slightly defective for recombination in mammals (Rijkers et al.1998). Later, it was shown that in mammals, the key protein for HR is not RAD52 but is BRCA2, with RAD52 playing an important role only in BRCA2-deficient cells (Liu and Heyer 2011).

Like Rad52 in *S. cerevisiae*, the human BRCA2 protein loads RAD51 on ssDNA and displaces RPA to stimulate strand exchange; it stabilizes RAD51-ssDNA complexes by inhibiting the ATPase activity of RAD51 (Yang et al. 2005; Liu et al.2010). MEILB2 (meiotic localizer of BRCA2) and BRME1 (BRCA2 and MEILB2-associating protein1) form a ternary complex with BRCA2 and during HR (Zhang et al. 2021). DSS1, the unique binding partner of BRCA2, controls the self-association, protein stability, and nuclear localization of BRCA2 and contributes to RPA removal (Le et al.2021). DSS1 and ssDNA locate on the opposite sides of BRCA2 crystal structures and contact different BRCA2 domains. In mammals, depletion of DSS1 dramatically decreases the formation of RAD51 focus and HR repair efficiency (Le et al. 2021). The BRCA2 has a helical domain, three oligonucleotide-binding folds that bind ssDNA and a three-helix bundle for dsDNA-binding, suggesting that BRCA2 targets RAD51 filament nucleation to the dsDNA junction at the resected end (Prakash et al. 2015). BRC repeats, consist of a set of eight 35-residue motifs, located in the central region of the protein and encoded by exon11 of the *BRCA2* genes. The BRC1-4 binds free RAD51 with high affinity, stimulating the formation of RAD51-ssDNA complexes, while BRC5-8 stabilize RAD51-ssDNA nucleoprotein filaments (Le et al. 2021). BRCA2 also bound RAD51 via a C-terminal motif unrelated to the BBC repeats and encoded within exon 27. BRCA2 binds to ~6 RAD51 molecules and promotes the replacement of RAD51 on ssDNA under the stimulation of DSSA (Liu et al. 2010). The CDK-cyclin A phosphorylates BRCA2 on serine 3291 during M-phase, enabling the interaction of the BRCA2 C-terminus with RAD51 (Heyer et al. 2010). BRCA2 have two models of RAD51-binding: the BRC repeats bind monomeric RAD51, disrupting RAD51 oligomers, whereas the TR2 region binds only an oligomeric form of RAD51 (Lord and Alan 2007). Furthermore, BRCA2 regulates the intracellular localization of RAD51 (Davies et al. 2001).

ScRad52 comprises three regions: 2 DNA-binding domains at the amino and carboxyl termini for ssDNA and dsDNA binding and the N-terminus domain that can bind to its paralogue Rad59. Both BRCA2 and ScRad52 promote Rad51 assembly on both ssDNA and dsDNA, with a preference for ssDNA. During HR, one DNA-binding domain of Rad52 catalyzes the exchange of RPA for Rad51; the

other catalyzes DNA annealing in the late stage, which BRCA2 does not involve (Mortensen et al.2019). In addition, Rad52 also regulates Rad51 filaments positively.

Rad52 is the most important protein for genome maintenance in yeast, and it is also necessary for efficient DNA synthesis in cells subject to replication stress (Bhowmick et al. 2016; Sotiriou et al. 2016). The mitotic DNA synthesis, termed MiDAS, depends on the pairing activity of RAD52 in human cells (Bhowmick et al. 2016). During HR, Rad52 mainly participates in two processes 1) removing RPA and recruiting Rad51 on ssDNA, 2) stabilizing Rad51 filaments and other proteins.

Rad52 in the competition between RPA and Rad51.

During HR, repair proteins accumulate at the damaging sites to form membrane-less subcompartments, dubbed repair foci. The replication protein A (RPA) first binds on ssDNA generated by Exo1 and/or Sgs1-Dna2 and is then displaced by Rad51 during the initiation of homologous recombination. RPA protects ssDNA from nucleolytic damage, prevents hairpin formation and blocks DNA reannealing until the processing pathway is completed (Fanning et al. 2006). RPA is a stable complex of three subunits (RPA70, RPA32 and RPA14) and six domains that adopt an oligonucleotide binding fold, a structure common to other known SSBs (Fanning et al. 2006). *In vitro* studies have shown that the efficiency of strand invasion decreases dramatically when ssDNA is incubated with Rad51 and RPA simultaneously, suggesting RPA competes with Rad51 for binding on single-stranded DNA (Sung et al. 1997). The molecular interaction between RPA and Rad51 supports the competition mechanism. RPA interacts with the N-terminal domain of Rad51through its DNA-binding domain A (RPA70A), which also binds to the ss-DNA, suggesting a competitive mechanism for the displacement of RPA from ssDNA by Rad51 where the RPA-Rad51 interaction displaces RPA from ssDNA (Stauffer et al. 2004).

Rad52 helps Rad51 to overcome this competition and loads it on ssDNA. Indeed, Rad51 filament formation occurs together with the displacement of RPA on ssDNA. The Rad51 nucleation rate is limited at the initiation stage of displacement, which is then accelerated by the Rad52-RPA-ssDNA co-complex as an intermediate (Sugiyama and Kowalczykowski 2002).

Single molecule microscopy *in vivo* reveals that Rad52 accumulating at break sites diffuses ~6 times faster within repair foci than the focus itself. On the contrary, Rfa1, a subunit of the RPA complex, has a diffusion that is similar to that of the focus or damaged chromatin. These results suggest that Rfa1 is bound to the ssDNA while Rad52 can move freely within the focus (Mine-Hattab et al. 2021).

Rad59, the paralog of Rad52, exhibits overlapping and distinct functions with Rad52. The *RAD59* gene was identified in a screen for mutants that reduce the rate of Rad51-independent recombination. It encodes a 238-amio-acid protein with significant homology to the N-terminal region of Rad52, the most highly conserved region among Rad52 family members. The C-terminal region of Rad52 is absent in Rad59, which is required for interacting with Rad51 (Davis et al. 2001). Both Rad52 and Rad59 mediate single-strand annealing, but only Rad52 can anneal an RPA-ssDNA complex and interact with Rad51. Unlike Rad52, which is found in most eukaryotes, Rad59 is only identified in fungal species, like *S. Cerevisiae* and *K. Lactis*. The deletion of *RAD59* has moderate effects, decreasing or delaying recombination between inverted sequences and delaying SSA (Sugawara et al. 2000, Wu et al. 2006).

Mus81-Mms4 / MUS81-EME1 cleaves branched molecules. During the classical HR pathway, DSBR and dHJ intermediate are formed and must be resolved to segregare the recombinant duplexes (Krogh et al. 2004). The Mus81-Mms4/Eme1 heterodimer can cleave various branched molecules, including simple Y-structures, duplex Y-structures, and X-forms, especially duplex Y-structures. Since Mus81 and Eme1 nuclease are important to resolve these recombination intermediates, the *MUS1* and *EME1* mutants in *S. pombe* can hardly produce viable spores. In these mutants, most of the time, the DNA is found only in one spore, suggesting that chromosome segregation is not occurring properly (Boddy et al. 2001). In contrast, in budding yeast, *MUS81* and *MMS4* mutants show a sporulation defect but only a two-fold decrease compared to wildtype (de Los Santos et al. 2003), suggesting the existence of alternative pathways for processing meiotic recombination intermediates (Heyer et al.2003, Hollingsworth and Brill 2004). Apart from Mus81-Mms4(EME1), the Sgs1-Top3-Rmi1 (BLM) are capable of resolving the dHJ to non-crossover products under the stimulation of RPA (Plank et al. 2006). The Mph1-Fml1 has a pre-recombination function during the S phase, specifically for promoting replication fork repair via HR (Sun et al. 2008). It also has been shown *in vitro* that Mph1-Fml1 (human FANCM) can dissociate D-loops and suppress the generation of crossover in ATP hydrolysis-dependent way (Daley et al. 2014).

In this paragraph, we have described the functions of some players of HR, excluding the Rad51 regulators that will be described in the next chapter.

4 Regulators of Rad51 filaments during HR

4.1 Difficulties during HR

The yeast nucleus, in its haploid state, contains ~13 Mb of DNA in a set of 16 chromosomes (Mine-Hattab and Taddei 2019). ChIP, PCR and Southern Blot on samples collected every 10 minutes after inducing DSB by HO endonuclease show that Rad51 is loaded on DNA ends within 30 minutes of DSB formation and takes around 60-90 minutes to find a donor that is 200 Kb away on the same chromosome (Hicks et al. 2010). Undoubtedly, finding the correct homologous donor sequence within the nucleus can be difficult and takes more time when the target is far away from the repair site. Additionally, homology search has a time constraint of 10-12 hours: indeed, the cell eventually adapts to the checkpoint and continues through the cell cycle even though the damage is still present (Toczyski et al. 1997; Paulovich et al. 1997; Pellicioli et al. 2001).

In the case of ectopic recombination, the time to identify the donor sequence can be further limited by the progressive loss of the homologous sequence due to exonuclease activity (Batté et al. 2017). Thus, the mechanism of homology search should ensure that the Rad51 nucleoprotein filament is able to find the donor sequence before the checkpoint adaptation if it is present within the nucleus, no matter how far it is from the break site. Widely considered to be error-free, several studies have shown that HR can be an error-prone pathway. It controls the equilibrium between genome stability and diversity but, on the flip side, jeopardizes the maintenance of genomic integrity (Guirouilh-Barbat et al. 2014).

Rad51 plays a major role during homologous recombination, but it can also be harmful to the cells. Several studies pointed out that Rad51 filaments can be lethal structures which should be dismantled by negative regulators (Fabre et al. 2002; Keyamura et al. 2016; Le Breton et al. 2008; Esta et al. 2013). When the nucleoprotein filament is deficient for strand invasion or no homologous sequence is available, it can result in toxic presynaptic Rad51 filaments and need to be removed from ssDNA. Some typical toxic Rad51 nucleoprotein filaments are shown in Figure 8. Let alone the involvement of many regulators during filament formation, homology search and strand invasion, HR is a sophisticated process, and many proteins regulate Rad51 filament. So, studying the positive and negative regulators on Rad51 during homologous recombination is worthwhile.

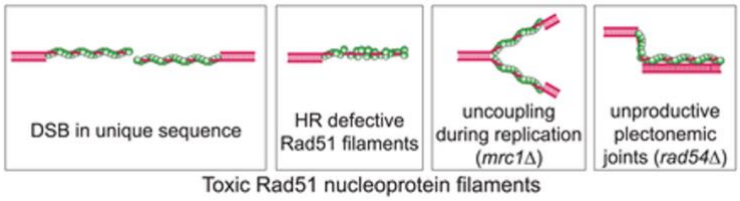

Figure 8 Schematic representation of the toxic Rad51 nucleoprotein filaments (Esta et al.2013)

4.2 ssDNA generated by Exo1 and Sgs1

As discussed above, ssDNA formation is a prerequisite for HR. DNA resection generates ssDNA that serves as a substrate for RPA and Rad51 during homologous recombination. There are two different kinds of resection: short-range DNA resection by MRX and long-range DNA resection by either Exo1 or Sgs1/Dna2 (Figure 9) (Cejka et al. 2015).

The MRX complex is one of the first to be recruited to DSBs. Once located at the DSB, MRX starts the short-range resection in a 3' to 5' direction back towards the DSB (Garcia et al. 2011). The MRX complex initiates resection and stimulates long-range resection by recruiting Sgs1 to the DSBs (Cejka et al. 2020). The ssDNA generated by MRX is the substrate for long-range resection machinery and stimulates Sgs1-Dna2 recruitment and activity by RPA binding. In addition, MRX physically interacts with Sgs1 (Myler et al. 2017). However, the short-range resection can be bypassed if the break ends are chemically "clean" like those generated by HO endonuclease (Figure 9A). In the absence of *RAD50* or *MRE11,* the long-range resection by Dna2/Sgs1 or Exo1 occurs at the same rate with only an initial delay. In some cases, the short-end processing starts at a position that is distant from the broken ends, up to 100-300 nucleotides away (Garcia et al. 2011).

There are two pathways for extended range resection modulated by either exonuclease Exo1 or endonuclease Dna2 working along with Sgs1. The Sgs1/Dna2 resection is a very conserved mechanism across organisms. Besides DNA resection, Sgs1 is a vigorous DNA helicase (Gangloff et al.1994) that works together with Top3 and Rmi1 to dissolve dHJs into non-cross-over products. Dna2 is a bifunctional helicase-nuclease that can remove DNA flaps caused by strand displacement synthesis (Bae et al. 2001). In the Sgs1-Dna2 resection pathway, the Sgs1 helicase unwinds dsDNA with a 3'-5' polarity providing a substrate for the ssDNA-specific Dna2 nuclease. Dna2 can resect DNA both in 3'-5' and 5'-3' directions but must load on ssDNA (Kao et al. 2004; Bae and Seo 2000). Exo1, on the other hand, does not require a helicase partner to unwind DNA; it degrades dsDNA from 5' to 3' and generates 3'-tailed ssDNA directly (Tran et al. 2002). Exo1 also plays an important function in post-replicative mismatch repair (Tran et al. 2007). The MRX complex, further enhanced by Sae1, can stimulate Exo1 resection. The 9-1-1 clamp and proliferating cell nuclear antigen (PCNA) promotes EXO1 in human cells (Tsai et al. 2014; Chen et al. 2013). These two pathways share a similar resection rate. In *exo1⊿* or *sgs1⊿* mutants, the resection rate is around 1kb/h, compared to ~4 kb/h in the WT strains. In the double deletion mutant (*exo1⊿ sgs1⊿*), only 30% and 10 % of cells generated ssDNA of more than 100 and 200 nucleotides (Zhu et al. 2008).

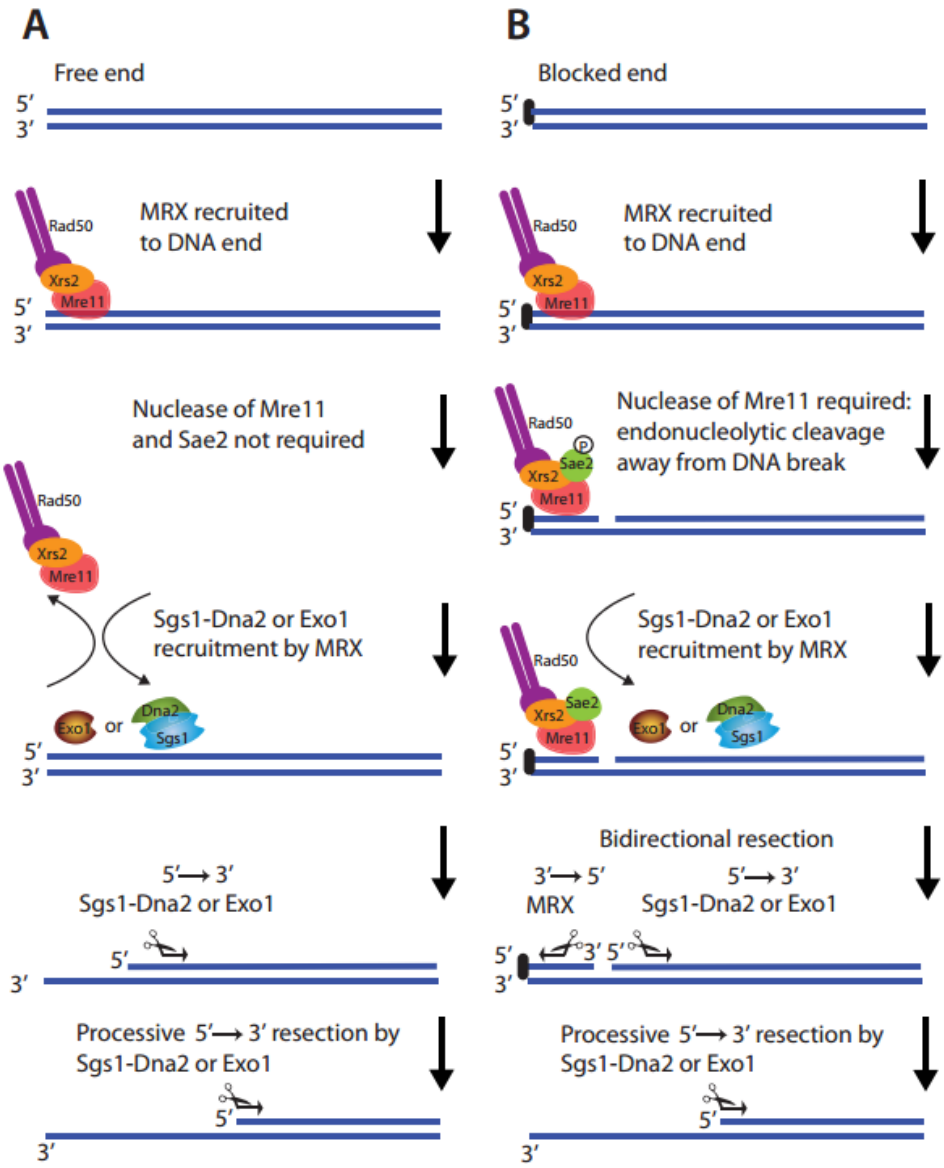

Figure 9 DNA end resection of free and blocked DNA ends.

A, resection of free (clean) DNA endsThe MRX complex is rapidly recruited to DNA ends upon break formation. The nuclease activity of Mre11 is not required for resection, but the MRX complex has a role to recruit components of the processive pathways that include either Sgs1-Dna2 or Exo1. In some cases, the structural role of the MRX complex can be bypassed. DNA is subsequently resected by either Sgs1-Dna2 or Exo1 in a processive manner. Only a monomer of MRX is depicted for clarity reasons. B, resection of blocked (dirty) DNA ends. The MRX complex is rapidly recruited to DNA ends, which is followed by Sae2. The nuclease activity of Mre11 is required, and it cleaves endonucleolytically the 5-terminated DNA strand away from the end in a reaction stimulated by phosphorylated (P) Sae2. Furthermore, MRX also likely recruits Sgs1-Dna2 or Exo1 to the endonuclease cut site. The endonuclease cut site provides an entry point for the Sgs1-Dna2 or Exo1 nucleases, which carry out long-range resection. The exonuclease of Mre11 then might degrade DNA in a 33 5direction back toward the DNA break (Cejka et al. 2015).

4.3 Srs2 helicase dismantles improper Rad51 filaments

The Srs2 helicase is a negative regulator of recombination and can reverse intermediate recombination structures of the Rad51 nucleoprotein filament (Veaute et al. 2003). Srs2 inhibits expansions, unwinds hairpins, and prevents triplet-repeat-induced chromosome fragility in yeast. Human RTEL1 serves as a human analogue to inhibit expansions and fragility (Frizzell et al. 2014). Sharing many similarities to Srs2, PARI presents a potential structural and functional mammalian homologue to Srs2 (Karpenshif and Kara 2012). The Srs2 shares homologies with the bacterial UvrD, Rep3, and PcrA helicases; it belongs to the SF-1 superfamily and translocates on ssDNA. Srs2 contains an additional C-terminal region with many interactions and regulatory domains responsible for other specialized functions (Marini and Krejci 2010). The ATPase activity of Srs2 is highly stimulated by the ssDNA, whereas the dsDNA has no effect. The Srs2 helicase unwinds 3' but not 5' end-tailed duplex DNA, indicating a preferential 3' to 5' polarity (Veaute et al. 2003).

The counteracting effects of Srs2 helicase during HR are suppressed by preventing the formation of Rad51 filaments (Fabre et al.2002). Srs2 can decrease the level of D-loop formation, and the inhibition effects of Srs2 become much more pronounced when RPA is present *in vitro* (Krejci et al. 2003). Stimulated by Rad51 bound to dsDNA, Srs2 can also unwind *in vitro* structures that resemble D-loops recombination intermediates (Dupaigne et al. 2008). Srs2 displaces Rad51 *in vitro* upon translocation on ssDNA (Dupaigne et al. 2008). Rad51 self-assembles into an extended polymer on ssDNA in the presence of ATP. During the disassembly of Rad51 NPFs by Srs2, a physical interaction between Rad51 and the C-terminal region of Srs2 triggers ATP hydrolysis within the Rad51 filament, causing Rad51 to dissociate from DNA (Antony et al. 2009). Electron microscopy work shows that the action of Srs2 on the nucleoprotein filament (Figure 10A) favours RPA over Rad51, inducing the loss of Rad51 presynaptic filament and the formation of RPA-ssDNA complexes (Krejci et al. 2003). Besides, Srs2 was shown to inhibit dsDNA invasion by a Rad51-ssDNA filament *in vitro* (Veaute et al. 2003).

To study the molecular mechanism of the anti-recombinase activity of Srs2, single-molecule Förster resonance energy transfer (FRET) was used. After the first clearance of Rad51 from ssDNA, the Srs2 monomer has a repetitive motion to prevent the re-formation of Rad51 filaments. Removing Rad51 from shorter fragments of ssDNA takes substantially less time than longer ones. When Rad51 polymerizes on dsDNA, the unwinding of dsDNA by Srs2 is inhibited (Qiu et al. 2013, Figure 10B).

In yeast, it is impossible to overexpress Srs2 protein significantly, suggesting that Srs2 might be toxic to the cells (Krejci et al. 2003). Fission yeast contains a sequence homolog of Srs2 that shares several

phenotypes with its budding yeast Srs2 homolog, including hypersensitivity to DNA damage agents, hyper-recombination, and several synthetic lethal interactions (Marini and Krejci 2010). Cells lacking Srs2 increase the incidence of mitotic crossovers. *In vitro* study supports a model where Srs2 actively prevents crossovers by unwinding the elongating invading strand from the donor strand and promoting SDSA (Dupaigne et al. 2008). On the other hand, in *srs2Δ* and in the *srs2* mutants defective in ATP binding and hydrolysis, HR is used to repair spontaneous DNA damage instead of alternative pathways of repair such as SSA-like repair (Marini and Krejci 2010). Besides, yeast cells show sensitivity to DNA damage and synthetic lethality with replication and recombination mutants in the *srs2Δ* strain. These negative genetic interactions are suppressed in the absence of Rad51, suggesting another role of Srs2: the elimination of lethal intermediates formed by recombination proteins. The *sgs1Δsrs2⊿* mutants accumulate toxic recombination intermediates that cannot be resolved without Srs2 and Sgs1 helicases (Marini and Krejci 2010). Srs2 is also involved in checkpoint activation, adaptation, and recovery (Ortiz et al. 2011). The interaction between Mrc1 and Srs2 is related to replication and the formation of inappropriate recombination intermediates (Xu et al. 2004).

Rad52 stabilizes Rad51 filaments against Srs2

In yeast, the Srs2 helicase is one of the major negative regulators of Rad51 nucleoprotein filaments. Rad52 can stabilize Rad51 nucleoprotein filaments and protect them from Srs2 activity. Thanks to random mutagenesis, various *RAD52* mutants were selected to study the relationship between Rad52 and Srs2. Mutations on the Rad52 N-terminal domain affect the Rad52 oligomeric ring structure and do not disrupt the Rad52-Rad51 interaction. These RAD52 mutants that can still load Rad51 with the same efficiency can suppress the Rad51 filament toxicity in Srs2-deficient cells. Hence, the Rad52 ring structure is important for working against Srs2 and, on the other hand, for increasing the Rad51 filament stability and toxicity in Srs2-deficient cells. (Godin et al. 2013 ; Ma et al. 2018 ; Ma et al. 2021).

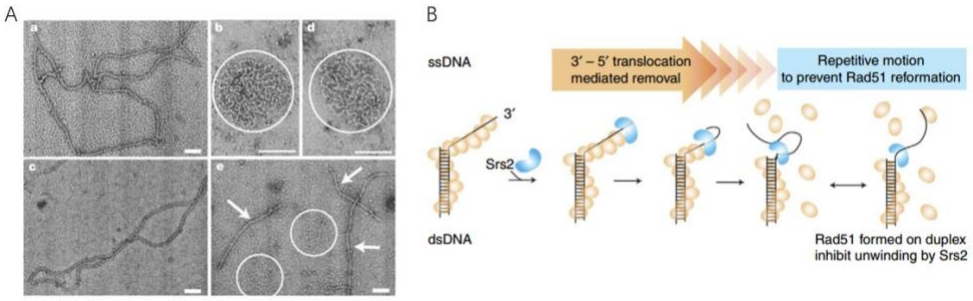

Figure 10 Rad51 filaments in EM and Scheme of Srs2 cleaving Rad51

A. EM analysis of Rad51 filament disruption by Srs2. a, b, Rad51 (a) and RPA (b) were each incubated with ssDNA; examples of the nucleoprotein complexes that formed are shown. c, RPA was not able to disrupt preformed Rad51 filaments; an example of the Rad51 filaments present is shown. d, Incubation of preformed Rad51 filaments with Srs2 and RPA caused the loss of filaments and concomitant formation of RPA–ssDNA complexes, an example of which is shown. e, when preformed Rad51–ssDNA filaments were incubated with Srs2, RPA and linear duplex, RPA–ssDNA complexes were formed (circled) and transfer of Rad51 onto the linear duplex was visualized (arrows). Scale bars, 100 nm (Veaute et al.2003) B. Schematic summary of Srs2 motion as an anti-recombinase mechanism for Rad51 clearance. Srs2 first translocates in the 30–50 direction along ssDNA to displace Rad51, and then remains bound near the duplex junction and displays repetitive motion on a short segment of ssDNA to prevent Rad51 re-formation. (Qiu et al.2013)

4.4 Rad51 paralogs during HR

Rad55 and Rad57, like the five paralogs in human (RAD51B, RAD51C, RAD51D, XRCC2, XRCC3), contribute to recombination without forming filaments. Deletion of one of them would cause recombination defects and sensitivity to DNA damage (Heyer et al. 2010).

How are these paralogs involved in recombination? One proposed mechanism is that the Rad55-Rad57 complex positively modulates Rad51 filaments by counteracting the effects of Srs2 helicase. *In vitro* and biochemical analyses showed that the heterodimer would associate with the Rad51 ssDNA filament, making it more stable. Besides, the Rad51-Rad55-Rad57 co-filament can block the Srs2 translocation to resist the Srs2-dependent disruption (Roy et al. 2021). The Rad51 presynaptic filament is a meta-stable reversible intermediate, while Rad55-Rad57 and Srs2 work against each other, respectively assembling and disassembling Rad51 on ssDNA (Liu et al. 2011) (Figure 11 A).

A recent single molecule study proposes a new mechanism of action for Rad55-57. When GFP-Rad55-Rad57 was injected into a sample chamber with assembled Rad51 filaments, little to no binding was observed. These results suggest that the binding between Rad51 and Rad55-Rad57 is transient, and the Rad55-Rad57 would dissociate very fast. With short-term binding, Rad55-Rad57 cannot block the Srs2 helicase. Instead, the Rad55-Rad57 would work against Srs2 by rapidly re-assembling Rad51 filaments after their disruption by Srs2 (Roy et al. 2021, Figure 11B). A different study showed that Rad55-Rad57 promotes HR at stalled replication forks and could control the recruitment of TLS polymerases. Besides, it is essential to promote of UV-induced HR independently of Srs2. (Maloisel et al. 2022).

Besides filament stabilization, Rad55-Rad57 heterodimer also functions against RPA to promote DNA strand exchange. Indeed, far fewer strand-exchange products are generated when the RPA complex is present during the nucleation phase, which the Rad55-Rad57 heterodimer can overcome (Sung et al. 1997).

The SHU complex, consisting of Shu1, Shu2, Csm2 and Psy3, also contributes to homologous recombination. Among these proteins, Csm2 and Psy3 are Rad51 paralogues, and Csm2 interacts with Rad51 and Rad55-Rad57 heterodimers. Interestingly, Csm2 requires Rad55 to interact with Rad51, while Rad51 is not necessary for the interaction between Rad55 and Csm2 (Godin et al. 2013). The SHU complex promotes Rad51 filaments and error-free repair through the Rad55-Rad57 complex in yeast (Sasanuma et al. 2013). In addition, Shu1 reduces Srs2 recruitment to both induced and spontaneous foci, where Srs2 recruitment anticorrelates with Rad51 foci intensity. It was thus

proposed that the SHU complex shifts the balance of repair toward Rad51 filament stabilization by inhibiting the disassembly reaction of Srs2 (Bernstein et al. 2011).

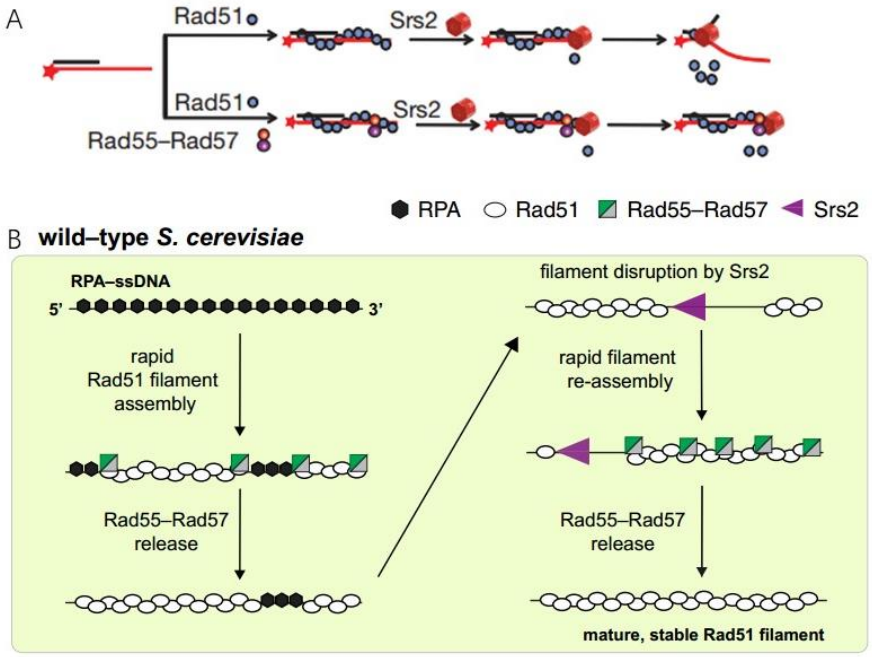

Figure 11 Rad55-Rad57 regulates Rad51 filaments

A. Helicase assay of Rad51 (28 nM) with or without Rad55–Rad57 (25 nM) were incubated with 1.5 nM 39-tailed substrate before addition of 120 nM Srs2 protein. (Liu et al. 2011) B, Rad55-Rad57 binds on Rad51 shortly, and promote fast Rad51 assembly after the disruption by Srs2 (Roy et al.2021),

4.5 Rad54 dismantles Rad51 filaments on dsDNA and promotes strand invasion

Rad54 protein belongs to the Snf2/Swi2 family, with a domain to bind and hydrolyze ATP on dsDNA but cannot separate DNA strands like other helicases (Vignali et al. 2000). With 48% identity and 68% similarity between scRad54 and hRAD54 (Petykhova et al. 1999), Rad54 is very conserved and required for homologous recombination and gene conversion in yeast and human cells. In yeast, the Rad51 filaments assembled in *srs2rad54* double mutants lead to recombination-dependent toxic intermediates that cause lethality. The hRAD54 cDNA partially suppressed the MMS-sensitivity of *rad54⊿* yeast cells. The ScRad54 is essential for forming the ScRad51 D-loop, while the hRad51 can form the D-loops in the absence of hRAD54. The hRAD54 only stimulates the D-loop formation and is implicated in the process of replication fork regression (Ceballos and Heyer et al. 2011). Like Rad51, Rad54 is also a significant player of HR, contributing to several stages of the process along with the Rad51 nucleoprotein filament (Figure 12) (Heyer et al. 2006).

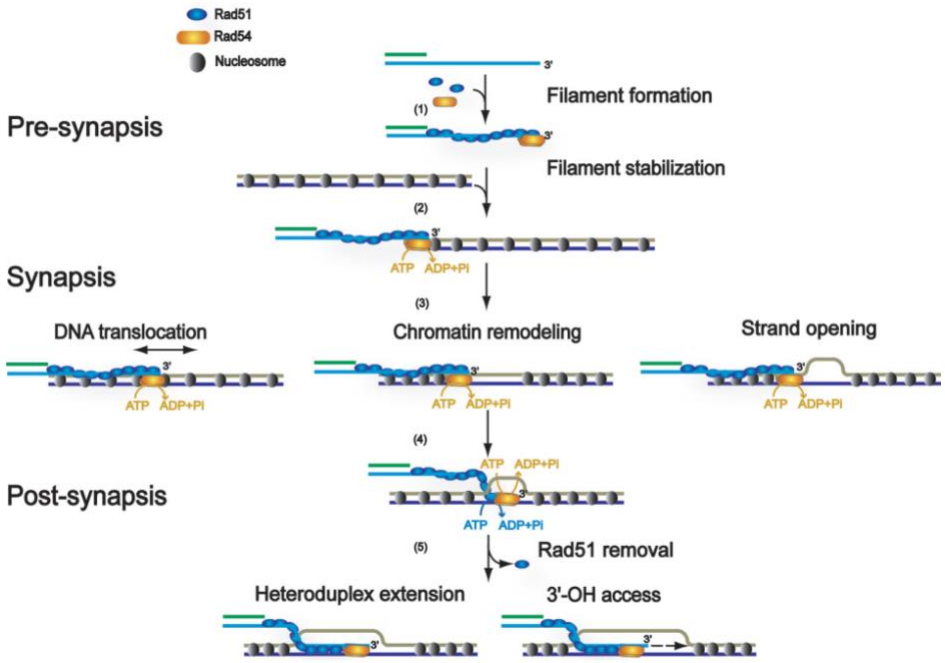

Figure 12 Mechanistic models for Rad54 function in HR.

The mechanistic models were derived from analysis of reconstituted *in vitro* recombination reactions and biochemical analysis of the Rad54 protein. For more details see text. Shown is one processed DSB end with a 30-ending ssDNA tail that invades a nucleosome duplex target DNA. Pre-synapsis: Rad54 was found to mediate formation or to stabilize Rad51 filaments on ssDNA. The pre-synaptic function does not require Rad54 ATPase activity and requires Rad51 binding to ATP but not hydrolysis. Synapsis: Rad54 augments the ability of Rad51-ssDNA filaments to form joint molecules, possibly involving translocating the Rad51-ssDNA filament along duplex DNA or inducing strand separation through induction of topological change. Rad54 also exhibits chromatin remodeling activity that may clear nucleosomes or other proteins from the pairing site. The synaptic function requires the Rad54 ATPase activity but not the Rad51 ATPase activity. Post-synapsis:

Rad54 was identified to catalyze heteroduplex extension (branch migration) and can dissociate the Rad51–dsDNA product complex, possibly to allow DNA polymerase access to the invading 30-OH end to prime DNA synthesis. Post-synapsis requires the ATPase activities of both the Rad54 and Rad51 proteins (Heyer et al.2006).

First, Rad54 can stabilize the nucleoprotein filaments during pre-synapsis by forming a co-complex with DNA-bound Rad51 (Mazin et al. 2003; Solinger et al. 2002). Second, Rad54 can promote nucleation of Rad51 similar to Rad52 and Rad55-Rad57 (Sung et al.2003), independently of its ATPase activity (Wolner et al. 2005). It can also increase the filament's resistance to cleavage by endonucleases (Wolner et al. 2003). Once a mature Rad51 filament is formed, Rad54 catalyzes homologous pairing and strand invasion with Rad51 filaments. The Rad54 would form a complex with the Rad51 filaments (Mazin et al. 2000; Solinger et al. 2001), and the potential target DNA sequence would be translocated by Rad54 and linked to the Rad51 filament. This process requires ATPase activity of Rad54 and would increase the efficiency of dsDNA delivery to the repair site within the filament (Mazin et al. 2000). From *in vitro* observations, it seems that Rad54 is not only crucial for Rad51-mediated synaptic complex formation and homology search, but its ATPase activity can also prevent the formation of non-productive Rad51 intermediates (Tavares et al. 2019). Stimulated by the Rad51-ssDNA nucleoprotein filament, Rad54 possesses chromatin remodelling by sliding nucleosomes along DNA. Rad54 can catalyze bidirectional nucleosome redistribution from the homologous DNA target site before the DNA pairing and DNA strand exchange (Alexeev et al. 2003).
Rad54 can regulate Rad51 filaments not only positively but also negatively. Rad51 is unable to release dsDNA. In a topological assay for the dissociation of Rad51 from dsDNA, Rad54 was shown to disrupt the Rad51-dsDNA filament in an ATP-dependent manner (Solinger et al. 2002).
It is worth mentioning that Rdh54, a Rad54 homologue in yeast, is also involved in maintaining genome integrity. Unlike Rad54, which functions primarily on homology search and strand invasion during HR, Rdh54 has a role in cell cycle recovery and pathway branch points at HR intermediates (Crickard et al. 2021). A recent study shows that Rdh54 and Rad54 act synergistically to function as key regulators of Srs2 and prevent the Srs2-mediated disruption of Rad51 presynaptic filaments (Meir et al. 2022). hRAD54B represents the only hRAD54 paralog clearly involved in the core mechanism of HR; it colocalizes with hRad51 and hRad54 in the nucleus. Likewise, the yeast rad54 rdh54 double mutant is completely deficient in meiosis, whereas the *RAD54 RAD54B* mutant mouse is fertile.

Though the ATPase activity is surprisingly low, hRAD54B is highly similar to hRAD54 (Ceballos and Heyer et al. 2011).

5 HR within the nucleus

5.1 Localization of HR proteins upon DSB

HR is a dedicated process involving plenty of repair proteins at different stages, which accumulate at damaged sites, forming membrane-less sub-compartments or foci upon DSB. By fusing repair proteins with fluorescent tags, we can observe their localization during HR. According to Lisby et al., repair foci progress through four distinct stages: first, DNA damage recognition and binding of DNA ends by the MRE11 complex; second, end-processing and binding of single-stranded DNA by replication protein A (RPA), which recruits checkpoint proteins; third, recombinational repair during S and G2 phase (Rad51 and Rad52 included) and fourth, disassembly of foci and resumption of the cell cycle (Lisby et al. 2004). Accordingly, Mre11, RPA and Rad52 are commonly used as markers for the different stages of HR, while the observation of Rad51 foci is limited because there is no functional tagged Rad51.

The Mre11 nuclease is the first protein detected at the DSBs; then Rfa1, the subunit of RPA, relocalizes at the break and recruits other key checkpoint proteins. The repair proteins for HR can only assemble in S or G2 phase (Lisby et al. 2004). With a Rad52-GFP strain that is functional in DNA repair and recombination, it has been discovered that Rad52-GFP proteins relocalize from a diffuse nuclear distribution to distinct foci, exclusively in the S phase (Lisby et al.2001). They also confirmed that Rad52 foci colocalize with the damaged site using a *lacO* array placed in close proximity to the DSB. The relocalization of Rad52 is a rapid and reversible process, whereby Rad52 foci are centres of DNA repair that can associate with more than one DSB (Lisby et al. 2003) (Figure 13A, B).

In recent years, cell compartmentalization has undergone a paradigm shift. It became clear that proteins concentrate in specific locations without the need for a lipid barrier. Recent evidence recently showed that repair foci likely arise from liquid-liquid phase separation. Two Independent studies showed that in Sc. yeast, Rad52 foci exhibit several hallmarks of liquid-liquid phase separation (Oshidari et al. 2021; Mine-hattab et al. 2021). Using a single molecule tracking approach to observe individual Rad52 molecules, Miné-Hattab et al., showed that Rad52 accumulates at DSB sites and diffuses ~six times faster within repair foci than the focus itself, exhibiting confined motion in yeast. Foci resulting from 2 DSBs are twice larger in volume than the ones induced by a unique DSB, and the Rad52 confinement radius scales accordingly (Figure 13C). On the other hand, Rfa1 diffuses similarly to the focus itself. Therefore, they conclude that unlike Rfa1 molecules, which are bound to ssDNA,

Rad52 molecules are free to explore the entire focus reflecting the existence of a liquid droplet around damaged DNA (Mine-Hattab et al. 2019).

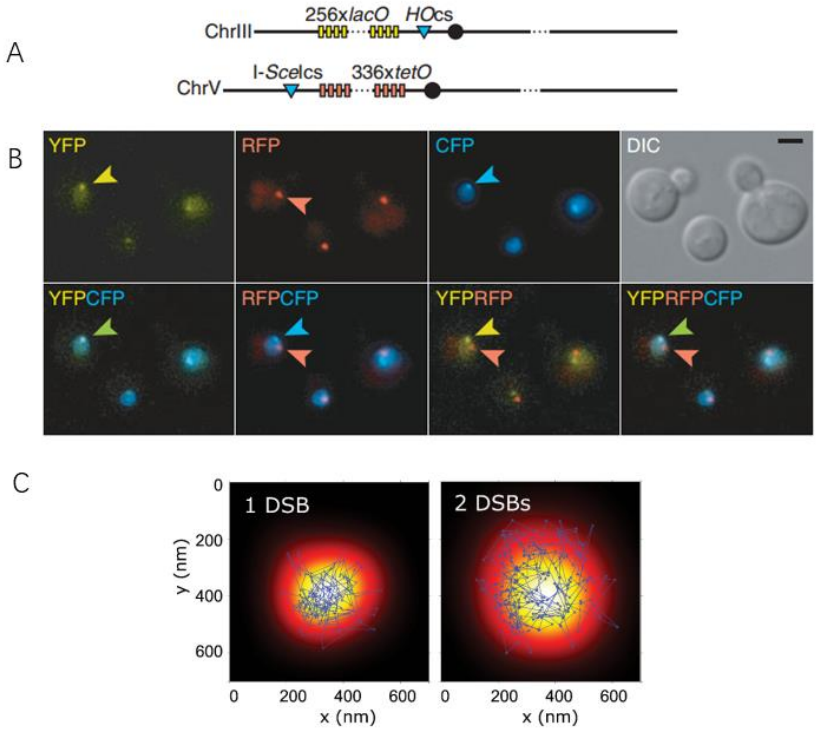

Figure 13 Localization of Repair proteins

A. Constructs for visualizing HO- and I-SceI-inducible DSBs. Yellow boxes: lacO sites. Red boxes: tetO sites. Cyan arrowheads: HOcs and I-SceIcs as indicated. Solid circles: centromeres. B. Relocalization of Rad52–CFP to a YFP-marked HO cut-site. W4292-14D was transformed with plasmid pJH132 harbouring a galactose-inducible HO gene. The panels show YFP, CFP, RFP, and combinations of merged images as well as DIC images of representative cells after HO induction. C. Typical example of a Rad52 trajectory represented in blue. The whole focus is shown in the background using a Gaussian blur of each Rad52 detections contained in this focus. Left: 1 DSB-induced focus; right: 2 DSBs-induced focus.

5.2 Chromatin dynamics upon DSB

The spatial organization of the chromosomes and chromatin mobility are central in the regulation of a wide range of cellular processes, such as gene expression, DNA replication and genome maintenance (Misteli 2007). In yeast and some mammalian cell lines, DNA mobility is dramatically altered upon DSB (Mine -Hattab and Rothstein 2013; Garcia-Fernandez et al. 2022). These changes are a double-edged sword, which promotes homology pairing in diploid yeast but also leads to mutagenic DNA repair and chromosomal translocations (Hansen et al. 2018, Mine-Hattab and Darzacq 2020).

Methodology to study DNA mobility in living cells:

Several diffusion models have been put forward to describe the movement of molecules in cells, which we will discuss before introducing the Coaggregate diffusion search model. To characterize the mobility of molecules, a common approach is to use a mathematical function called “mean square displacement” (MSD): it = represents the amount of space a particle has explored as a function of different time intervals, and its shape reveals the nature of the motion. When there is no external force and a particle moves freely, the MSD curve is linear with time. This type of movement is called “Brownian diffusion” (Figure 14). When molecules move slower than Brownian diffusion, it is called “sub-diffusive”. There are two major sub-diffusive models: confined sub-diffusion, where movement is limited in a sub-volume and anomalous sub-diffusion, where movement is restricted with scaling properties in time and space (Barkai et al. 2012; Metzler et al. 2014). The MSD curves for these two models are also presented in Figure 13. In the anomalous model, although the sub-diffusive loci are constrained, molecules can still diffuse without boundary and thus reach further targets with enough time.

For sub-diffusive motion, the MSD exhibits a power law (MSD $\sim At^{\alpha}$), where α, the anomalous exponent, is smaller than one. When α is small, the locus explores recurrently the same environment for a long time, while a large α indicates that the locus is able to frequently explore new environments. The anomalous diffusion coefficient A represents the amplitude of DNA motion. Previous DNA mobility studies reported the confined diffusion of chromatin (Marshall et al. 1997; Heun et al. 2001; Taddei et al. 2006; Maeshima et al. 2010; Masui et al. 2011; Miné-Hattab et al. 2012, Backlund et al. 2015), while others have reported anomalous diffusion (Maeshima et al. 2010; Weber et al. 2010; Burnecki et al. 2012; Hajjoul et al. 2013; Lucas et al. 2014; Backlund et al. 2015, Miné-Hattab et al. 2017).

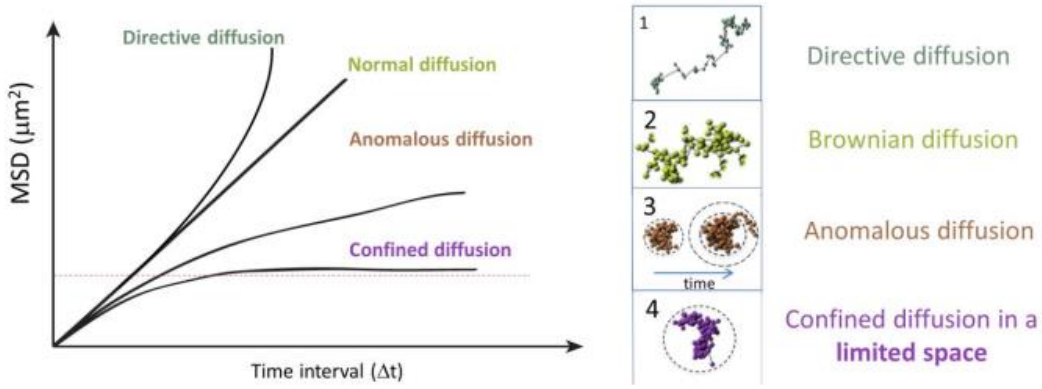

Figure 14 Models of molecular diffusion.

Left, theoretical Mean Square Displacement (MSD) curves for directive, Brownian, anomalous, confined and diffusion. Right: corresponding typical trajectories for each mode of diffusion (Klein et al, 2019).

Evidence of increased mobility in response to DSB

During the last decade, several studies suggested that chromatin mobility is strongly modified in response to DSB in living Sc. yeast (Fernandez et al. 2022). Locally, chromatin shows a faster motion after a transient mobility reduction in response to an HO-induced DSB (Saad et al.2014). Chromatin mobility is dramatically increased at the damaged site in diploid yeast in the presence of donor sequence, allowing the damaged locus to explore the nuclear volume 10 times larger (Miné-Hattab and Rothstein 2012). Haploid yeast cells also exhibit such increased mobility in response to DSBs, even if no homologous template is present in the nucleus (Dion et al. 2012). The two broken ends probably stay in contact to explore the nuclear space together during HR (Lisby and Rothstein 2004). Importantly, chromatin mobility is increased in the case of zeocin-induced DSBs associated with Rad52 foci. In contrast, in spontaneous DSBs, chromatin mobility is decreased (Dion et al. 2012), which might owe to the number of DSBs within the nucleus. Interestingly, in the case of one-end DSBs induced by protein-DNA adduct and camptothecin (CPT) at replication forks, a Rad52 focus is formed, but no change in chromatin mobility is observed (Dion et al.2012). Different types of damage have very different consequences on DNA mobility (Dion et al.2013; Mine-Hattab and Darzacq 2020). Surprisingly, several studies show that changes in chromatin mobility are not an intrinsic property of the damaged locus (Miné-Hattab et al 2012; Miné-Hattab et al. 2017; D'Angelo et al. 2022). During the early stage of HR, a strong inhibition of chromatin mobility has been reported in yeast (Mine-Hattab and Darzacq 2020). Indeed, the broken chromosome is not the only locus to be affected; other chromosomes also display increased mobility in haploid and diploid strains. This change in chromatin dynamics is named “global increased mobility” and suggests that changes in chromatin dynamics are

a general feature of the cellular response to DSBs. The global mobility increase is dose-dependent since the chromosomes explore almost the entire yeast nucleus upon inductions of approximately 20 DSBs (Miné-Hattab and Rothstein 2012). More induced DSBs cause a higher increase in global mobility. Finally, it is important to note that the diffusion coefficient chromatin (at the damaged site or genome-wide) is not significantly altered after DSB induction (Miné-Hattab et al. 2012). Thus, increased DNA mobility enlarges the space sequences can explore without increasing the speed at which they move.

Several studies investigate the origin of increased chromatin mobility upon DSB. It has been shown that both local and global increased mobility are dependent on Rad51 in diploid (Miné-Hattab et al. 2012; Miné-Hattab et al. 2017) and Mec1 and Rad9 dependent in haploid (Dion et al. 2012). Possible mechanisms to explain the origin of chromatin mobility upon DNA damage are shown in Figure 14 (Zimmer and Fabre 2018).In undamaged conditions, chromosomes are tethered to SPB; upon DSB, changes in chromatin mobility could be due to a change in the flexibility/topology of chromatin throughout the genome at both damaged and undamaged, for example, chromatin stiffening, while in an alternative model, it would be due to a change in tethering changes enhancing the chromatin dynamics.

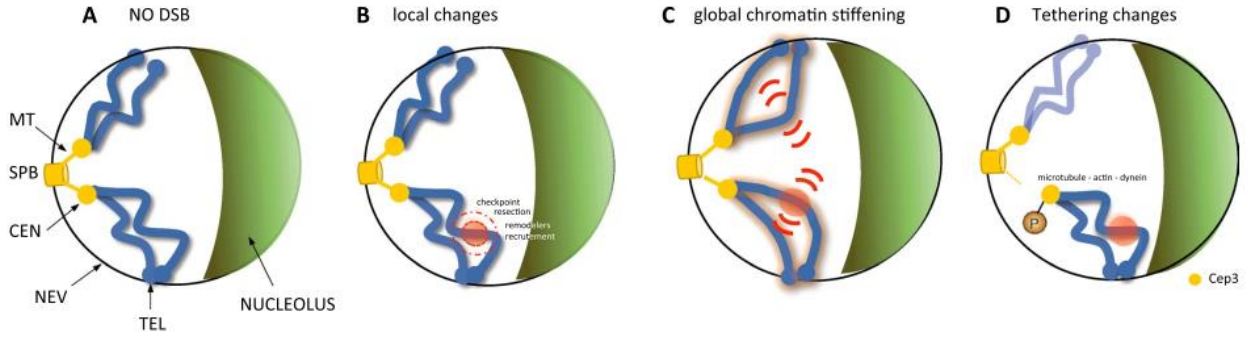

Figure 15 Possible mechanisms for chromatin mobility upon DNA damage.

Two chromosomes in a Rabl configuration of a haploid yeast cell are shown (a). In undamaged conditions, chromosomes are tethered to the spindle pole body (SPB) by their centromere (CEN) via a nuclear microtubule (MT) and to the nuclear envelope (NEV) by their telomere (TEL). b Possible scenarios of enhanced chromatin dynamics following DNA damage at the site of DNA damage is shown. Proposed mechanism for global mobility includes c stiffening (or alternatively, decondensation) of the chromatin fiber and d relaxation of the link between centromere and SPB through microtubule, loss of telomeres tethering and impaired function of nuclear actin (Zimmer and Fabre 2018)

In mammalian cells, there is no clear consensus on the effect of DSB on chromatin mobility. In HeLa cells, after a-particle-induced DSBs, gH2AX foci are more mobile, supporting the notion that distant DSBs can be juxtaposed (Aten et al. 2004; Krawczyk et al. 2012). Similarly, ICM is associated with uncapped telomeres in mouse cells, and this movement is dependent on the 53BP1 repair protein

(Dimitrova et al. 2008). Finally, the movement of heterochromatic DSBs toward euchromatin was observed in mouse embryo fibroblasts (MEFs), HeLa cells (Jacob et al. 2011), and Drosophila cells (Chiolo et al. 2011). By contrast, in other studies using MEFs (Kruhalk et al. 2006), HeLa, or U2OS cells (Jacob et al. 2009), DSBs generated by UV laser or γ-irradiation did not significantly alter chromosome mobility. Only energy-dependent local expansion of chromatin was observed around the initial damaged zone immediately after DNA damage. Similarly, in G1-phase NIH3T3, no mobility increase was observed in the presence of an *I-SceI*-induced DSB (Soutoglou et al. 2007). These observations in mammalian cells may result from different repair pathways, variations between cell lines, the regions of chromatin damaged, or the type of damage induced.

5.3 Homology search in the nuclear space

The principal steps in recombination and the key components of its machinery are well known, but homology search, the step to explore the genome for a homologous sequence, remains enigmatic. Once formed, the Rad51-ssDNA complex keeps exploring the nucleus and contacts nearby dsDNA molecules until it finds the homologues sequence, or the checkpoint adaptation starts. HR can occur between sister chromatids, homologous chromosomes in diploid cells, or ectopic homologous sequences. Since the genome size is relatively large compared with the donor sequence, the nucleofilament is extremely efficient for homology search. In yeast, a single recipient locus and a single donor locus that share only 1.2 kb of homology can find each other in 12Mb of the condensed genome and engage in repair with 20% efficiency within 4 hours after DSB formation (Aylon et al. 2003; Inbar et al. 2000). Nuclear organization affects the repair efficiency, which is limited by spatial proximity, double-strand break resection and chromatin status (Agmon et al. 2013; Batté et al. 2017). Here are some popular searching models through *in vitro* and *in vivo* studies.

The Null model is an oversimplified search model in many respects (Barzel and Kupiec 2008). It assumes that during ectopic recombination, both chromatids are cut by an endonuclease, so there are two DSBs defining two sister recipients searching for two sister ectopic donor sequences. As each DSB divides the chromatid in two, there are indeed four independent homology searches. This model contrasts with the results from Lisby and Rothstein in that the chromatids and the two ends of a DSB stay attached during the search (Lisby and Rothstein 2004). In this model, each base will be tested independently. Considering that the homology search takes around 1-2h and there is 3×10^7 base pairs in a G2 haploid yeast cell, each trial should be 2.5×10^{-4} seconds to ensure all base pairs are aligned. Even though there are four independent homology searches, one trial must be finished within 10^{-3} seconds.

Three base-pair seed model. To overcome the difference in pitch between the dsDNA and the nucleofilament, which is stretched from the canonical *B* state to *S* state, Dorfman thinks that the time costs of homology search are dependent on the intracellular fluid viscosity and ionic strength. Moreover, the initial homologous recognition involves a three base-pair seed (Dorfman et al. 2004). In this model, 1 kb of dsDNA strand recognizes one RecA-ssDNA in around 500s, which agrees with the experimental data from Dutreix (Dutreix et al. 2003). The lifetime of synapsis is around 10 seconds (Sagi and Stavas 2006), so a RecA filament could form 50 synapses before finding a homology sequence.

These two first models are not considering the time spent to make the DSB in proximity to the donor sequence.

Coaggregate diffusion search model. The biochemical analysis led to a proposal that strand exchange proceeds through an intermediate "coaggregate" and that homology search involves facilitated diffusion within these coaggregates (Tsang et al.1985; Gonda et al. 1985). Some studies on RecA reveal that ATP hydrolysis is not required for strand invasion, suggesting it might be driven by thermal energy (Menetski and Kowalczykowski 1990). It was proposed that this acts primarily by concentrating the DNA into a small volume. This, along with the multiple bindings of duplex DNA and presynaptic filaments, could greatly accelerate the rate at which duplex DNA sequences are sampled by the presynaptic filaments during the search for homology. The homologous substrates that interact with RecA can be as short as 8 bp so that the homologous sequences might be a length-based recognition. Since there is no preferential recognition of the outermost targets, long-distance one-dimensional sliding does not contribute to the search (Adzuma 1998). This mechanism is quite plausible, but there is no definite proof available to support this mechanism so far. In addition, it is also against the dynamics of the RecA bundle and repair foci that Wiktor observed in a recent paper (Wiktor et al. 2021).

Increased chromosome mobility.

Many studies have shown that DNA mobility is greatly increased in *Saccharomyces cerevisiae* and some mammalian cell lines after the occurence of DSB (Dimitrova et al. 2008; Chiolo et al. 2011; Jakob et al. 2011; Dion et al. 2012; Miné-Hattab and Rothstein 2012; Neumann et al. 2012; Roukos et al. 2013; Lawrimore et al. 2017). The former models only take the mobility of broken DNA ends but no other DNA into consideration and are only applicable when the donor is close to the broken site.

To investigate the mechanism of homology search *in vivo*, Mine-hattab et al. tagged two homologous loci in diploid yeast cells. They investigated their dynamic in the absence and presence of DNA damage. First, they observed that when neither locus is damaged, homologous loci occupy largely separate regions, exploring only 2.7% of the nuclear volume in 15min. In contrast, following the induction of a single DSB, homologous loci colocalize ten times more often. The mobility of the cut chromosome markedly increases, allowing it to explore a nuclear volume that is more than ten times larger. Of note, increased nuclear exploration does not correlate with a higher speed of locus

movement. In fact, the diffusion coefficient does not significantly change in response to damage, both at damaged and undamaged loci (Miné-Hattab et al. 2012; Miné-Hattab et al. 2013). In other words, changes in mobility allow chromatin to go further but not faster. Interestingly, the mobility of uncut chromosomes also increases, allowing them to explore a four times bigger volume of nucleus, also inducing a general increase in dynamics, and multiple DSBs produce even more DNA movement. Both local and global increased mobility are Rad51-dependent in diploid cells. Mine-hattab et al., proposed that increased mobility in response to DSB facilitates homologous pairing by increasing the efficiency of homology search. More recently, it has been shown that changing the timing of chromosome mobility results in a corresponding change in essential downstream HR events, reinforcing its mechanistic role in the DNA repair process (Joseph et al. 2022). However, in this paper, it is not clear whether it is resection or mobility that matters, as both are affected at the same time.

Accelerated random search model. With the advances in single-molecule studies *in vitro*, a mechanistic model, namely the accelerated random search model (Figure 16), was proposed. Besides homology search in the genome, this model takes homology recognition into account through DNA pairing between the broken end and the template at the site of homology. The presynaptic nucleoprotein filament is formed and probes inside the DNA of the broken chromosome (Forget and Kowalczykowski 2012). If no homologous DNA is detected, the filaments would immediately probe other chromosome segments that are close to the broken site. The efficiency of probing decreases with distance in three dimensions (San Filippo et al. 2008). Additionally, chromatin movement increases to enable the filament to find more distant sequences (Mine-Hattab and Rothstein 2012). Besides search by diffusion, the presynaptic nucleofilaments can also slide along DNA to test several segments at the same time (Regunathan et al. 2012). The sliding can accelerate the process of searching since it smoothens the process and avoids recurring dissociation and association within a short range. However, the factors that facilitate the extent of sliding are still unclear (Greene 2016). After the homologous sequence is recognized, chromatin opens for probing and exchange. This mechanism presents a higher efficiency in organisms with small genomes or where homologous DNA locates in spatial proximity (San Filippo et al. 2008; Branzel et al. 2010). For example, since the nuclear volume of mammalian cells is around 1000-fold larger than yeast, but the chromatin mobility is comparable (Misteli and Soutoglou 2009), the homology search would be restricted to small volumes but unable to explore faraway regions. (Renkawitz et al. 2014). In addition to this mechanism, the filaments can reduce the search complexity by ignoring tracts with less than eight nucleotides.

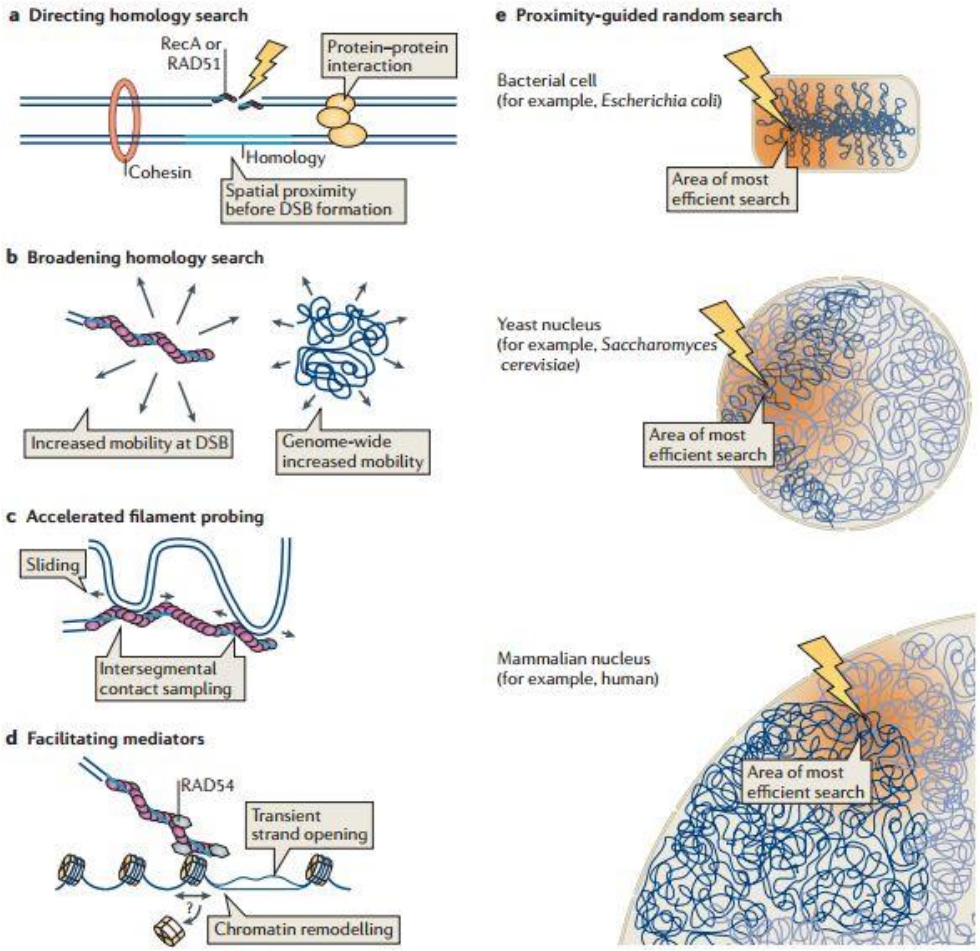

Figure 16 Accelerated Random homology search model.

Homology search is principally based on random probing events within an area of spatial proximity. However, dependent on the context in which it occurs, homology search is also influenced by additional parameters. a | As spatial proximity is a crucial factor for recombination efficiency, homologous recombination efficiency is increased if the DNA double-strand break (DSB) and the respective donor homology sequence are already juxtaposed before DSB formation. An archetypical mediator for this function is cohesin. b | Conversely, if probing in a larger volume is desired (for example, to enable ectopic (non-allelic) recombination), increased mobility of the DSB and/or the entire genome might be beneficial. c | Homology probing might be accelerated by intersegmental contact sampling or sliding, or it might even occur simultaneously through these processes. d | Finally, homology probing is actively facilitated by protein mediators that increase DNA accessibility, such as the conserved RAD54 protein, potentially through the remodelling of nucleosomes (indicated by arrows and the question mark). e | As the mobility of chromatin is approximately the same in different species, including bacteria, yeast and mammals, the percentage of the genome that is effectively probed by random homology search in each species is mainly dictated by the size of the respective genomes and their nuclear volumes. DSBs are indicated by lightning symbols. (Renkawitz et al.2014)

Spatial chromosome organization. In eukaryotes, chromosomes have a preferred position within the nucleus, and the high-order spatial organization is related to replication, transcription, and recombination (Aparicio 2013; Dekker and Mirny 2016). Comparing repair efficiency in strains where the DSB and the donor loci are at various initial distances within the nucleus reveals that the closer to the repair template, the easier the DSB would be repaired, indicating an evolutionary impact on

both chromosome organization and recombination (Agmon et al. 2013; Lee et al. 2016; Batte et al. 2017).

Reduced dimensionality search model. Through conventional and super resolution microscopy, it has been shown that RecA bundles extend along the long axis of an *E. coli* cell and mediate homology pairing between sisters that are segregated to the opposite halves of the cell. The RecA bundles can facilitate the long-range homology search by channelling the movement of DNA DSB ends (Lesterlin et al. 2014). Furthermore, Wiktor et al., propose the reduced dimensionality search model based on visualizing the process of DSB repair in single cells. They found that the search takes less than 9 ± 3 min and is mediated by a thin, highly dynamic RecA-YFP (expressed on top of the endogenous, untagged protein) filament that stretches throughout the *E. coli* cell. By this stretching along the z-axis, the RecA filament reduces the -search dimensionality from 3D to 2D by aligning with various dsDNA templates along the Z-axis at the same time (Figure 17). 2D search is approximately 100 times faster than 3D search and is consistent with the search time observed from single cell experiments (Wiktor et al. 2022).

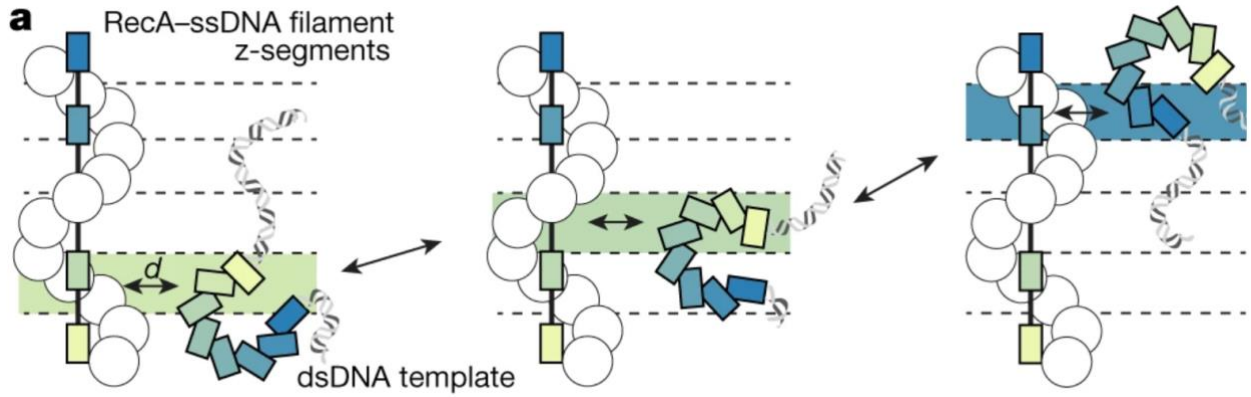

Figure 17 Reduced dimension search model.

The RecA–ssDNA filament and the repair template share one homologous segment (coloured bars) at each z coordinate along the length of a cell. As the repair template moves along the cell, only the segment at the current z coordinate is relevant. The search by the relevant segment thus occurs in 2D.

6 Aims of this work

Though intensively studied, there is still an open question of how Rad51 filament performs homology search in the nucleus and how Rad51 identifies a donor sequence among metabases of DNA. So far, this question is unsolved because of the lack of tools to monitor Rad51 in living cells.

To solve this problem, we collaborated with Raphael Guerois (CEA) and found a specific position to tag Rad51, predicted to minimize the effects of the tag on Rad51. Based on this strategy and through Crispr-Cas9, we constructed two internally GFP-tagged Rad51 strains (Rad51-yeGFP and Rad51-sfGFP) that make the study *in vivo* possible.

My PhD project was to study the dynamics of Rad51 in living yeast:

1. Observe Rad51 structures after inducing DSB in haploid and diploid strains.
2. Study effects of negative and positive regulators on Rad51 filaments, some chemical drugs effects on Rad51.
3. Use a time-lapse movie to explore how Rad51 filaments are formed and possible models of homology search.

I have used an I-*Sce*I cutting site to induce DSB at will to achieve these goals. It uses a galactose promoter to cut the DNA sequence in the middle of gene LYS2, and its efficiency is nearly 100% after adding galactose for 4h. With this system, we can induce a unique and specific DSB and estimate an appropriate time for observation. Most induced DSBs should finally be repaired by homologous sequence since the outcome of NHEJ can be cut up again. So, it is irreparable in our haploid strains and reparable in diploid strains. Besides, ilastik, a machine learning open-source software, Fiji and Matlab, have been used for analyzing images and quantification.

For the first goal, I checked the functionality of our internal GFP tag before experiments, including spot assay on YPD-MMS plates, western blot, immune fluorescence, and gene conversion efficiency test, making sure Rad51-intGFP in our strain behaves as well as WT strain and capable of homologous recombination. Then, I use microscopy to observe Rad51-sfGFP after inducing DSB for different hours in both haploid and diploid strains. Then using ilastik to quantify the percentages of different Rad51 filaments, measuring 3D lengths and intensities of filaments after deconvolution.

For the second goal, lots of mutant strains have been constructed. We have deleted the genes coding for the main known regulators of Rad51 filament (SRS2, RAD54, RAD52, SGS1, EXO1, RAD57, RDH54, PSY3, and CSM2) to study their effects on Rad51 filaments. Double-deleted strains are constructed by transformation or spore dissection for some interesting regulators, like *sgs1exo1Δ, rad52srs2Δ,*

and *rad57srs2Δ*. Besides tagging Rad51, Rfa1, Rad52 and Rad54 were also tagged in red to see the position relationship between Rad51 filaments and these factors. HU treatments have also been done in the Rad51-intGFP strains for studying Rad51 during replication.

As for the dynamics of Rad51 filaments, we have used time-lapse microscopy and a microfluidic system to take acquisitions every 2-5 min in haploid, diploid, and mutant strains. A laco/lacI system was designed to label the donor sequence, so we can observe how Rad51 structures interact with the homology sequence during HR.

These results are presented in the next chapter: Part A for the manuscript Liu et al. 2022, Part B for the unpublished results.

II. RESULTS

1. Section A

Title:

In vivo Dynamics of Rad51 filaments reveals a robust homology search strategy

Authors: Siyu Liu [1], Judith Mine-Hattab [1]‡, Marie Villemeur [1*]‡, Raphael Guerois [2], Leonid Mirny [3], Angela Taddei [1*].

Affiliations :

[1]Institut Curie, PSL University, Sorbonne Université, CNRS, Nuclear Dynamics ; Paris, France.

[2]Université Paris-Saclay, CEA, CNRS; Institute for Integrative Biology of the Cell (I2BC); Gif-sur-Yvette, France

[3] Department of Physics and Harvard-MIT Division of Health Sciences and Technology, Massachusetts Institute of Technology; Cambridge, Massachusetts, USA.

* Corresponding author. Email: angela.taddei@curie.fr

Abstract:

Homologous recombination (HR) is a major pathway to repair DNA double-strand breaks (DSB). HR uses an undamaged homologous DNA sequence as a template for copying the missing information, which requires identifying a homologous sequence among megabases of DNA within the crowded nucleus. In eukaryotes, this search is mediated by the conserved Rad51-ssDNA nucleoprotein filament (NPF). Although NPFs have been extensively studied *in vitro* by molecular, and genetic approaches, their formation and dynamics *in vivo* could not be assessed due to the lack of functional tagged versions of this protein. Here, we developed and characterized in budding yeast the first fully functional tagged version of Rad51. Following induction of a unique DSB, we observed Rad51-ssDNA forming exceedingly long filaments, spanning across the whole nucleus and finally contacting the donor sequence. Emerging filaments adopt a variety of shapes, not seen *in vitro*, and modulated by Rad54 and Srs2, shedding new light on the function of these factors. The filaments are also surprisingly dynamic, undergoing cycles of compaction and extension. Our biophysical model demonstrates that formation of extended filaments, particularly their compaction-extension dynamics constitute a robust search strategy, allowing DSB to rapidly explore the nuclear volume and thus enable efficient HR.

1.1 Introduction

Among the different kinds of DNA insults, double-strand breaks (DSBs) are the most genotoxic. DSBs can arise from errors in DNA metabolism, such as during DNA replication, as well as by exposure to exogenous DNA-damaging agents. Failure to repair such lesions leads either to cell death or genomic instability. Homologous recombination (HR) is one of the main pathways to repair DNA double strand breaks (DSB) and stalled replication forks [1–3]. HR uses an undamaged homologous DNA sequence as a template for copying the missing information. When available, the sister chromatid provides an ideal donor sequence as it is perfectly homologous and in spatial proximity. However, in the absence of an intact sister, homologous sequences on either the homologue or a different chromosome can be used as a template leading to inter-homologue or ectopic recombination, respectively. In this case, identifying the homologous sequence among the megabases (Mbs) of the genome within the nuclear space represents a real challenge with the risk of using the wrong donor sequence, thus leading to genomic instability [4–6].

At the molecular scale, homology sampling is carried out by a nucleoprotein filament (NPF), formed by the recombinase, RecA in bacteria and Rad51 in eukaryotes, coating ssDNA [7]. *In vitro*, this leads to a rigid right-handed helix around ssDNA, (50% extended relative to B-form duplex) [8] with a persistence length ranging from 190 to 550 nm. These micrometer-long, rigid structures could sample surrounding dsDNA in parallel, in search for a homologous sequence to use as template for repair [9].

Rad51 engages into HR following the formation of ssDNA by the combined actions of the nucleases Mre11, Exo1, and Dna2 [10]. Once generated, ssDNA is rapidly covered and stabilized by the ssDNA-binding protein complex, RPA, that is then replaced by the recombinase Rad51 [2]. While Rad51 filament formation is a key step for HR, it is also potentially harmful for cells if intermediates are formed that cannot be processed normally [11]. Several regulators of Rad51 filament formation and stability have been identified including the recombinase loader Rad52, the helicase Srs2, and the member of the SNF2 family of chromatin remodeling DNA-dependent ATPase Rad54 [9,12].

Although Rad51 has been intensively studied by combination of genetics, *in vitro,* structural and molecular approaches [2,7,9,12,13], how the nucleofilament is being formed, and how it mediates homology search *in vivo* remained elusive owing to the lack of functional tag to monitor Rad51 in living cells. While micrometer long RecA structures are observed upon DSB in bacteria [14,15], cells expressing terminal tagged version of Rad51 showed unresolved foci at DSB sites in eukaryotic cells [16–18], in contradiction with the long rigid structures predicted from *in vitro* studies.

Here we established the first functional tagged version of the eukaryotic recombinase Rad51, thanks to which, we could follow the dynamics of Rad51 assemblies undertaking homology search in living cells.

1.2 Results

A functional tagged version of Rad51

So far, no fluorescent tagged Rad51 has been shown to be fully functional. We reasoned that the difficulty to design a functional Rad51 tag was due to the structural constraints imposed to form a functional filament and allow access to regulatory factors. Taking in consideration these physical constraints, we thought to introduce a fluorescent tag in the least conserved region of the N-terminal domain of Rad51 (Figure 1A). After several adjustment of GFP version and linker properties, we obtained an endogenous tagged version of Rad51 (Rad51-iGFP2, Fig1B ; here after Rad51-iGFP), which allowed wild-type resistance to the damaging agent MMS when expressed as the only copy of *RAD51*, in contrast to the commonly used N or C-terminal tagged version (Figure 1B [16,17]).

Furthermore, our tagged version of Rad51 is as competent as the wild-type version to perform gene conversion following the induction of unique DSB in the presence of a homologous donor sequence located on a different chromosome (figure 1C).

Finally, we checked by western blot that the GFP tag did not affect the expression levels of Rad51 even following the induction of an unrepairable DSB by the I-*Sce*I endonuclease (Figure S1A).

Together, these data show that our internal tagged version of Rad51 is functional for homologous recombination. We could thus use this system to monitor Rad51 during HR events.

Rad51 forms filaments to perform homology search in living cells

Using our functional Rad51-iGFP expressing strain, we monitored Rad51 localization *in vivo* before and after induction of a unique un-repairable DSB in haploid cells. In the absence of induced DSB, we observed spontaneous foci in 5 % of the cells (Fig. 1D) as previously shown using a N-terminal tagged version of Rad51 [16]. Similar foci are visible in cells 2 hours after I-*Sce*I induction, together with brighter globular and elongated structures that were not reported for strains expressing either N- or C-terminal tagged Rad51 (Fig. S1B-C [16,17]).

The percentage of cells showing Rad51 structures, quantified using machine-learning-based image analysis ([19]), increased over time after induction to reach 90 % after 6 hours (Fig. 1D-E and S1D). The

proportion of elongated structures as well as their length also increased over time, some of them exceeding 1 µm in length at late time points (see below for quantification) akin the RecA filaments observed in bacteria [14,15]. Here, we use the term filaments to refer to Rad51 elongated structures and NPFs to refer to the nucleoproteic filaments.

We observed similar filaments by immuno-fluorescence in untagged cells using an antibody raised against Rad51, after inducing an un-repairable DSB (Fig. 1F), ruling out potential artefact owing to the presence of the tag.

Filamentous structures were also observed in diploid cells in which the homologous chromosome provide a perfect donor sequence (Figure S1E-F). In all situations, Rad51 structures were observed mainly in S and G2/M phases, as expected.

In diploid, the percentage of cells showing Rad51 structures peaks 4 hours after induction, a timing consistent with the disassembly of the nucleofilament once HR is achieved (Fig. 1G). We next assessed which of the Rad51 structures interact with the donor sequence on the homologous chromosome, tagged with the FROS system (Fig. 1H). Rad51 filaments showed a maximal level of association (50%), 2hrs after DSB induction in good agreement with the kinetic of homologous pairing observed in living cells [20] and ectopic donor invasion monitored by molecular assay [21–23]. In contrast, Rad51 foci or globular structures associate 3-fold less with the donor sequence, showing little variation over time after DSB induction, and a rate close to the one observed for association with a non-homologous sequence. We thus conclude that Rad51 filaments observed here in living cells correspond to the functional structures performing the homology search and strand invasion.

Rad51 filaments form on ssDNA resulting from long range resection of the DSB ends.

After deconvolution and segmentation, we measured the distribution of Rad51 filaments length over 2, 4 and 6 h DSB induction in haploid and diploid strains (Fig. 2A and S2A). As expected, in haploid cells, in the absence of a donor sequence, filament lengths increased over time with a median length of 0.9 µm at 2h, 1.3 µm at 4h and 1.7 µm at 6h after DSB induction. Diploid cells show longer filaments at 2h and 4h (respectively 1.5 and 1.7 µm), reflecting the higher efficiency of the HR pathway in diploid versus haploid cells. In contrast, filaments are shorter after 6 hours in diploid cells (1.4 µm), where the DSB can be repaired using the homologous chromosome as a perfect donor sequence.

In vitro, Rad51 coated ssDNA is extended by 50% relative to B-form duplex [8]. Assuming a similar extension *in vivo*, 1 µm would correspond to approximately 2 kb of ssDNA. This is consistent with chromatin immunoprecipitation (ChIP) performed against Rad51, 4 hours after I-*Sce*I induction

showing a broad 4-6Kb peak for both tagged and untagged versions of Rad51 (Fig. 2B). Therefore, the length of the Rad51 filaments that we observe *in vivo* is compatible with the extent of Rad51 association as detected by ChIP.

Accordingly, deleting either *EXO1* or *SGS1*, which both contribute to the long range resection of DSB [10], decreased the number of cell showing Rad51 filament 4hrs after DSB induction (Fig. 2C-D). Moreover, the double *sgs1Δ exo1Δ* strain, where long-range resection is abolished, shows very few Rad51 structures with weaker intensity than the wildtype strain 4 hours after DSB induction (Fig. 2C-D and S2B). We thus conclude that the formation of Rad51 filaments requires long-range resection for the extension of Rad51 filament along ssDNA.

Rad51 filament formation requires the Rad51 loader Rad52 and are modulated by the helicase Srs2 and the DNA-dependent ATPase Rad54.

We next tested in living cells, the impact of factors identified as Rad51 regulators through genetic and molecular studies. We first tested whether Rad51 filaments and foci depend on the Rad51 loader Rad52. Consistently, Rad51 nuclear structures were rarely observed in *rad52Δ* cells (less than 1%) 4 hours after DSB induction (Fig. 3A).

To avoid the generation of toxic filaments and protect favorable ones, many regulators participate in the competition between dismantling and stabilizing NPF [9,12]. The Srs2 helicase is proposed to be the major negative modulator that restricts HR by disassembling the NPF. Rad54 is a critical HR factor, with both pre-synaptic and post-synaptic functions, as it was shown to stabilize the presynaptic complex, destabilize dsDNA-bound Rad51, promote strand invasion, catalyze branch migration, remodel nucleosomes, and promote strand invasion on chromatin substrates (13). We observed Rad51 filaments in both *rad54Δ* and *srs2Δ* strains in the absence of DSB (Fig. 3A-B), suggesting that both Srs2 and Rad54 prevent the formation of filaments at spontaneous damages. Following DSB induction, these two mutants showed more Rad51 structures after 2 hours, but similar levels after 4h.

However, our quantification revealed that the filaments are also getting longer in the *rad54Δ* (p=1E-4) strain than those in the WT strain. Although the ability of Rad54 to remove Rad51 from dsDNA was mainly proposed to act on the heteroduplex dsDNA product of strand invasion, our results indicate a presynaptic role of Rad54, possibly preventing the formation of rad51 filaments on the dsDNA flanking the damaged site.

In the absence of the helicase Srs2, Rad51 filament median length was not significantly affected, although we observe a decrease in the proportion of short filaments. Furthermore, Rad51 filaments are brighter in the *srs2Δ* strain (p=6E-14), which could be interpreted as an increased density of Rad51 along the filament, probably related to the known activity of Srs2 that dismantles Rad51 on ssDNA *in vitro* (12). We thus conclude that the formation of Rad51 filaments in living cells requires the Rad51 loader Rad52, and is negatively regulated by the Srs2 helicase and the ATPase Rad54, in good agreement with activities reported for these factors [9,12].

Recurrent patterns in Rad51 filaments regulated by Rad54

We noticed that Rad51 filaments can adopt a variety of patterns (Fig. 3D and S3A) that we categorized into 5 subclasses: rods, bent filaments, circles, branched structures with a single node and others (including more complex or multiple structures). Rad51 mainly forms rods and bent filaments at the early stage after DSB induction, while other shapes, are commonly observed after a 6h galactose induction in the wildtype strain, suggesting that the simple filaments convert into branched and circular structures over time (Fig. 3E and S3B). The same classes of structures were observed in the diploid strain, where the DSB is repaired, with notably a lower proportion of very complex structures ("others" in Fig 3D). We thus conclude that rod filaments, bent filaments, 1-node and circles filaments are all functional structures.

Quantifying these subclasses on strains with different genetic background, we observed that *srs2Δ* strain show a close to wildtype distribution (Fig. 3E and S3C). However, we noticed that rods and bent filaments are significantly longer in this strain (Fig. S3D) in good agreement with the anti-recombinase activity of Srs2 (12). Strikingly, *rad54Δ* strain has nearly no branched filaments but accumulates circular structures (>25% at 6 hours after DSB induction versus less than 10%, in WT and *srs2Δ,* Fig. 3E).

Although we expect up to four NPF in each cell (corresponding to the two sides of the break on the two sister chromatids), most cells show a single Rad51 structure. These structures thus correspond to up to four NPFs, which precise organization need to be determined. The one- node structures showing a maximum of 4 branches and being Rad54 dependent could correspond to individual NPFs interacting with small tracks of homology belonging to different parts of the genome (13). Although there is no homologous sequence available for a faithful HR event in this case, short tracks of homology (9 to 15 nt) are sufficient for Rad54 to promote association of the presynaptic complex with dsDNA *in vitro* (14).

Together this analysis shows that timing and shapes of nuclear-size structures formed by Rad51 filaments are controlled by Srs2 and Rad54, possibly through modulation of Rad51 polymerization and depolymerization, and capacity to invade dsDNA.

Dynamics of Rad51 filament *in vivo* reveals rapid compaction/extension cycles.

To monitor the dynamics of Rad51 filament formation in living cells, we acquired time laps, taking one Z-stack of 21 images every 5 min, starting 90 min after I-*Sce*I induction. As shown in Fig. 4A, Rad51 first accumulates as a focus, whose intensity increases, before forming a more elongated structure or filament (Movie S1). Imaging cells, at 2 min time interval (Fig. S4A) we could estimate the median time between the appearance of the first focus and the formation of a structure larger than 300 nm as 22 min in wild-type cells (n=12). Consistently, this transition was faster in the absence of Srs2 or Rad54 (9 and 8.23 min respectively, Fig. S4B), indicating that both factors delay Rad51 filament elongation.

Once formed, Rad51 filaments are very dynamic, bending, changing orientation and shapes over time, switching from rod to bent filaments, to more complex structures, eventually disappearing in diploid cells, probably reflecting repair events (Fig. 4B, Movie S2-4-5; and S4C-D). All classes of filament shapes observed in a population of cells could be observed in single movies. Therefore, the different classes of filament shapes reflect the dynamics behavior of Rad51 structures rather than cell to cell variability. Furthermore, we frequently observed abrupt changes in filament length, seemingly collapsing as bright foci, yet followed by a rapid re-extension (Fig. 4C and S4C-E, Movies S3-4). Careful inspection of individual Z-stack confirmed that these foci did not correspond to filament truncated in the Z axis or oriented perpendicularly to the XY plan. Furthermore, the intensity of these foci was close to the total intensity of the extended filaments observed on the previous and following frames (Fig. 4D, grey, green, and purple areas for examples). We thus conclude that these bright foci are compacted filaments. This is reminiscent to the contraction events observed *in vitro* on Rad51 nucleoprotein filaments, which are hydrolyzing ATP, leading to shorter filaments associated with Rad51-ADP molecules that dissociate slowly from DNA [24,25].

Within over 26 hours of movies imaged at a 2 min rate we observed on average one contraction event every 18 min. These events also occur in the absence of Srs2 or Rad54 (Fig. S4E-F, Movies S6-7) indicating that none of these factors are necessary for these events.

As we demonstrate below, these cycles of extension/compaction/re-extension provide an efficient strategy for homology search.

Rapid compaction-extension cycles of Rad51 filaments allow a fast and robust search.

Identifying the homologous sequence among megabases of DNA is a rate-limiting step for HR [26,27]. Inter-homologue recombination, however, is highly efficient in diploid cells, despite a large initial separation (~1.5 μm (20)) between the DSB and the homologous locus. Movement of a chromosomal locus, however, is highly constrained due to its polymer nature. To understand the role Rad51 filament and its dynamics can play into the efficacy of the search process, we developed a biophysical model of the search process. We consider various scenarios of search (Fig. 4E): (i) "no filament" where the DSB and the donor are compact chromosomal loci undergoing random polymer dynamics; (ii) the "static filament" where the DSB is stretched into a stable filament, while the donor searches via random polymer dynamics; (iii) the "dynamic filament", where the filament undergoes rounds of extension and compaction. In all scenarios, chromosomal loci undergo Rouse diffusion, that is characterized by $\mathrm{MSD} = At^{0.5}$, and is now well-supported and characterized by a broad range of locus-tracking experiments [28,29]. Since DSB leads to about 20% increase in the value of *A (28),* we used a higher range for A=0.01 um^2/sec$^{1/2}$ (28). For each scenario we use experimentally measured parameters to analytically compute the characteristic search time, and then use simulations to validate the theory and to obtain the full distribution of the search time.

Direct simulations of Rouse-diffusive loci and theory provide a very consistent picture of search facilitation through filament formation and dynamics (Fig 4E). Starting at a random position within a nuclear volume a compact donor locus explores the nuclear volume in search for the DSB-proximal region (compact or filamentous); the search ends when the DSB-proximal region touches the complementary donor region, irrespective of where the donor touches the filament. The idea being that the compact donor contains a region complementary to any part of the filament. Rouse diffusion leads to search via compact exploration of the volume, and allows estimating the search time as the time it takes the Rouse-diffusing donor to explore the nuclear volume (see [30], and Supplemental Information). For the no-filament case, theory and simulations yield the median search of ~9-11h. In the case of a static ~1.2μm filament, the search is estimated to take ~5h. Dynamic filament drastically changes the search process from the slow volume exploration to the intermittent search that consists of rounds of extended (and compacted filament). In each round, a new section of the nuclear volume is probed by the extended filament for time □□□ followed by the compacted state for time □₀.□□Akin to other intermittent search processes [31], from animal foraging to protein-DNA search [32,33] where rounds of local exploration (e.g. sliding in 1D or an extended filament) are combined with flights (3D

diffusion or re-extension), rounds of filament compaction and elongation facilitate the homology search (see SI) yielding the median search time of ~1.5-3h (for τ_0=100sec and τ=1000sec). Like in other intermittent search processes [31], there is an optimal time for having a stable filament: having filament for a shorter period of time would require many more rounds of search each incurring an additional τ_0 in the less-exposed collapsed state, while having a filament stable for too long makes the whole process inefficient due to redundant probing of the same part of the nuclear volume. Consistently, both theory and simulations show (Fig. 4F) that for τ_0=100sec experimentally measured τ=1000sec, provides search times slower but close to the optimal value through efficient intermittent search. Cumulative distributions of the search time from simulations (Fig 4F, right) also show that models differ in their ability to provide robust search, *i.e.* having a large fraction of cells succeeding with a required time interval. Interestingly, the effect of the filament dynamics becomes more pronounced for shorter (0.9μm) filaments that we observe at earlier times after DSB (see SI). Our models do not consider tethering of chromosomes and topological constrains that can further slowdown polymer dynamics. This, however, could provide more advantage to facilitated search through filament dynamics that relies more on cycles of compaction and extension rather than polymer mobility to probe the nuclear volume.

Our estimates have several functional consequences. As cells need to complete search within 8-10h, before cells adapt to checkpoint activation and undergo cell division despite the presence of an unrepaired broken chromosome [35,36], no-filament and stable filament mechanisms can deliver successful search for only 45% and 68% of cells. The dynamic filament, on the contrary provides successful search at 8h for 92% of cells. The time to identify the donor sequence can be further limited by the progressive loss of the homologous sequence owing from exonuclease activities, in the case of ectopic recombination [27]. Together, our biophysical modeling demonstrates that formation of elongated filaments and particularly their rapid compaction and re-extension provides a fast and robust search strategy, like other intermittent search strategies.

1.3 Conclusion

Here we report the first functional tagged version of a eukaryotic recombinase allowing to monitor the dynamics of the nucleofilament upon homology search in living cells. Our study reveals that genome- and nucleus-wide homology search proceeds through a radically different mechanism from the prevailing view of broken ends seeking the homologous sequence as a compact focus. In contrast,

we show that homology search is performed by micrometer long Rad51 filaments, exposing the ssDNA to a big area of the nucleus and allowing the simultaneous scanning of sequences located in different nuclear region in good agreement with observed complex genomic rearrangement [6]. Furthermore, our study reveals that Rad51 filaments are dynamic, occasionally compacting and extending, allowing robust exploration of the nuclear space, compatible with repair efficiency observed *in vivo*, as demonstrated by simulations and theoretical analyses. Consistently, we observe a strong correlation between the ability of the different Rad51 tagged version to form long filaments and HR efficiency. While Rad51 filament dynamics ensures that the resected ssDNA can reach the donor sequence, other factors such as decreased nucleosome occupancy could facilitate the invasion of the template sequence once in proximity [37]. The observations of dynamics filaments reported here call for the reinterpretation of previous work. For instance, the dynamics of the filament itself could be in fact the cause of the increased in mobility reported for the damaged chromatin and to a lesser extent the undamaged chromatin upon DSB induction [20,38]. Finally, the capacity to monitor the dynamics of Rad51 in living cells opens new avenues to screen genetic factors and small molecules impacting on HR regulation with strong implications for both our understanding of HR regulation in living cells and the development of new intervention of therapeutic value.

1.4 References

1. Ait Saada, A., Lambert, S. A. E. & Carr, A. M. Preserving replication fork integrity and competence via the homologous recombination pathway. *DNA Repair* **71**, 135–147 (2018).
2. Wright, W. D., Shah, S. S. & Heyer, W.-D. Homologous recombination and the repair of DNA double-strand breaks. *Journal of Biological Chemistry* **293**, 10524–10535 (2018).
3. Kowalczykowski, S. C. An Overview of the Molecular Mechanisms of Recombinational DNA Repair. *Cold Spring Harb Perspect Biol* **7**, a016410 (2015).
4. Barzel, A. & Kupiec, M. Finding a match: how do homologous sequences get together for recombination? *Nat Rev Genet* **9**, 27–37 (2008).
5. Haber, J. E. DNA Repair: The Search for Homology. *BioEssays* **40**, 1700229 (2018).

6. Piazza, A. & Heyer, W.-D. Homologous Recombination and the Formation of Complex Genomic Rearrangements. *Trends in Cell Biology* **29**, 135–149 (2019).
7. Bonilla, B., Hengel, S. R., Grundy, M. K. & Bernstein, K. A. *RAD51* Gene Family Structure and Function. *Annu. Rev. Genet.* **54**, 25–46 (2020).
8. Sung, P. & Robberson, D. L. DNA strand exchange mediated by a RAD51-ssDNA nucleoprotein filament with polarity opposite to that of RecA. *Cell* **82**, 453–461 (1995).
9. Kong, M. & Greene, E. C. Mechanistic Insights From Single-Molecule Studies of Repair of Double Strand Breaks. *Frontiers in Cell and Developmental Biology* **9**, 20 (2021).
10. Cejka, P. & Symington, L. S. DNA End Resection: Mechanism and Control. *Annu. Rev. Genet.* **55**, 285–307 (2021).
11. Lehmann, C. P., Jiménez-Martín, A., Branzei, D. & Tercero, J. A. Prevention of unwanted recombination at damaged replication forks. *Curr Genet* **66**, 1045–1051 (2020).
12. Carver, A. & Zhang, X. Rad51 filament dynamics and its antagonistic modulators. *Seminars in Cell & Developmental Biology* **113**, 3–13 (2021).
13. Sun, Y., McCorvie, T. J., Yates, L. A. & Zhang, X. Structural basis of homologous recombination. *Cell. Mol. Life Sci.* **77**, 3–18 (2020).
14. Lesterlin, C., Ball, G., Schermelleh, L. & Sherratt, D. J. RecA bundles mediate homology pairing between distant sisters during DNA break repair. *Nature* **506**, 249–253 (2014).
15. Wiktor, J. *et al.* RecA finds homologous DNA by reduced dimensionality search. *Nature* **597**, 426–429 (2021).
16. Lisby, M., Barlow, J. H., Burgess, R. C. & Rothstein, R. Choreography of the DNA Damage Response: Spatiotemporal Relationships among Checkpoint and Repair Proteins. *Cell* 15 (2004).
17. Waterman, D. P. *et al.* Live cell monitoring of double strand breaks in S. cerevisiae. *PLoS Genet* **15**, e1008001 (2019).

18. Essers, J. Nuclear dynamics of RAD52 group homologous recombination proteins in response to DNA damage. *The EMBO Journal* **21**, 2030–2037 (2002).
19. Berg, S. *et al.* ilastik: interactive machine learning for (bio)image analysis. *Nat Methods* **16**, 1226–1232 (2019).
20. Miné-Hattab, J. & Rothstein, R. Increased chromosome mobility facilitates homology search during recombination. *Nat Cell Biol* **14**, 510–517 (2012).
21. Piazza, A. *et al.* Dynamic Processing of Displacement Loops during Recombinational DNA Repair. *Molecular Cell* **73**, 1255-1266.e4 (2019).
22. Jain, S., Sugawara, N., Mehta, A., Ryu, T. & Haber, J. E. Sgs1 and Mph1 Helicases Enforce the Recombination Execution Checkpoint During DNA Double-Strand Break Repair in *Saccharomyces cerevisiae*. *Genetics* **203**, 667–675 (2016).
23. Aylon, Y., Liefshitz, B., Bitan-Banin, G. & Kupiec, M. Molecular Dissection of Mitotic Recombination in the Yeast *Saccharomyces cerevisiae*. *Mol Cell Biol* **23**, 1403–1417 (2003).
24. Hilario, J., Amitani, I., Baskin, R. J. & Kowalczykowski, S. C. Direct imaging of human Rad51 nucleoprotein dynamics on individual DNA molecules. *Proc. Natl. Acad. Sci. U.S.A.* **106**, 361–368 (2009).
25. Robertson, R. B. *et al.* Structural transitions within human Rad51 nucleoprotein filaments. *Proc. Natl. Acad. Sci. U.S.A.* **106**, 12688–12693 (2009).
26. Agmon, N., Liefshitz, B., Zimmer, C., Fabre, E. & Kupiec, M. Effect of nuclear architecture on the efficiency of double-strand break repair. *Nat Cell Biol* **15**, 694–699 (2013).
27. Batté, A. *et al.* Recombination at subtelomeres is regulated by physical distance, double-strand break resection and chromatin status. *EMBO J* **36**, 2609–2625 (2017).
28. Miné-Hattab, J., Recamier, V., Izeddin, I., Rothstein, R. & Darzacq, X. Multi-scale tracking reveals scale-dependent chromatin dynamics after DNA damage. *MBoC* **28**, 3323–3332 (2017).

29. Hajjoul, H. *et al.* High-throughput chromatin motion tracking in living yeast reveals the flexibility of the fiber throughout the genome. *Genome Res.* **23**, 1829–1838 (2013).

30. de Gennes, P. G. Kinetics of diffusion-controlled processes in dense polymer systems. I. Nonentangled regimes. *The Journal of Chemical Physics* **76**, 3316–3321 (1982).

31. Chupeau, M., Bénichou, O. & Voituriez, R. Cover times of random searches. *Nature Phys* **11**, 844–847 (2015).

32. von Hippel, P. H. & Berg, O. G. Facilitated Target Location in Biological Systems. *Journal of Biological Chemistry* **264**, 675–678 (1989).

33. Slutsky, M. & Mirny, L. A. Kinetics of Protein-DNA Interaction: Facilitated Target Location in Sequence-Dependent Potential. *Biophysical Journal* **87**, 4021–4035 (2004).

34. Berg, O. G. & von Hippel, P. H. Selection of DNA binding sites by regulatory proteins. *Journal of Molecular Biology* **193**, 723–743 (1987).

35. Toczyski, D. P., Galgoczy, D. J. & Hartwell, L. H. CDC5 and CKII Control Adaptation to the Yeast DNA Damage Checkpoint. *Cell* **90**, 1097–1106 (1997).

36. Sandell, L. Loss of a yeast telomere: Arrest, recovery, and chromosome loss. *Cell* **75**, 729–739 (1993).

37. Challa, K. *et al.* Damage-induced chromatome dynamics link Ubiquitin ligase and proteasome recruitment to histone loss and efficient DNA repair. *Molecular Cell* **81**, 811-829.e6 (2021).

38. Dion, V., Kalck, V., Horigome, C., Towbin, B. D. & Gasser, S. M. Increased mobility of double-strand breaks requires Mec1, R

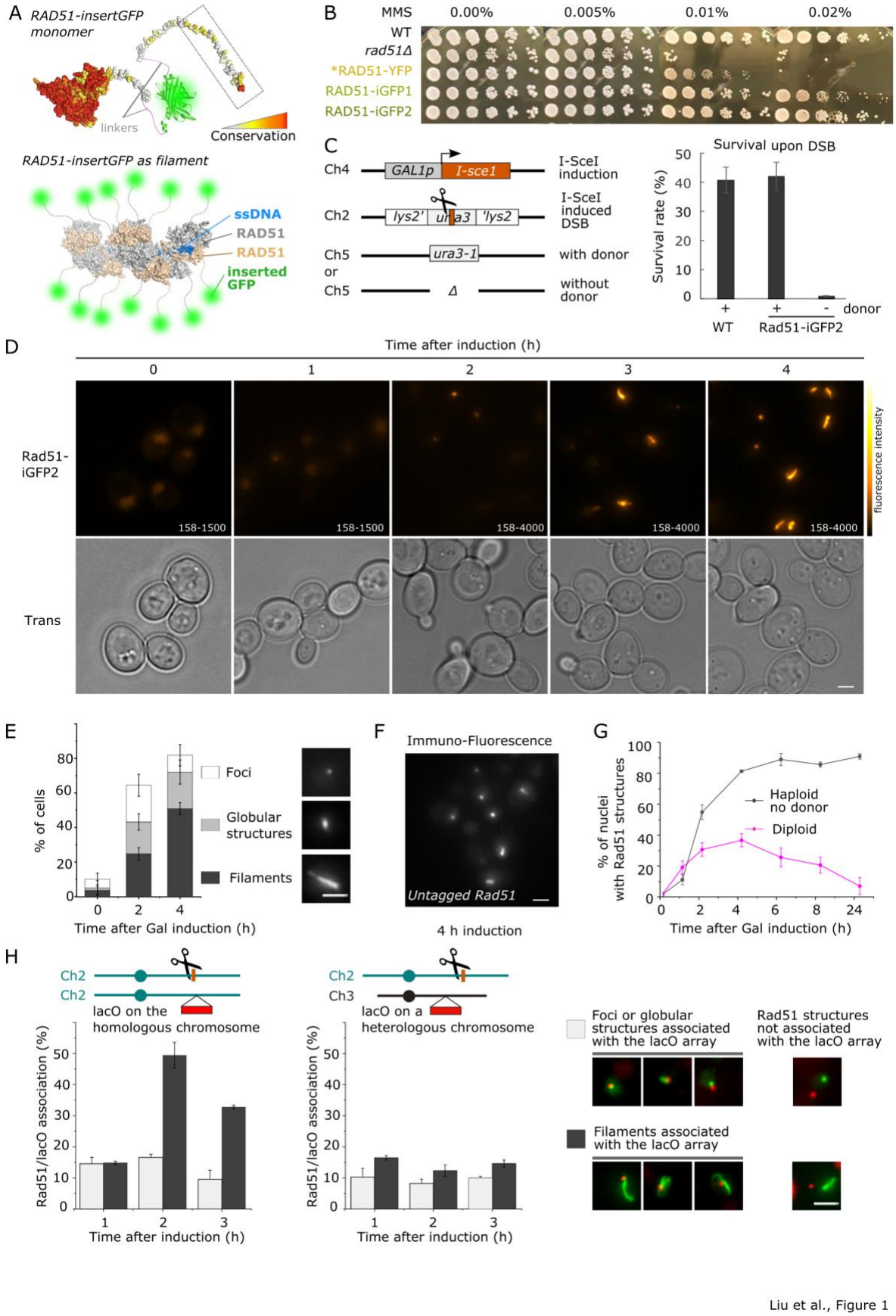

Liu et al., Figure 1

SecA_Figure 1 **Rad51 forms filaments upon DSB to perform homology search in living cells**

A. Strategy to tag Rad51. The top view represents a single monomer of RAD51-iGFP2 with positions of Rad51 amino acids shown as spheres colored with respect to their conservation in Rad51 homologs. It highlights that the N-terminal tail of RAD51, predicted as disordered, contains sequence motifs partially conserved among closely related yeasts to *S. cerevisiae* which might have a functional role. The GFP was inserted just downstream of these motifs in the least conserved stretch of amino acids. The bottom part shows the structure of the nucleofilament formed by Rad51-iGFP2 around ssDNA.

B. Sensitivity of WT, *rad51Δ*, N-terminally tagged YFP-Rad51, and our internally tagged Rad51-iGFP expressing strains to the genotoxic agent Methyl Methane Sulfonate (MMS). **C.** Schematic description of the galactose induced DSB by I-*Sce*I and survival rate of the untagged or Rad51-iGFP strain upon DSB induction (galactose plate) in the presence or absence of a donor sequence. **D.** Representative images (Transmitted-light image and the GFP channel fluorescent image) of a Rad51-iGFP expressing strain at different time after DSB induction. Z-projection is applied on fluorescent images. **E.** Untagged Rad51 localized by Immunofluorescence 4 hrs. after DSB induction. **F.** Percentages of Rad51 foci, globular structures, and filaments at different time after DSB induction. **G.** Percentages of Rad51 structures in haploid (without donor) and diploid strains over time after DSB induction. **H.** Top: Schematic representation of the strains used to monitor the donor locus (on the homologous chromosome) or a control locus, labelled by insertion of lacO array in a strain expressing RFP-LacI and Rad51-iGFP strain. Bottom: percentages of Rad51 foci/globular structures or filaments associated with lacO array at different time after DSB induction (examples of lacO spot associated or not associated with Rad51 are shown on the right).

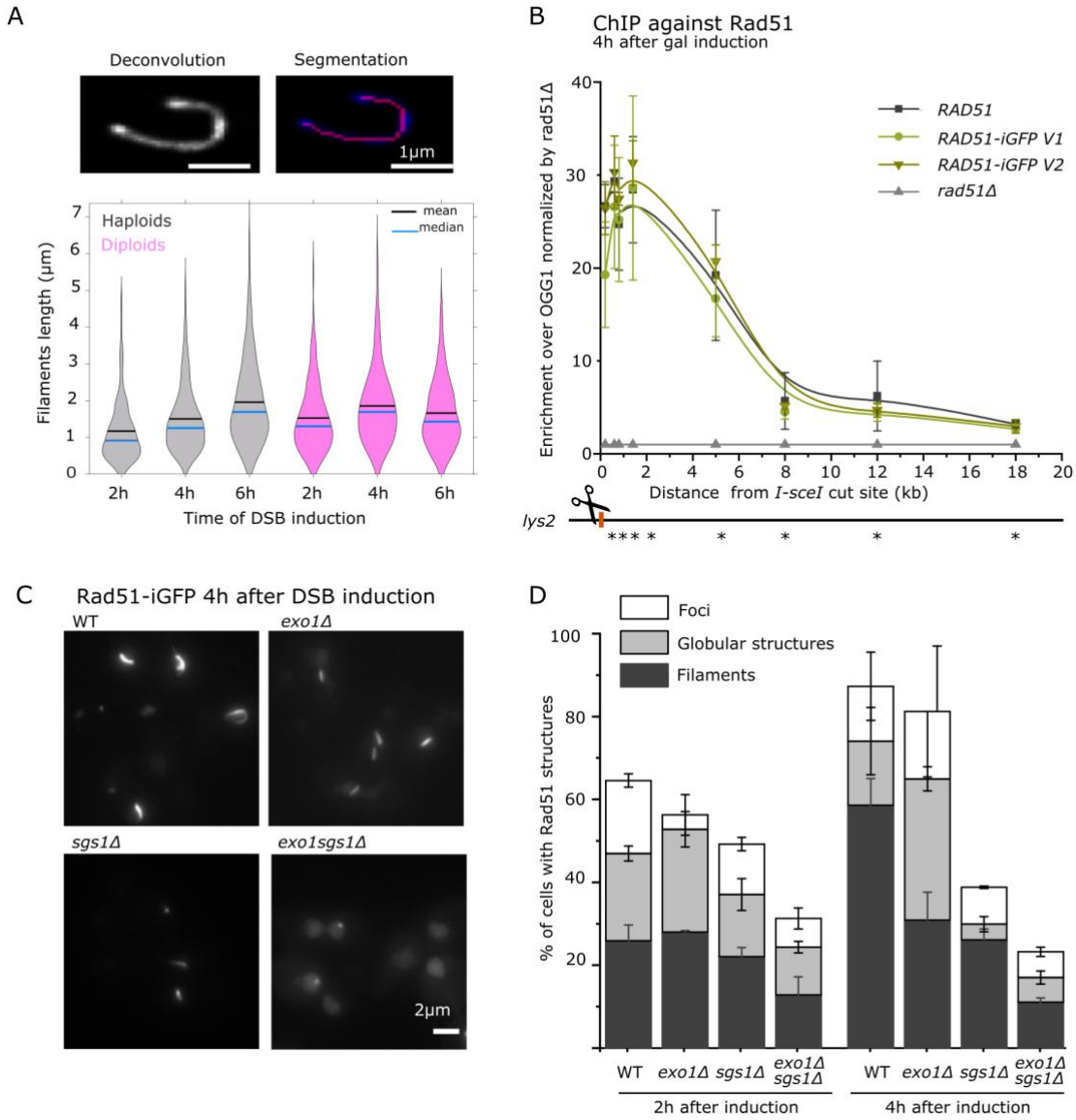

SecA_Figure 2 **Rad51 forms micrometer long filaments on ssDNA**

A. Distribution of filaments 3D lengths after 2, 4 and 6 h of galactose induction in haploid (un-repairable DSB) and diploid strains (where the homologous chromosome provides a donor sequence for HR). **B.** Enrichment of Rad51 as a function of the distance from the DSB site monitored by ChIP on *RAD51, RAD51-iGFP1, RAD51-iGFP2* and *rad51⊿* strains, 4 hours after DSB induction. **C.** Z projection of GFP images in WT*, exo1⊿, sgs1⊿,* and *exo1sgs1* strains expressing Rad51-iGFP 4h after DSB induction. **D.** Percentages of Rad51 foci, globular structures and filaments in WT and mutant strains. Data obtained through ilastik [19], n>100, 2 experiments.

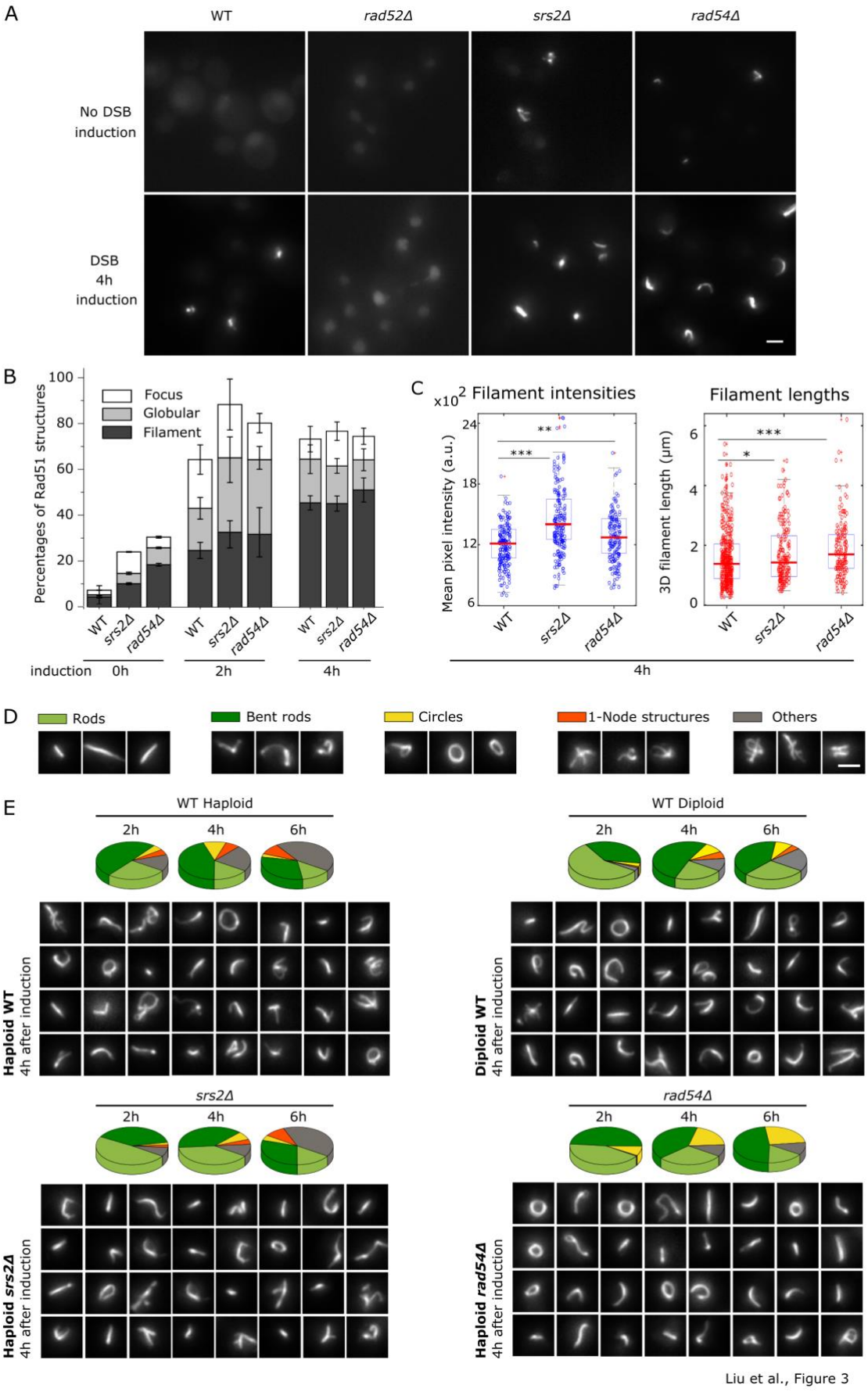

SecA_Figure 3 **Rad51 filament structures are regulated by Rad52, Srs2 and Rad54**.

A. Representative images of RAD51-iGFP 4h after galactose induction in WT, *rad52△*, *srs2△*,and *rad54△* strains. **B.** Percentages of Rad51 foci, globular structures, and filaments in the indicated strains. Data obtained through Ilastik [19], n>100, 3 experiments. **C.** Comparison of mean intensities within Rad51 filaments and their lengths in WT and mutant strains. **D.** 5 classes of Rad51 filaments are observed. **E.** Distribution of the 5 classes in WT (haploid and diploid), *srs2△, and rad54△* strains after 2, 4, 6h DSB induction, and presentative filaments 4 h after induction.

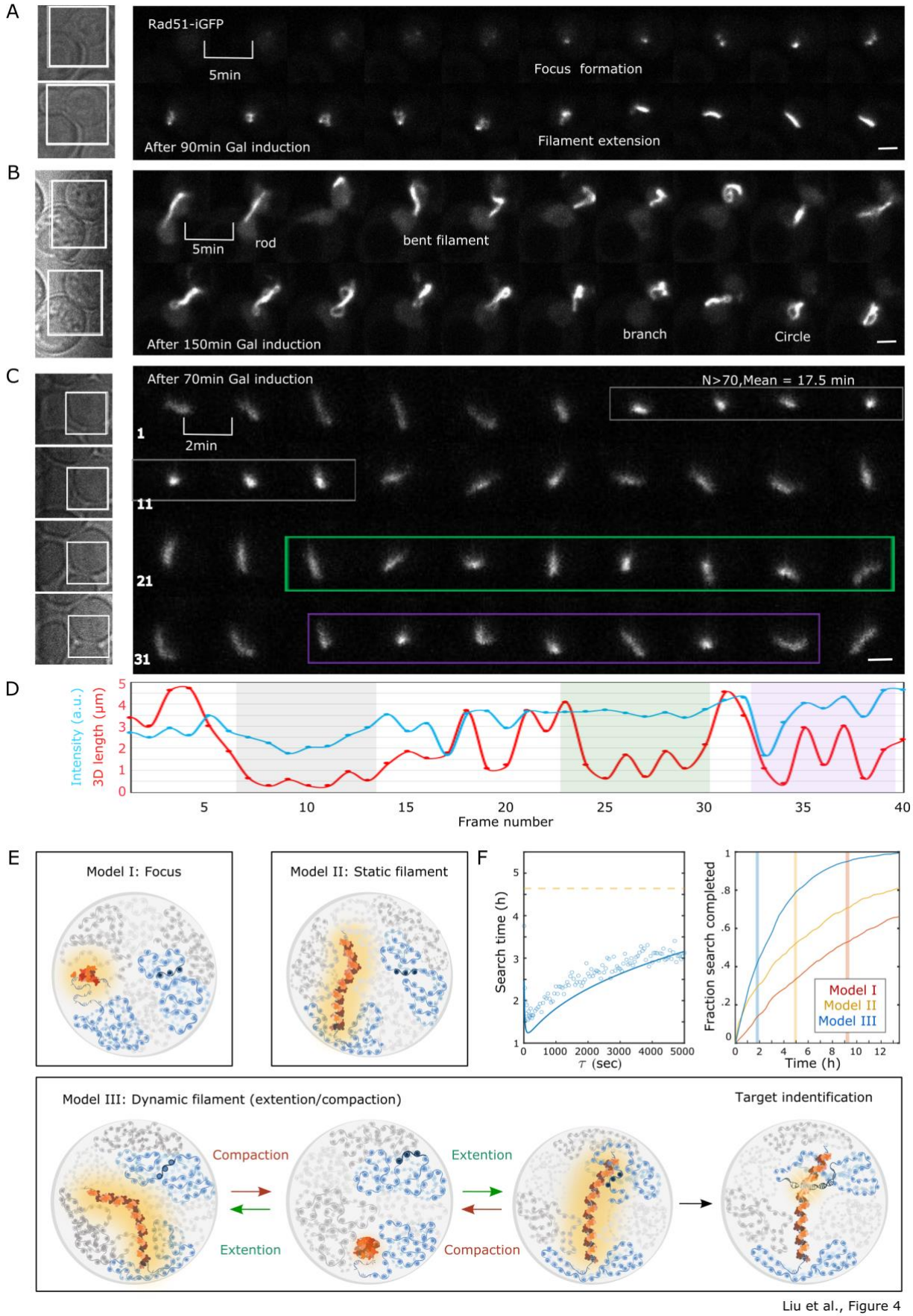

Liu et al., Figure 4

SecA_Figure 4 ***In vivo*** dynamics of Rad51 filaments suggest a new strategy of homology search.

A-B. Representative time-lapse images acquired every 5 min, 90 min after galactose addition (I-SceI induction) showing the formation of Rad 51 filament (A, Movie S1), or 150 min after Galactose addition (B, Movie S2) showing the dynamic of a mature Rad51 filament adopting different shapes over time. **C.** Images acquired every 2 mins, 70 min after galactose addition showing Rad51 filament undergoing compaction and extension events (Movie S3). **D.** Normalized fluorescence intensity and 3D length over time of the images shown in C. **E.** Different models for homology search: the nuclear space is explored by the Rouse diffusion (with D=.01 $\mu m^2.s^{-1/2}$ for the broken DNA and the donor: model I), a static filament (of length 1.2 µm, model II) or a dynamic filament undergoing cycles of extension and compaction, as observed in living cells. The yellow areas illustrate the volume explored over time. **F.** Left: theoretical prediction and simulation of the mean search time for model III as a function of τ (time the filament spends in an extended form) for a compaction time τ_0 = 100 s. The dotted line corresponds to the mean search for static filament (model II) from the simulation. Right: Search time estimated by theory and simulations: cumulative distribution of fraction of cells in which the DSB has reached the donor sequence as a function of time for the 3 models in simulations. Vertical lanes show characteristic times computed analytically and serving as good approximations of the median times from simulations. Note that different models provide very different fractions of cells able to find homolog within 8-10h when cells adapt to checkpoints and divide even if the DSB is not repaired [35,36].

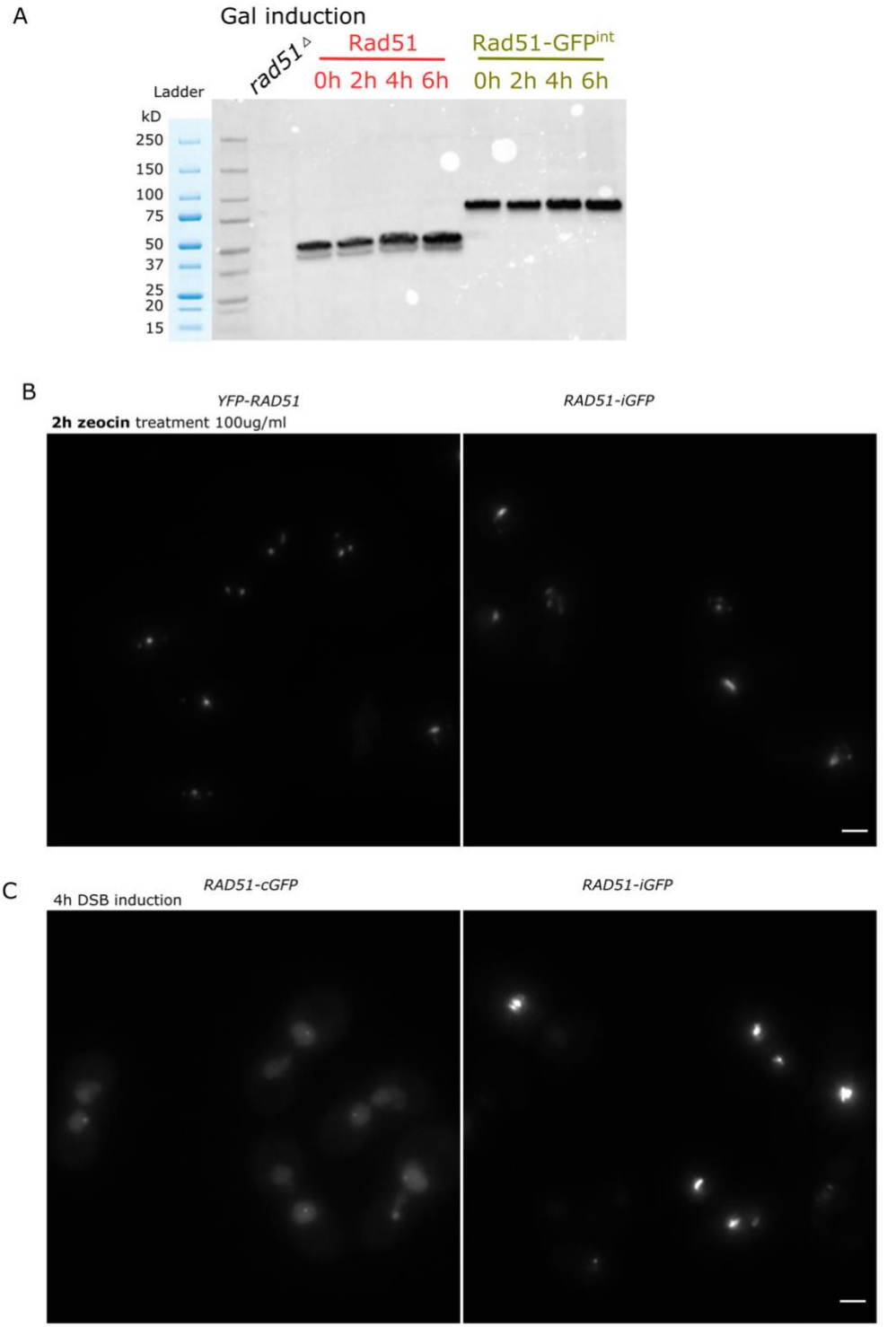

Liu et al., Figure S1A-B-C

D

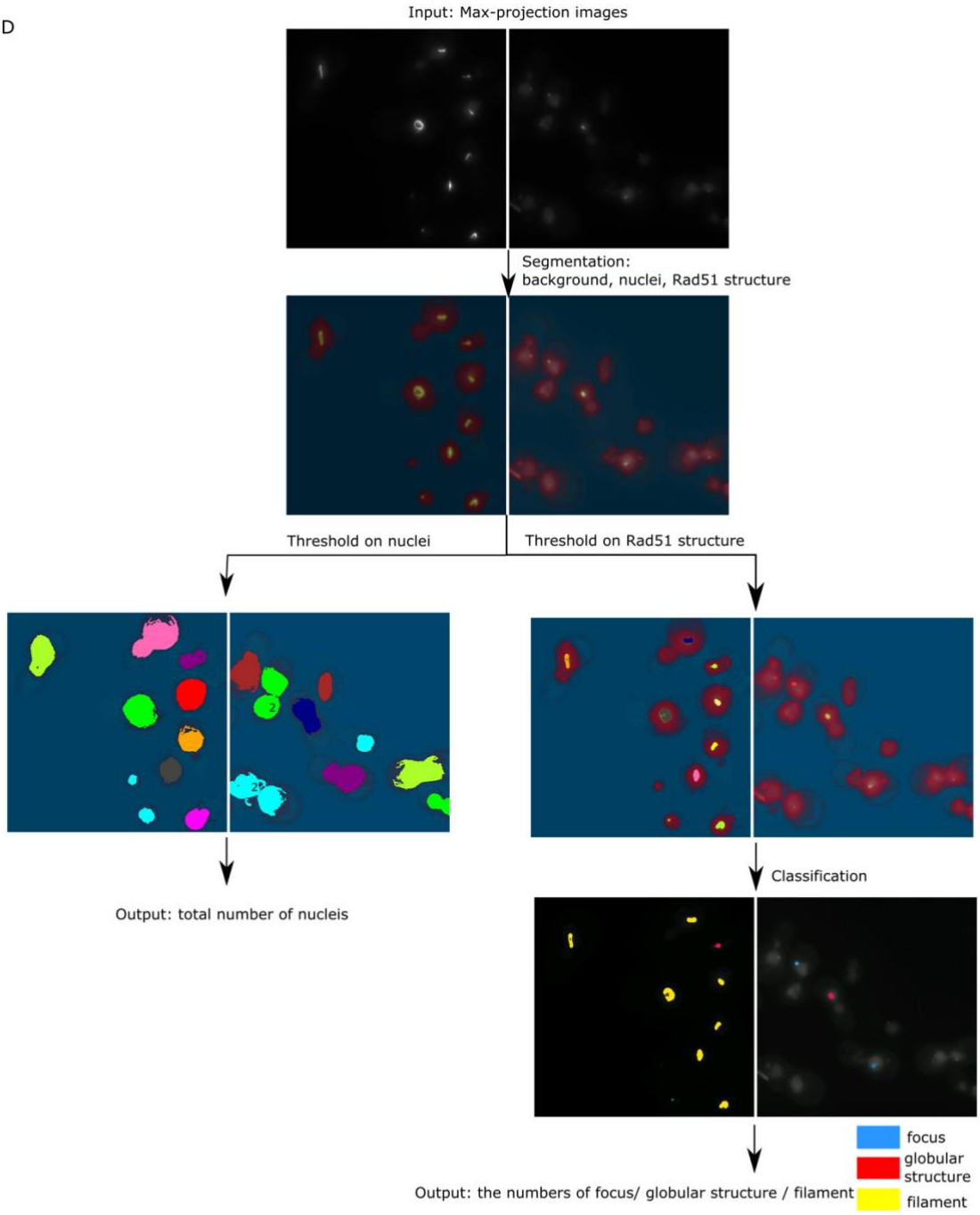

Liu et al., Figure S1D

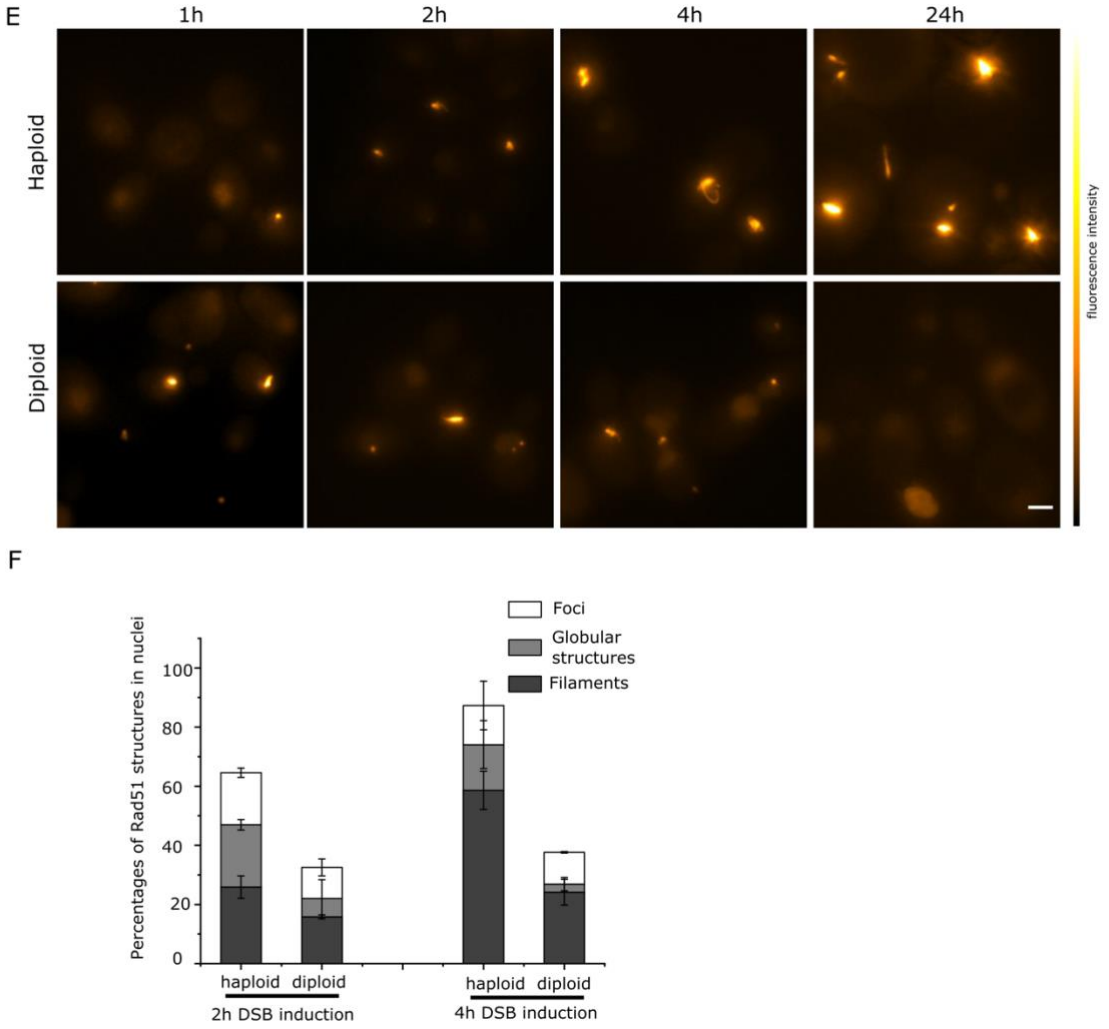

SecA_Figure S 1 **Functional Rad51-iGFP strain can form filaments**

A. Western blot on WT and Rad51-iGFP expressing strains at different time after DSB induction, *rad51Δ* is shown as negative control.

B. Representative GFP channel fluorescent images of YFP-Rad51 (from [27], N-terminal tag) and Rad51-iGFP after 2h Zeocin treatment, maximal Z-projections are shown.

C. Representative GFP channel fluorescent images of Rad51-GFP (C-terminal tag) and Rad51-iGFP with I-SceI cutting site after 4h galactose induction, Z-projection is applied.

D. Quantification of Rad51 structures using the machine-learning-based image analysis tool, Ilastik [28]. Input: Z-projection fluorescent images. Output: left, number of nuclei; right, numbers of Rad51 foci, globular structures and filaments.

E. Representative images GFP channel fluorescent images of a Rad51-iGFP in haploid and diploid strain at different time after DSB induction maximal Z-projections are shown.

F. Percentages of Rad51 foci, globular structures, and filaments at different time after DSB induction in haploid (without homologous donor sequence) and diploid strains quantified as in D.

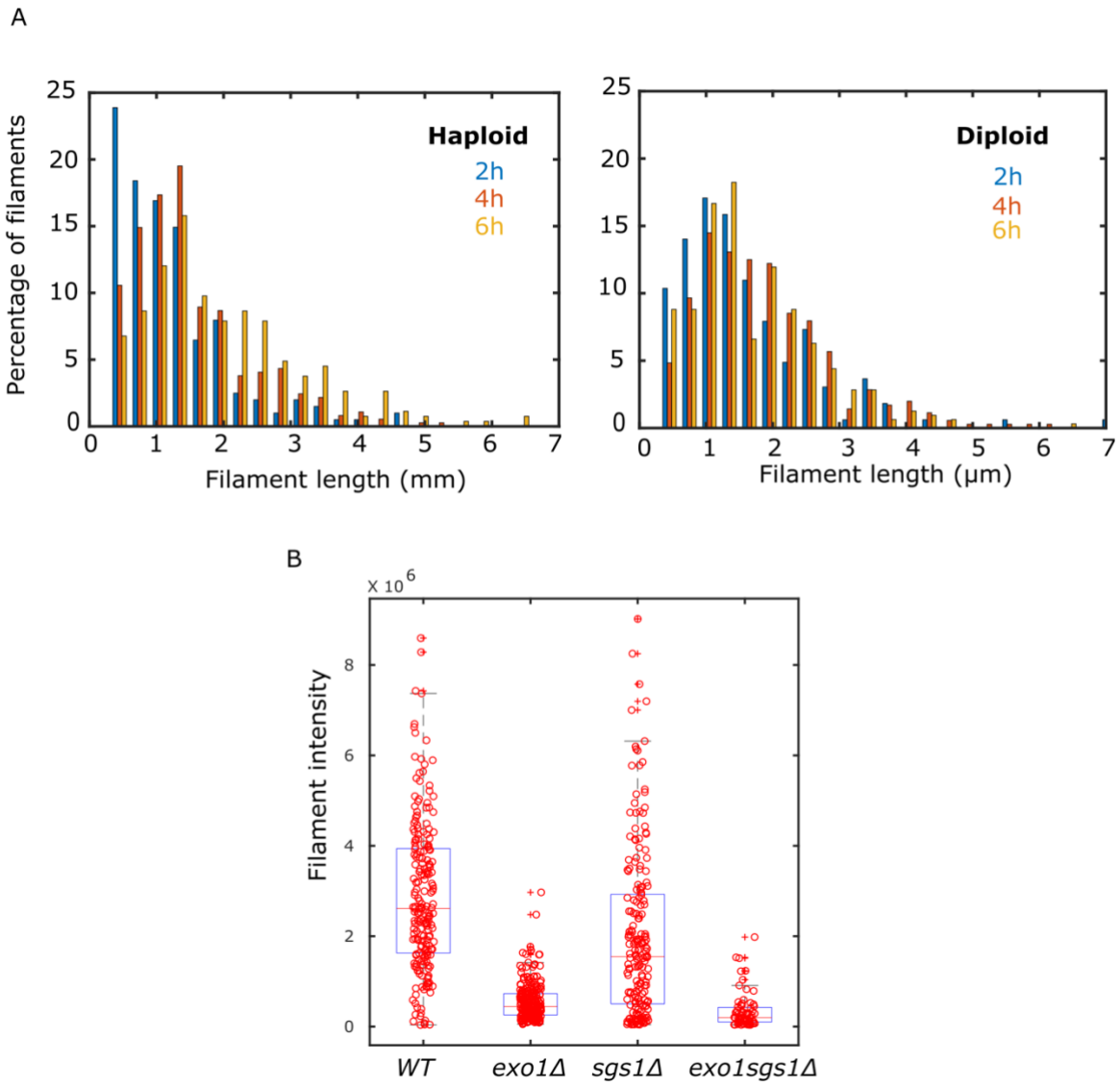

SecA_Figure S 2 **Effects of Sgs1 and Exo1 on Rad51 filaments**

A. Distributions of filament length in haploid (left) and diploid (right) strains

B. Comparison of total intensities of Rad51 filaments in WT, *sgs1Δ, exo1Δ, sgs1Δ exo1Δ* strains as indicated.

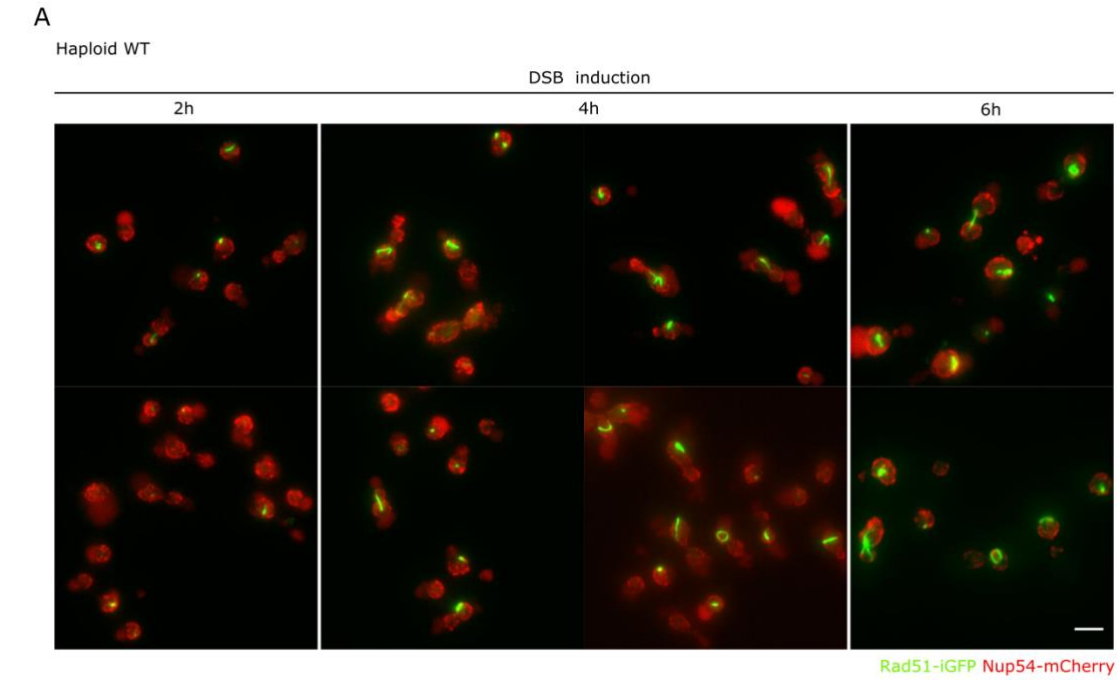

Liu et al., Figure S3AB

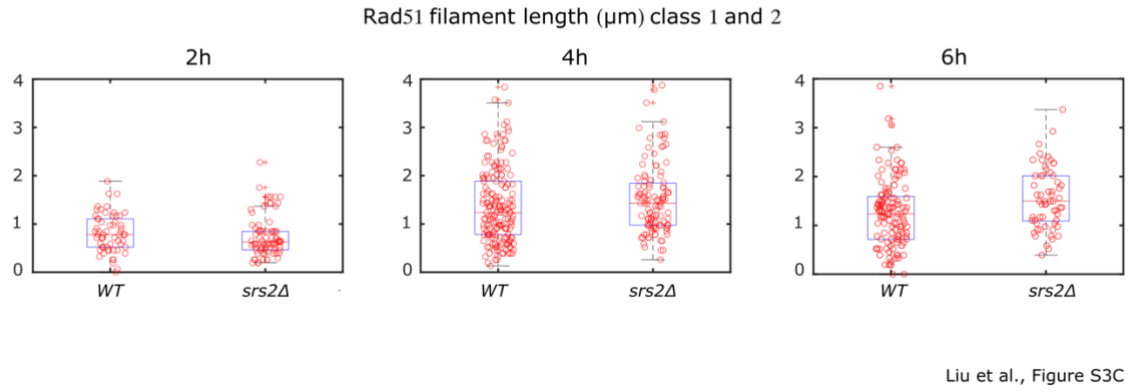

SecA_Figure S 3 **Rad51 filaments form different shapes**

A. Representative fluorescence images a Rad51-iGFP Nup-mCherry strain at 2,4,6h after DSB induction. GFP channel and RFP channel are combined, Z-projection is applied on fluorescent images.

B. Representative filaments of WT haploid and diploid strains at different time after galactose induction

C. Representative filaments of WT and mutants at 6h after DSB induction, Z-projection is applied

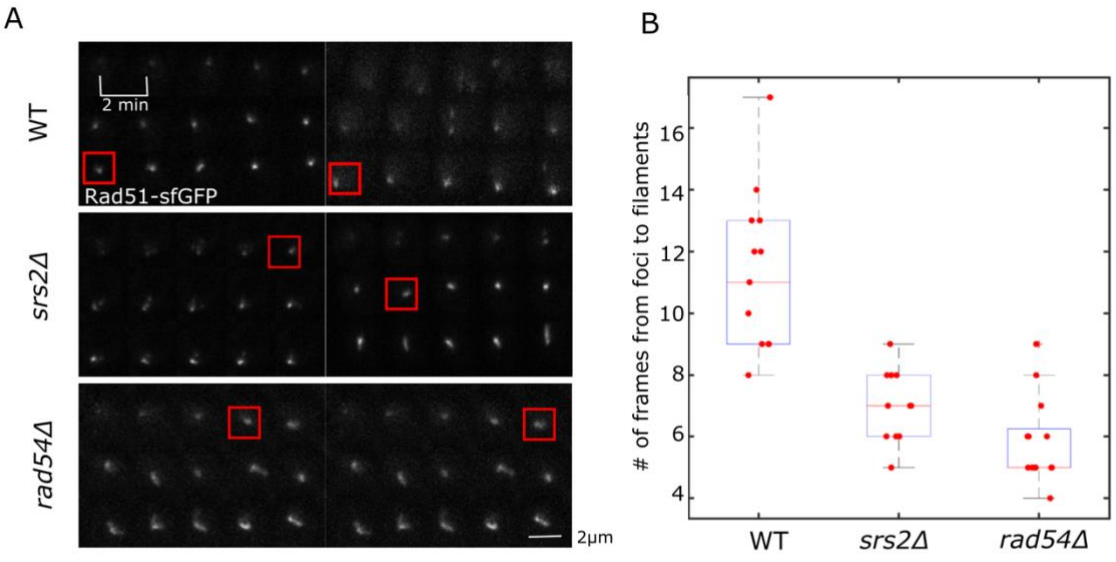

Liu et al., Figure S4AB

C Rad51-iGFP diploid after 70min Gal induction

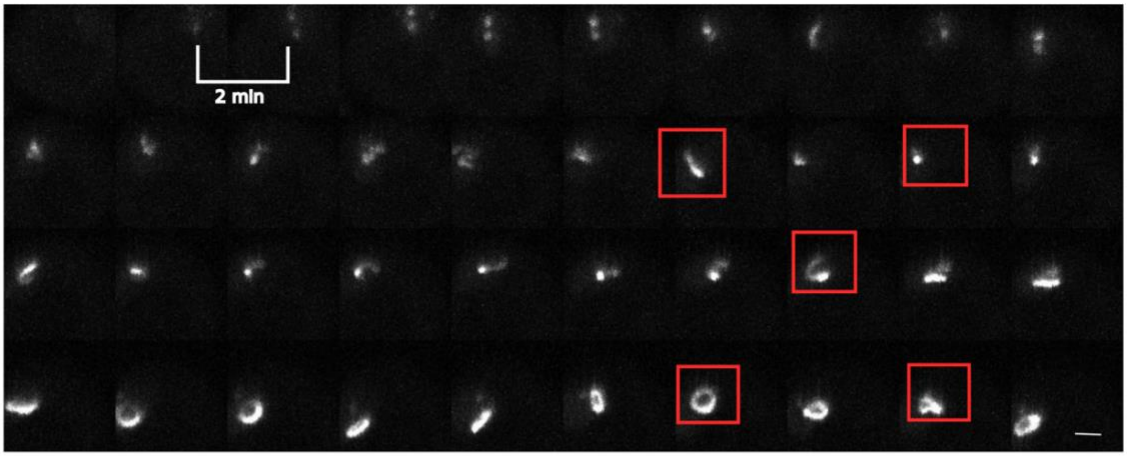

D Rad51-iGFP diploid after 225min Gal induction

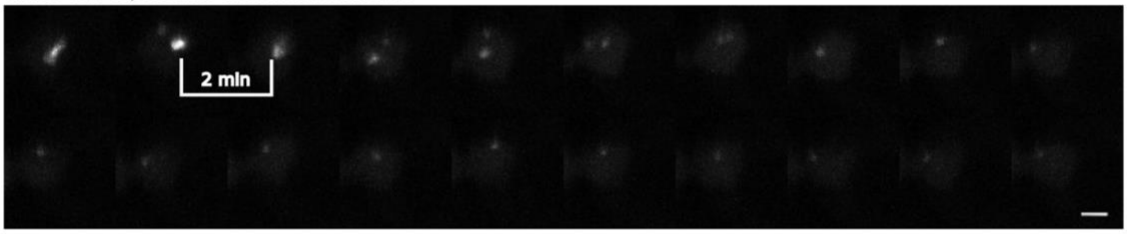

E Rad51-iGFP *srs2 Δ* after 70min Gal induction

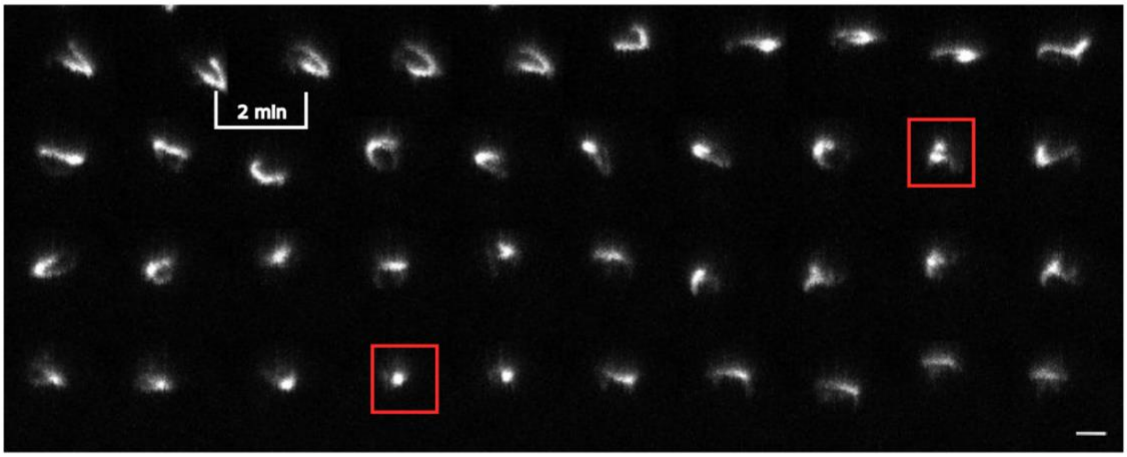

F Rad51-iGFP *rad54Δ* after 190 min Gal induction

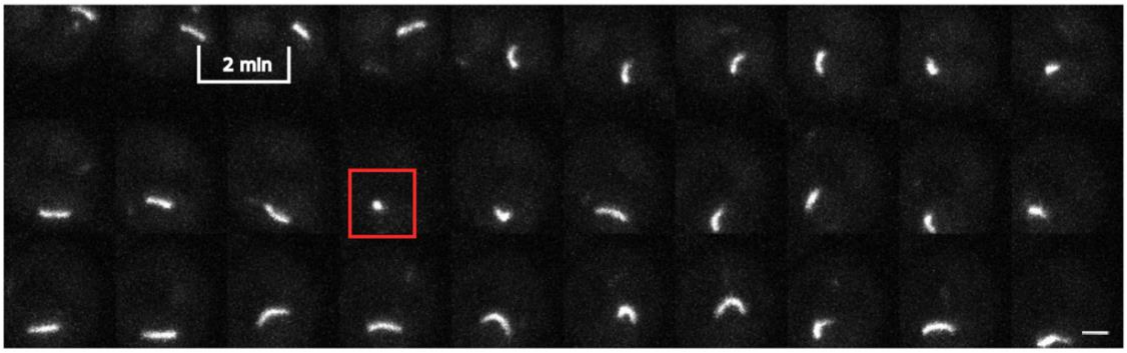

Liu et al., Figure S4C-D-E-F

SecA_Figure S 4 **Dynamics of Rad51 filaments**

A. Examples of time-lapse images in WT and mutants upon DSB, images acquired every 2 minutes, Z-projection is applied

B. Number of frames from Rad51 foci to filaments (>6 pixel) in WT and mutants upon DSB

C-F. Examples of time-lapse images in Rad51-iGFP diploid strain upon DSB, images acquired every 2 minutes, Z-projection is applied (Movie S4-7).

Scale bar: 2µm

2. Section B

2.1 Position relationship between Rad51 filaments and other proteins

Unlike Rad51 that forms filaments during HR, most HR associated proteins were shown to form repair foci. Thus, our observation raises the following question: what is the spatial organization of other repair proteins with respect to Rad51 structures? We wonder if these foci are located outside or inside the Rad51 filaments and if inside, where in the filament? To answer these questions, we have tagged other recombination factors, including Rad52, Rad54, and Rfa1 (the subunit of replication protein A, RPA), in the functional Rad51-sfGFP strain. These unpublished results are presented in the following section.

2.1.1 Rad52 foci and Rad51 filaments

Rad52 is widely regarded as the loader of Rad51: it removes RPA and recruits Rad51 on ssDNA to form nucleofilaments. We have already shown that no nuclear Rad51 focus or filament were visible in the *rad52Δ* strain, suggesting that Rad52 is essential for their formations. To study the relative position of Rad52 foci and Rad51 filaments upon DSB, we obtained a C-terminal tagged Rad52-RFP strain from Lisby (Khadaroo et al.2009). This strain grows significantly slower than WT in the presence of 0.01% of MMS, indicating that the Rad52-RFP is not fully functional (Figure1A line3). We then constructed a double-tagged strain by crossing and dissecting the Rad52-RFP and Rad51-yeGFP strains. This double-tagged strain is even more sensitive than the single Rad52-RFP strain (Figure 1A line 4) and forms only Rad51 foci after DSB induction (Figure 1B). Considering the elongated Rad51 structures in the single-tagged Rad51-yeGFP strain, we guess that the missing of Rad51 filaments might be caused by the unfunctional Rad52-RFP in the double-tagged strain. It is possible that the Rad52-RFP can recruit Rad51 but cannot stabilize the Rad51 filament or counteract the Srs2 activity. Furthermore, the fact that MMS sensitive strains are unable to form Rad51 filaments is a strong indication that functionality is important for forming filaments.

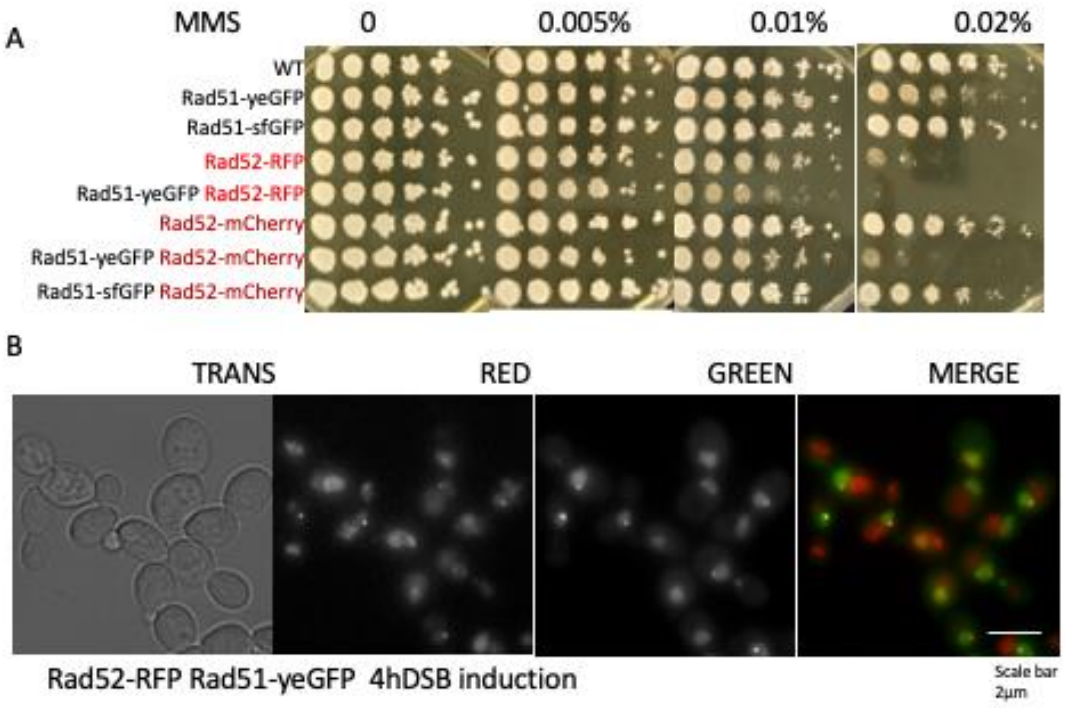

SecB_Figure 1 Rad52-RFP Rad51-yeGFP

A. FL images of Rad52-RFP Rad51-yeGFP strain. Only Rad52 foci and Rad51 foci are observed, no Rad51 filament after 4h DSB induction. B. Spot assay of WT, 2 versions Rad51-intGFP strains, Rad52-RFP, Rad51-yeGFP Rad52-RFP, Rad52-mCherry, Rad51-yeGFP Rad52-mCherry and Rad51sfGFP Rad52-mCherry strains on YPD-MMS plates. Rad51-sfGFP functions better than Rad51-yeGFP and as well as WT. Rad52-mCherry is more benefit than Rad52-RFP. The Rad51-sfGFP Rad52-mCherry is the best choice to study the relationship between Rad52 foci and Rad51 structures.

We thus constructed a Rad52-mCherry strain through CRISP/Cas9, which is also a C-terminally tagged strain with a long linker between Rad52 and the mCherry. As opposed to the Rad52-RFP, this strain shows wild-type sensitivity to MMS (Figure 1A, line 6), so does the Rad52-mCherry Rad51-sfGFP strain (line 8). Rad51 foci as well as filaments are observed in this new double tagged strain with DSB induction (Figure2A). It is noteworthy that Rad51 structures are not systematically associated with Rad52-mCherry foci possibly because of low level fluorescence intensity or photobleaching. We choose the Rad51-sfGFP Rad52-mCherry strain and merely focus on the nucleus present both Rad51 filaments and Rad52 foci, to study the positional relationship.

As shown in the small crops, Rad52 foci are preferentially located at the brighter part of nonhomogeneous Rad51 filaments (Figure2B), this dense part being in the middle or at the end of the filaments. Considering there are 2 ssDNA ends at the broken site and only one Rad52 focus, the 2 DSB ends should be associated together and share the Rad52 focus to load Rad51 and form nucleofilament on ssDNA. The dense part of the filament associated with the Rad52 focus could correspond to the root of several NPF while the distant part could correspond to only one filament.

Alternatively, the dense part could correspond to a partially compacted filament. Two color time-lapses are required to understand better the relationship between Rad52 foci and Rad51 filaments.

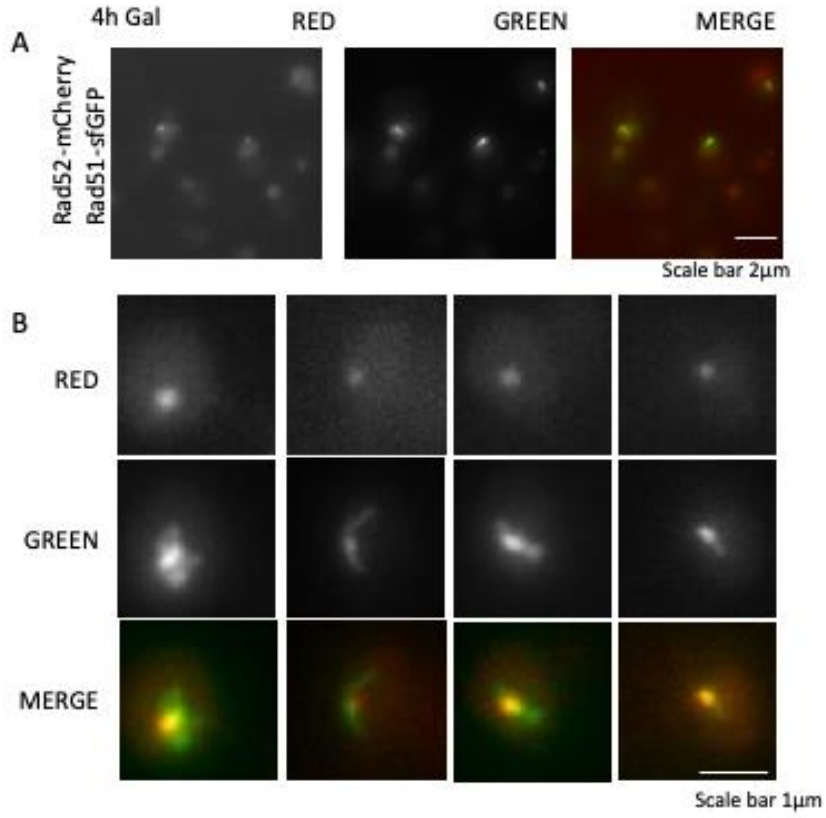

SecB_Figure 2 FL images of Rad52-mCherry Rad51-sfGFP

A. Rad51 can form filaments in the Rad52-mCherry Rad51-sfGFP strain. B. Rad52-RFP foci locate at the bright part of the Rad51 filaments

2.1.2 Rad54 forms similar structures as Rad51

Rad54 is crucial for Rad51-mediated synaptic complex formation and homology search. The Rad54 ATPase not only prevents the non-productive intermediates, but also forms a functional unit with Rad51 for homology search, synaptic complex, and D-loop formation (Tavares et al. 2019). The negative effects of Rad54 on Rad51 filaments have been studied by deleting *RAD54* in the Rad51-sfGFP strain. Former studies observed Rad54 with the non-fully functional Rad51 or Rad52 tagged proteins (Lisby and Rothstein 2004, Tan et al. 1999, van Veelen et al. 2015), which prevent the formation of Rad51 filament (see above). So, how is the Rad54 structure and its location in the presence of Rad51 filament?

Therefore, we constructed a Rad54-mCherry Rad51-sfGFP strain through CRISPR/Cas9 to investigate the distribution of Rad54 during HR. This strain grows as well as Rad51-sfGFP on MMS plate (Figure 3A, line3), showing the functionality of Rad54-mCherry.

Previous studies have reported that Rad54 form foci with analogous appearance than other repair proteins such as Rad52 (Lisby and Rothstein 2004). While in our strain, we found that the Rad54-mCherry can form structures with shapes similar to the corresponding Rad51 filaments (Figure3B). Compared with the Rad51 filaments, these Rad54 structures are mostly shorter, weaker, and not visible in all nuclei (Figure3C). When we colocalized the red and green channel together, the Rad54-mCherry coats part of the Rad51 filaments. To exclude channel crosstalk caused by the leaking of the GFP signal in the red channel, we constructed strain only expressing Rad54-mCherry and observed similar structures. Taking the function of Rad54 in the former research into consideration, the Rad54 might motor the homology search through attaching on Rad51 filaments (Heyer et al.2006). However, only less than half Rad51 filaments are associated with a similar Rad54 structure. We propose two explanations for the lack of Rad54 structures: the mCherry signal is too weak to be observed in some nucleus; or the Rad54 only recruits around Rad51 at a specific stage during homology search. Monitoring the localization of Rad54 and Rad51 over time after DSB induction would be necessary to answer this question.

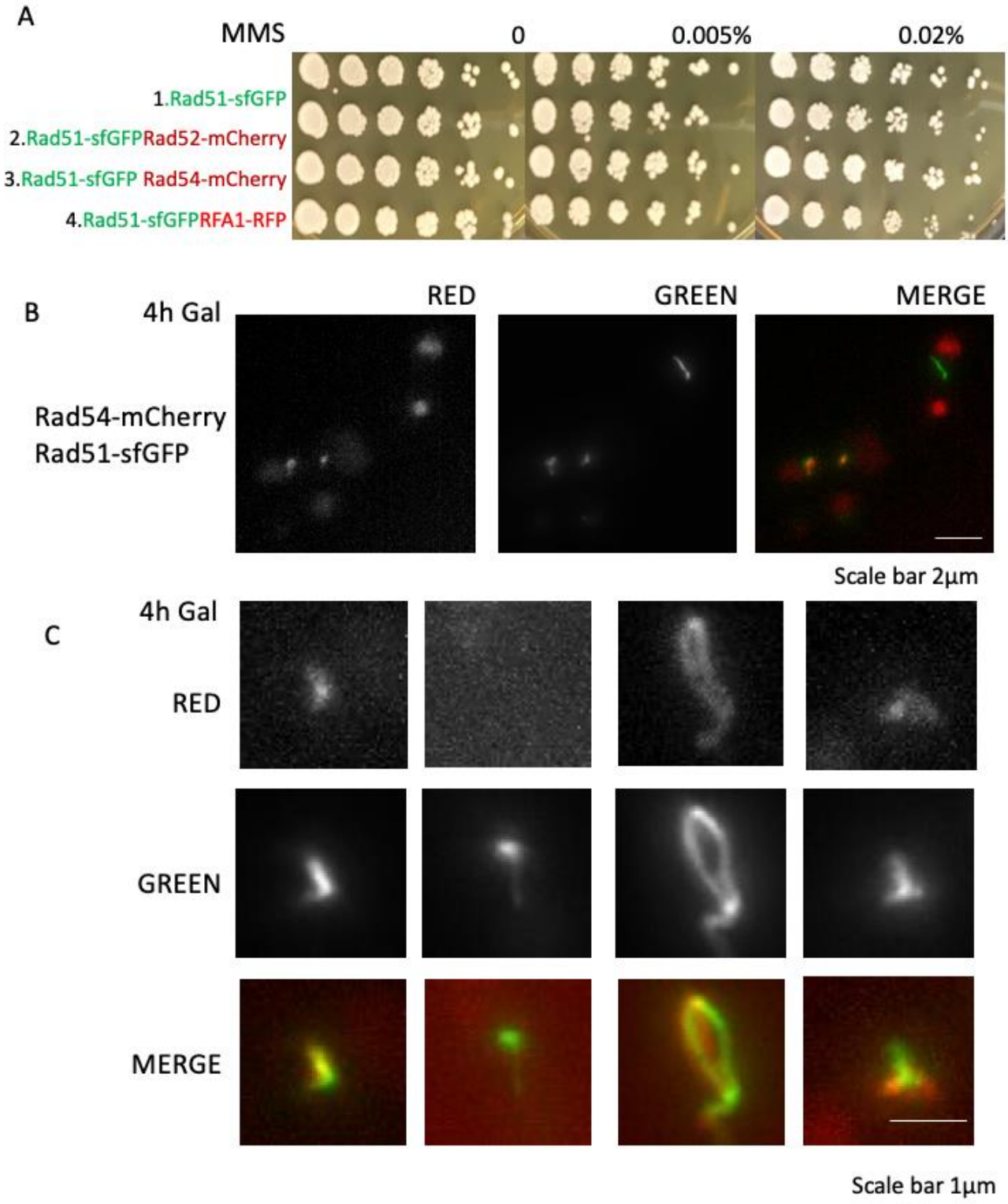

SecB_Figure3 Rad54-mCherry and Rad51-sfGFP strain.

A. Spot assay of Rad51-sfGFP, Rad51-sfGFP Rad52-mCherry, Rad51-sfGFP Rad54-mCherry and Rad51-sfGFP RFA1-RFP on MMS plates B. GFP, RFP and composite images Rad51-sfGFP Rad54-mCherry strain after inducing DSB for 4h C. Crops of Rad51-sfGFP filaments and Rad54-mCherry structures after inducing DSB for 4h.

2.1.3 RFA1 foci and Rad51 filaments

Replication protein A (RPA) is a heterotrimeric single-stranded DNA-binding protein, that is highly conserved in eukaryotes. RPA plays essential roles in many nucleic acid metabolisms, including DNA replication, nucleotide excision repair and HR (Iftode et al. 1999), where it binds ssDNA. In S phase, Rfa1, the subunit of RPA, localizes to small, speckled foci that associate with replication centers and colocalize with PCNA (Wang et al. 2020) and also binds to ssDNA that may be engaged in HR events (Lisby et al. 2004).

We have constructed a Rad51-sfGFP RFA1-RFP strain, which shows a mild defect on MMS plate compared with WT (Figure3A). After inducing DSB for 4h, there is one bright focus or several weaker foci in the cell (Figure4A). We quantified that most nuclei have several spontaneous spots in the absence of DSB, while 20% nuclei after 2h and 36% nuclei after 4h DSB induction have only one bright focus, suggesting the only source of ssDNA is the DSB at these points as the S phase has proceeded during this time.

The bright Rfa1-RFP foci can localize at both the middle and at the end of Rad51 filaments (Figure4B). Our preliminary observations suggest that when the Rad51 forms a homogeneous filament, the Rfa1 foci are located in the middle of it. While in the inhomogeneous structures, the Rfa1 foci is preferentially found at the brighter part of Rad51 filaments. In the case of one node branched Rad51 structures, Rfa1 foci are often found at the node. If DSBs are induced after DNA replication, both sister chromatids are cut and there are 4 broken ends, which will be resected to form 4 long ssDNA. Therefore, we can expect up to 4 Rad51 filaments within one nucleus (Figure4C). Figure 4B shows how we interpret the different possible organization of the filaments with respect to the Rfa1 focus. More quantification is needed to draw definitive conclusions.

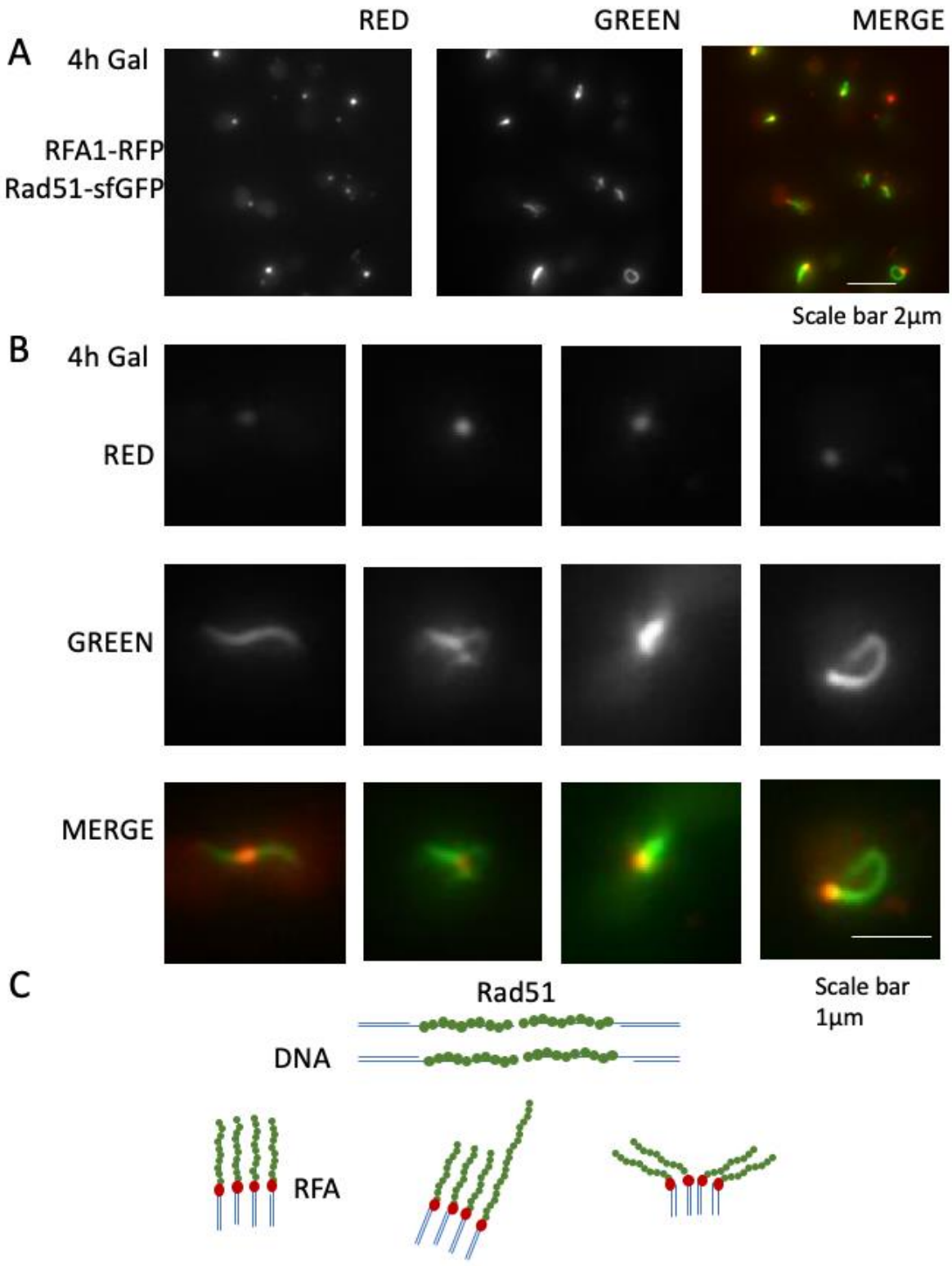

SecB_Figure 4 Rad51-sfGFP and Rfa1-RFP

A. RFP, GFP and composite FL images of Rad51-sfGFP and RFA1-RFP strain after 4h DSB indcution B. Crops of Rad51 filaments and Rfa1 foci C. Schemes to show the possible position relationship between Rad51 and Rfa1

2.2 Impact of Rad51 regulator on Rad51 structures in living yeast

2.2.1 Rad55-Rad57 stabilize Rad51 filaments

Rad55-Rad57, the paralogs of Rad51, were shown to be the positive regulators of Rad51 filaments (Heyer et al.2010). The *rad57Δ* has been constructed to check its impact on the Rad51 filaments we observe in living cells. Four hours after DSB induction, Rad51-sfGFP only form foci or very short structures (Figure 5). Through ilastik quantification (Figure 6), we estimate that 14.7% of nuclei harbor Rad51 foci, 7.7% globular structures and 7.4% filaments after 4h DSB induction in the *rad57Δ* strain. Compared with more than half of the nuclei forming filaments in the wildtype strain after 4h DSB induction, it suggests that the Rad55-Rad57 have a positive effect on filament elongation or stability.

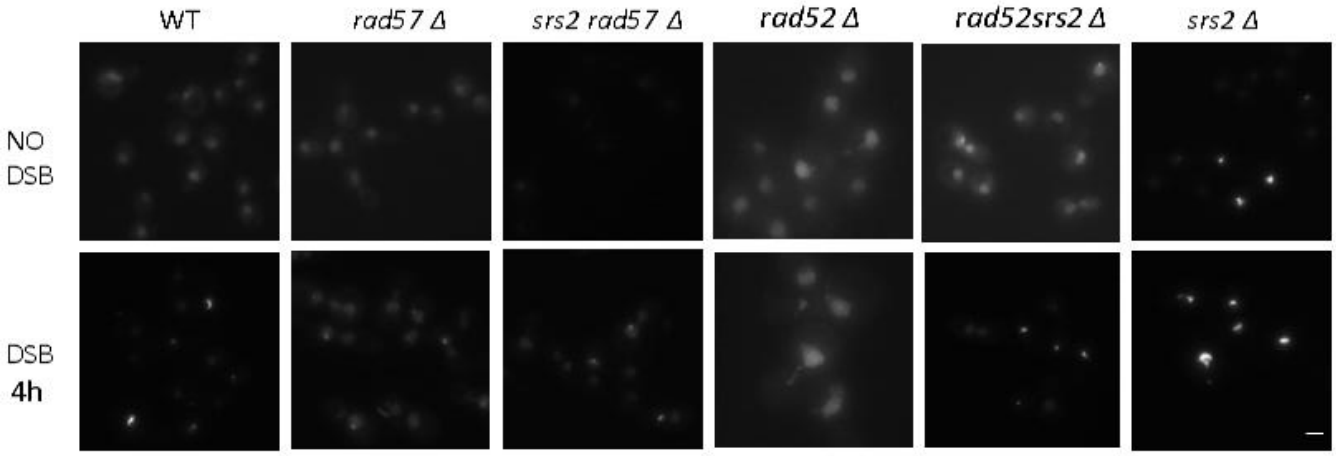

SecB_Figure 5 Rad51-sfGFP in *srs2rad57Δ* and *srs2rad52Δ strain.*

Inducing *DSB in the WT and mutants for 4h*

In the last part, we have already shown that the Srs2 helicase is a negative modulator of Rad51 filament in living cells: spontaneous Rad51 structures are observed in the *srs2Δ* strain. We wonder if the Rad55-Rad57 paralogs work against the Srs2 helicase or work independently. Therefore, we constructed the double-deleted strain. No more spontaneous Rad51 structures is observed in the *srs2rad57Δ* strain (Figure5). Therefore, the Rad55-Rad57 complex is required for the spontaneous structures to form in the absence of Srs2. The positive effect of Rad55-Rad57 on Rad51 filaments has been proven, but we don't know whether Rad55-Rad57 prevents the dismantling or favours the formation of filaments, which requires further investigation with an inducible system. In the presence of DSB for 4h, the double-deleted strain can form more and longer Rad51 structures than the *rad57Δ* strain (Figure5 and Figure6) but still less than the *srs2Δ* and WT strain; in other words, the deletion

of *RAD57* can partially rescue the *srs2Δ* strain. We thus conclude that the Rad55-Rad57 complex stabilizes Rad51 filaments by working against Srs2 as well as independently of Srs2.

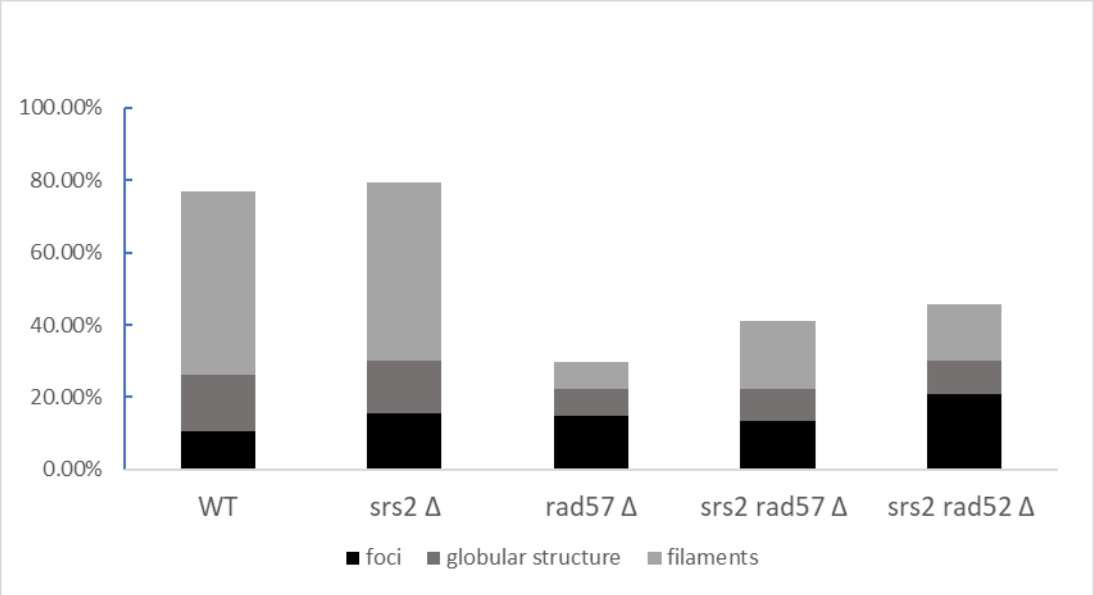

SecB_Figure 6 Quantification of the double mutants

Quantification through Ilastik, the percentages of Rad51-sfGFP foci, globular structures and filaments in wildtype strain and mutants after inducing DSB for 4h

2.2.2 Rad52: the loader and the protector of Rad51 filaments

We already showed that Rad52 is necessary for the formation of Rad51 filaments as no Rad51 structures are detected in *RAD52* deleted cells even after 4h DSB (Figure5). However, it has been shown that Rad54 and Rad51 can still form foci in a *rad52Δ srs2Δ* strain expressing a non-fully functional Rad51 tagged protein, which doesn't form recombinant proficient Rad51 filaments (Burges et al. 2009). We thus decided to test whether this would also be the case with our functional Rad51-GFP version in the *rad52srs2Δ* strain.

When we deleted both *RAD52* and *SRS2*, Rad51 structures are observed with or without DSB induction (Figure5), in agreement with the study that interaction between Rad51 and Rad52 is dispensable for Rad52 mediator function (Krejci et al.2002, Burges et al.2009). The existence of Rad51 structures suggests that the Rad52 is not the only loader of Rad51 during HR, and we hypothesize the paralog of Rad52, Rad59, might be involved in the process of Rad51 recruitment. Another explanation is that Rad52 is not essential for loading Rad51 on RPA coated ssDNA. The Rad51 filaments are independent of the loader during HR but requires Rad52 as a regulator to counteract the dismantling activity (Ma et al. 2018). That's why there are Rad51 structures in *srs2rad52Δ* strain but none in *rad52Δ* strain.

There are around 25% nuclei with Rad51 filaments in the *srs2rad52Δ* strain (Figure 6) when DSB is induced, and spontaneous Rad51 structures are weaker in the double mutant strain than in the *srs2Δ* strain. Thus, Rad52 has a very important role in counteracting Srs2 activity which is in good agreement with previous work (Ma et al, 2018). Rad52 can stabilize Rad51 filaments independently of the Srs2 helicase like Rad55-Rad57. Indeed, most spontaneous Rad51 structures disappear after deleting Rad52 in the *srs2Δ* strain. Since the *rad52Δ srs2Δ* strain have more and brighter filaments than the *rad57Δ srs2Δ* strain, we conclude that the Srs2 independent stabilizing activity of Rad52 is less important than the one of the Rad55-Rad57 paralogs.

We also tested the impact of the Rad52 partially functional allele of Rad52-SUMO on Rad51 filament *in vivo* (Figure7). Rad52-SUMO bypasses the requirement for Srs2 specifically for the prevention of toxic Rad51 filaments and cannot restore viability of *srs2*Δ cells that accumulate intertwined recombination intermediates which are normally processed by Srs2 post-synaptic functions. Remarkably, the *srs2Δ* cells are less sensitive to DNA damage by replacing Rad52 by a Rad52-SUMO fusion protein. Therefore, the sumoylation modifies Rad52 activity thereby changing the properties of Rad51 filaments (Esta et al. 2013).

Consistent with this hypothesis, cells expressing Rad52-SUMO Rad51-yeGFP can form foci but can't form long filaments. While long Rad51 filaments are observed with or without DSB induction in the Rad52-SUMO *srs2Δ* strain. This indicates that the Rad51 filaments produced by the partially functional Rad52 are more sensitive to Srs2 than the one formed by the wildtype allele.

To conclude, Rad52 is not only the loader of Rad51 during HR, but also protect Rad51 filaments by counteracting Srs2 activity. Besides Rad52, there might be other unknown recombinase loaders of Rad51 when Rad52 is missing, which is worthwhile to study.

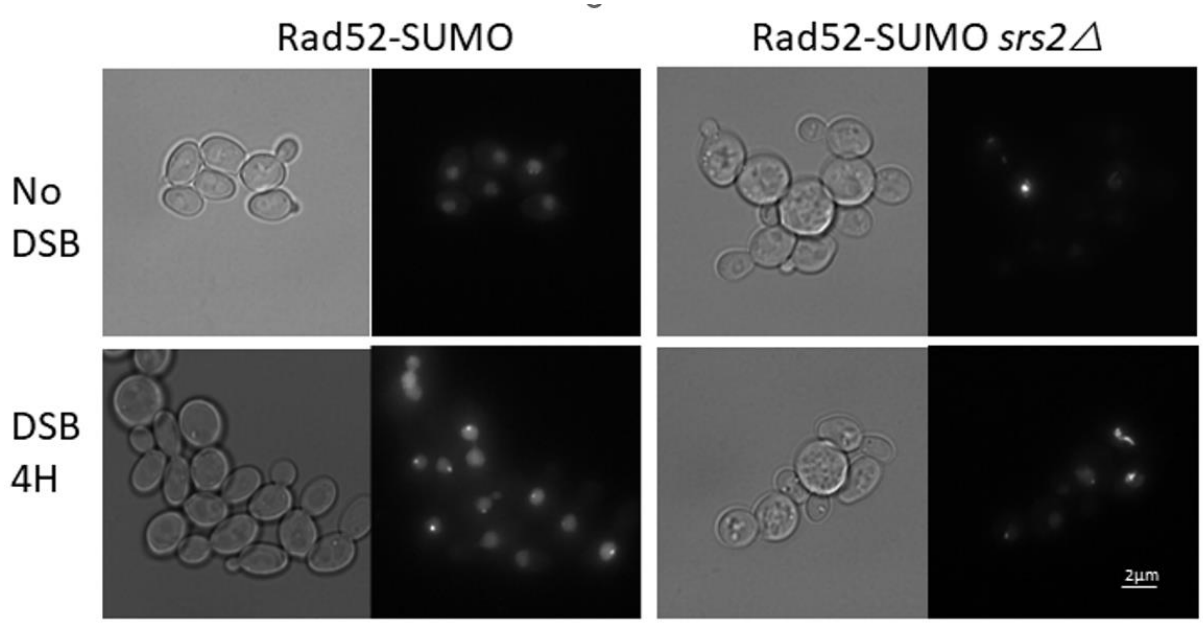

SecB_Figure 7 Rad52 -SUMO

FL and trans images of Rad52-SUMO strains after 0 and 4h DSB induction

2.2.3 Rdh54, the Rad54 paralog

Both *RAD54* and *RDH54* are *RAD52* epistasis group genes and belong to the Swi2/Snf2 protein family. It is said that *RAD54* serves a more prominent role than *RDH54* in mitotic DSB repair, intra-chromosomal recombination, and sister chromatid-based recombination, whereas *RDH54* is more relevant to inter-homologue recombination in both mitotic and meiotic cells. In budding yeast, Rdh54 can also interact with Rad51 and catalyze Rad51 removal from DNA through *in vitro* study (Chi et al.2006). To observe this effect in living cells, we deleted *RDH54* in the Rad51-sfGFP strain and observed spontaneous Rad51 structures in the absence of DSB (Figure8). Unlike Rad54 or Srs2, there are several Rad51 foci within one nucleus and these foci exist in nearly all nuclei, which cannot be explained by spontaneous DSB. So, we hypothesize that Rad51 would attach on ssDNA during DNA replication or transcription but are rapidly removed by Rdh54. When a DSB is induced, a long Rad51 filament is observed in some nuclei along with several foci. I thus conclude that Rdh54 catalyzes the Rad51 removal independently of DSB and HR.

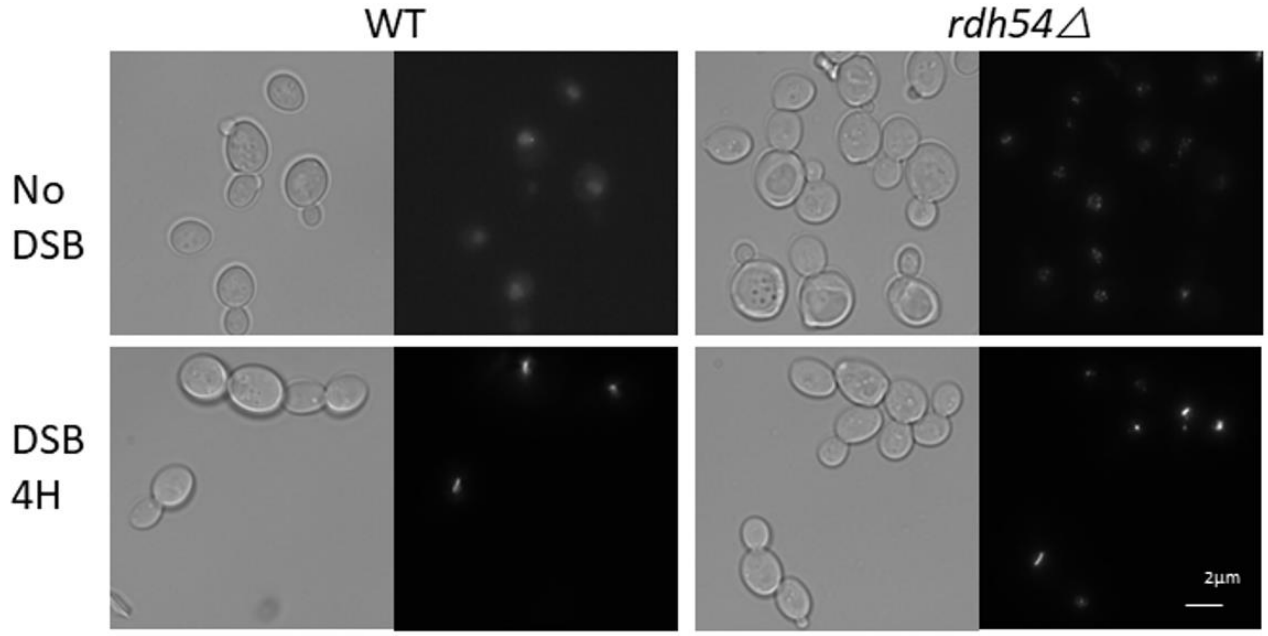

SecB_Figure 8 FL images of rdh54*Δ* strain

FL and trans images of rdh54*Δ* strain after 0 and 4h DSB induction

2.2.4 The SHU complex

The SHU complex, including Csm2 and Psy3, is thought to positively regulate the Rad51 filaments through interacting with Rad55-Rad57. However, the *csm2Δ* strain is capbale of forming Rad51-yeGFP filaments as WT strain after inducing DSB for 4h (Figure9). The effects of Csm2 and Psy3 is thus vastly weaker than Rad55-Rad57. Interestingly, the *csm2srs2Δ* strain shows a decline in the number of spontaneous Rad51-yeGFP structures compare to the *srs2Δ* strain, suggesting that the SHU complex might be required for these spontaneous structures to occur. This could point to a specific role of the SHU complex during replication (Ball et al. 2009). As shown in Figure 10, the *csm2srs2Δ* strain has slightly more Rad51-yeGFP filaments than *csm2Δ* strain but less than *srs2Δ* strain (N>300). This result indicates the function of SHU complex against Srs2 during HR and requires repeats in Rad51-sfGFP strain to draw a convincible conclusion.

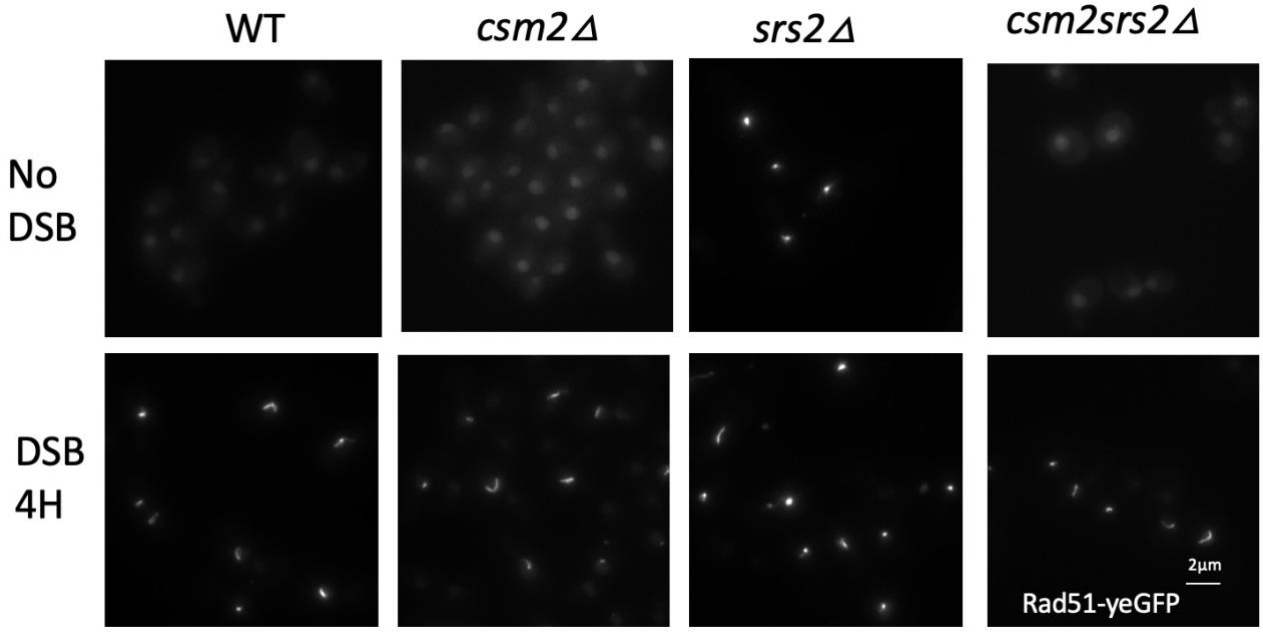

SecB_Figure 9 Shu complex on Rad51 structures

FL and trans images of Rad51-yeGFP WT, *csm2Δ*,*srs2Δ* and *csm2srs2Δ* strain after 0 and 4h DSB induction

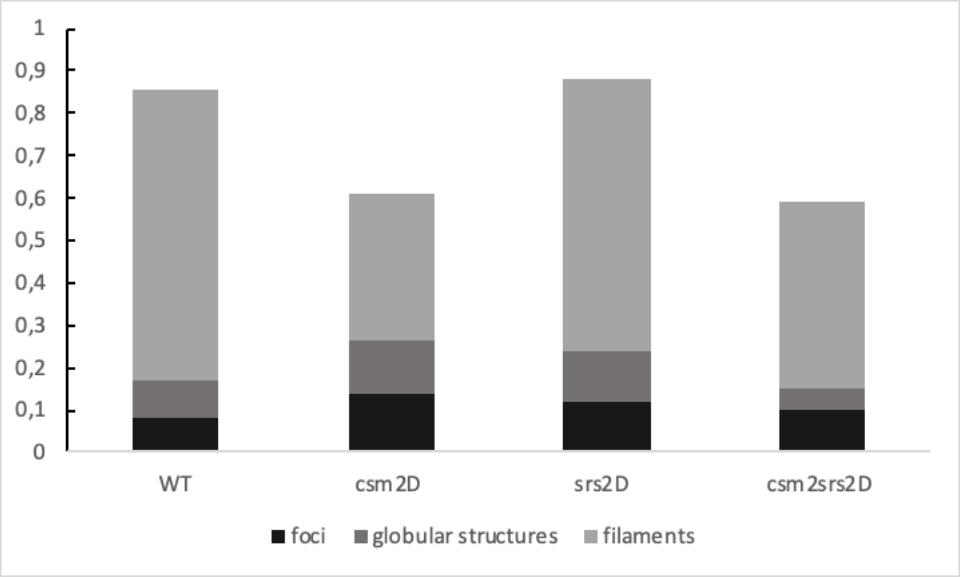

SecB_Figure 10 Quantification of the Shu complex mutants

The fraction of Rad51-yeGFP foci, globular structures and filaments in wildtype strain and mutants after inducing DSB for 4h (N>300).

2.3 Rad51 structures upon replication stress.

Hydroxyurea (HU) causes replication stress by limiting the generation of dNTP pools. We first add 0.2M HU in the Rad51-yeGFP strain and detect no particular Rad51 activity. To make sure that the HU does work, we quantify the percentages of cells in different stages, and confirm that around 78% of cells accumulate in the G2 phase after 4 h 100mM HU treatment *versus* 11% of G2 cells in control. Cells did not show Rad51 structures under the circumstances of HU treatment. However, when we release cells in YPD for another 1h after HU treatment, structures appear in the nucleus (Figure11 A), 51% of nuclei have several foci, and 8% have filaments. This result is congruent with the sensitivity or *rad51Δ* strain to HU treatment. The cells continue their cycles after the recovery in YPD medium and generate ssDNA due to the lack of dNTP, serving as substrate for Rad51.

Mrc1 and Tof1 are two factors ensuring the DNA helicase and polymerase coupling at replication forks. When one of these factors is missing, ssDNA accumulates ahead of replication forks (Katou et al. 2003) upon HU treatment. In these conditions, we observe several Rad51 structures within S-phase nuclei (Figure11B), with more than 60% of cells showing several Rad51 structures after a 90 min HU treatment in the *mrc1Δ* or *tof1Δ* strains. We can assume that without Tof1 or Mrc1's inhibition on replication folk, DNA continues uncoupling to generate long ssDNA segments, leading to the Rad51 recruitment and formation of Rad51 structures.

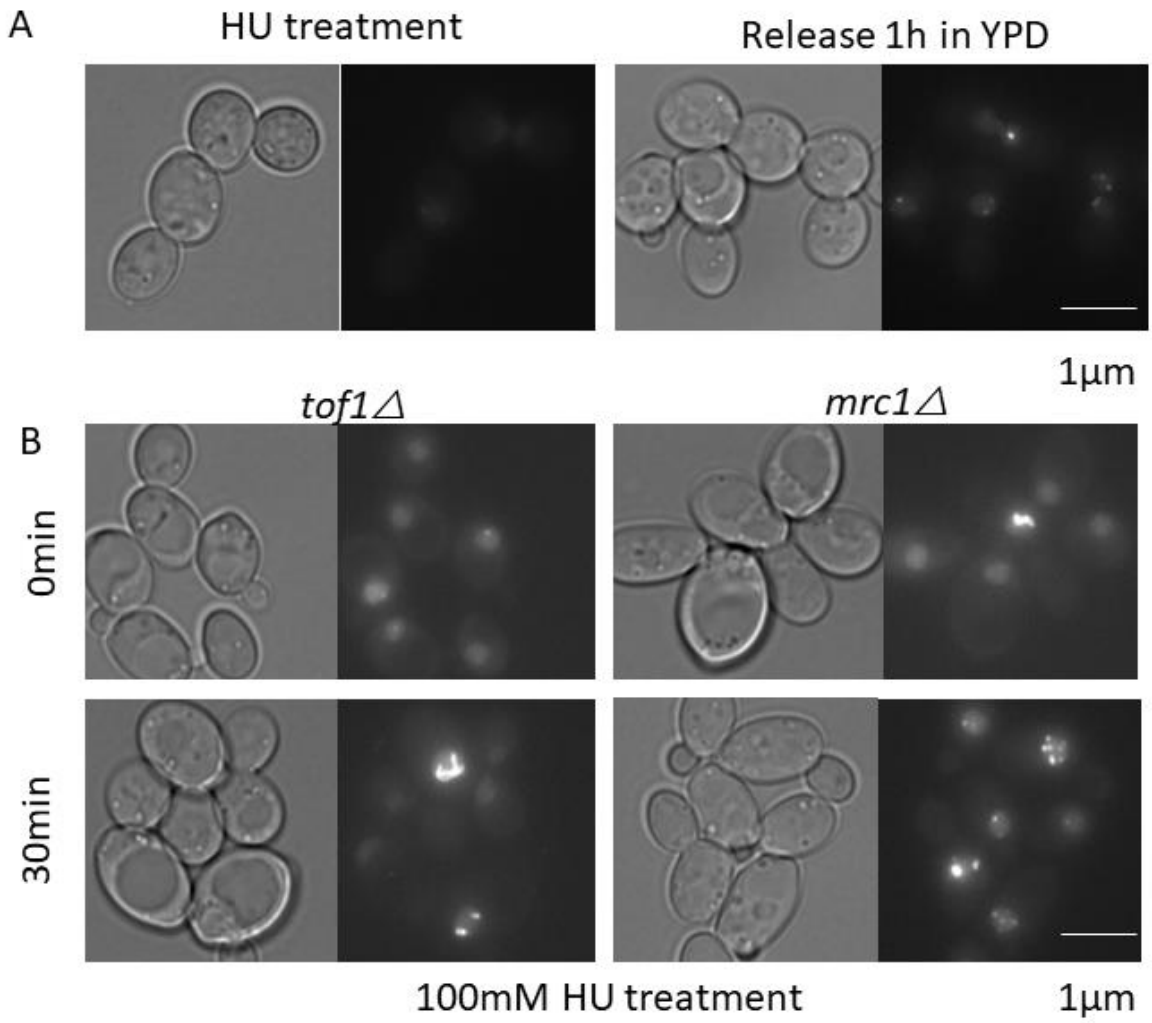

SecB_Figure 11 Rad51-yeGFP upon replication stress by HU

A. FL and trans images of cells after 1h 100mM HU treatment, and another 1h recovery in YPD medium B. FL and trans images of cells after 0 and 30min HU treatment in the *mrc1Δ or tof1Δ* strain.

III. METHODS

Design of the Rad51 GFP insert

A multiple sequence alignment of *S. cerevisiae* Rad51 (RAD51_YEAST) was generated using HHblits against the UniRef30 database and secondary structure were predicted using PsiPred from this MSA. A structural model of full-length Rad51 was generated using the RaptorX server (Kallberg et al. 2012) and used as a basis to map the evolutionary rates which were estimated using the Rate4Site algorithm[3] and the Rad51 MSA. Secondary structure predictions obtained from the RaptorX server suggests that the N-terminal end of *S.c.* Rad51 harbors some helical propensities with a few positions slightly conserved. These features could be due to functional constraints that account for the poor functionality of the N-terminal tagged versions of Rad51 tested so far. To identify a more favorable insertion site, we analyzed the MSA looking for a more flexible and variable region. The site between Gly54 and Gly55 fulfilled these criteria and a first version of a tagged Rad51, named Rad51-iGFP1, was generated using two 11-residues flexible linkers flanking the GFP of sequence 'GGAGSAGGAGG-GFP-GGAGSAGGAGG'. The promising results obtained for that first construct prompted us to further optimize the sequence of the linkers. We reasoned that to reduce as much as possible the influence of the acidic tag on the properties of the Rad51 filament, we could increase further the length of the linker and add positively charged residues in the vicinity of the GFP-tag. This led to the design of the Rad51-iGFP2 construct with two 16-residues flexible linkers with the following sequence 'GGAGSAGGAGNRKRNG -GFP- GNRKRNGAGSAGGAGG'. The structural model of the filament was built using the structure of *S.c.* Rad51 (Conway et al. 2004) (PDB: 1SZP). The Pymol software was used to draw the different structures [PyMOL, The PyMOL Molecular Graphics System, Version 2.0 Schrödinger, LLC].

Strain and plasmid construction

All strains are derivatives of W303. Gene deletions, insertions of alternative promoters and gene tagging were performed by PCR-base gene targeting, except Rad51-iGFP strains. For Rad51-iGFP strains, the internal tagging of Rad51 between the 54th and 55th amino acid was obtained using the CRISPR-Cas9 technique. A guide rDNA obtained by hybridization of primers oAT2449 and oAT2450 was inserted into the pRS425-Cas9-2xSap1 (Kind gift of Bruce Futcher, State University of New York, Stoney Brook) yielding pAT569. The Rad51-iGFP strains were obtained by co-transformation of pAT569 together with a donor sequence that contained *RAD51* homologous sequences on either side

of a fluorescent tag flanked by identical linkers (11 amino acids for the Rad51-iGFP1 and 16 amino acids for Rad51-iGFP2). The donor for the Rad51-iGFP1 strain was generated by PCR on the yeGFP sequence of pYM25 with primer oAT2334 and oAT2335. The donor of the Rad51-iGFP2 strain was generated by PCR on pAT624 (a fragment of Rad51-isfGFP: synthetic construct from Genescript, this study) with primer oAT558 and oAT2401.

List of strains and primers used in this study can be found in Supplemental Table 1 and 2.

Viability assay

Strains were grown overnight in YPD and plated in fivefold serial dilutions starting at OD_{600nm}=1 on YPD plates containing 0%, 0.005%, 0.01% and 0.02% MMS (Methyl methanesulfonate). Plates were then incubated at 30°C for 48h.

Gene conversion experiment

Strains were grown overnight in YPA+3%Raf medium, and diluted to $OD_{600nm}=10^{-4}$. 100µl culture (corresponding to 100 cells) was plated separately on YPD and YP 2% galactose plate for 48h incubation at 30°C. Gene conversion efficiency was calculated by the number of colonies on YP-Gal plate divide by the corresponding number on YPD plate.

Immunofluoresence

A total of 20 OD_{600nm} equivalent cells was fixed in 0.9% paraformaldehyde (Sigma-Aldrich) and incubate at 30°C for 15min. Samples were centrifuged, washed twice with H_2O, and resuspended in 1.25ml solution (0.1M EDTA-KO, 10mM DTT, pH=8.0) for 30 min incubation with a gentle agitation. After centrifugation, the pellets were resuspended in 1.25ml YPD-Sorbitol (1.2M) and 15µl zymolyase-100T. Cells were incubated at 30°C and their shape was checked every 5 min by microscopy (transmitted light). The reaction was stopped by adding 40ml YPD-Sorbitol when cells became round and didn't reflect anymore. The spheroplasts were washed twice with YPD-Sorbitol and finally resuspended in YPD without sorbitol. Cells were dropped on microscope slides (Polylabo, super-teflon slides) and and air dried for 3 min. Then, slides were put in methanol for 6 min and acetone for 30s at -20°C. After 3min air dry, the slides were incubated in 1xPBS with 1%BSA and 0.1%Triton X-100 for at least 20 min. Spots were covered by 1xPBS with 0.1% Triton X-100, anti-Rad51 antibody (PA5-34905 ThermoFischer, 1/500), and 1h incubation at 37 °C. After 3 washes in 1xPBS

with 0.1% Triton X-100, the slides were dried and covered by Invitrogen goat anti-rabbit IgG(H+L) cross-adsorbed secondary antibody (Alexa fluor 568, catalog #A-11011, 1/100 in spheroplast suspension). After 1h incubation at 37°C and three times wash with 1xPBS,0.1% Triton X-100, nuclei were dyed with 1x DAPI (in 1xPBS) for 5min. After 2 washes with 1xPBS, 15µl antifading (DABCO, pH7.5) was added to each spot. Slides were covered with a cover slip and stored at 4°C in the dark.

Western blot.

Cell lysates were extracted by the TCA method and 10min vigorous vortex at 4°C. After centrifuging, the pellets were resuspended in TCA-Laemmli loading buffer (120 mM Tris base, 3.5 % sodium dodecyl sulfate (SDS), 8 mM EDTA, 5 % β-mercaptoethanol, 1 mM PMSF, 15 % glycerol, 0.01 % bromophenol blue). Samples were incubated at 95°C for 10min. For immunoblotting, a polyclonal antibody anti-Rad51 (PA5-34905 ThermoFischer) was used at 1:3000.

ChIP and quantitative PCR analysis

A total of 20 OD_{600nm} equivalent cells was fixed in 0.9% formaldehyde for 15 min at 30°C, and quenched with 0.125M glycine for 5 min. The following steps were done at 4°C, unless indicated. After washing in cold 1x TBS, the pellets were resuspended in 1 mL 1x TBS. After a second centrifugation, the pellets were frozen in liquid nitrogen and stored at -80°C. The pellets were suspended in 500 µl cold lysis buffer (0.01% SDS, 1.1% Triton X-100, 1.2 mM EDTA pH8, 16.7mM Tris pH8, 167mM NaCl, 0.5% BSA, 0.02 g/L tRNA, and 2.5 µl of protease inhibitor from Sigma-Aldrich P1860, Sigma-Aldrich, St. Louis, MO, USA), then 500µl 0.5mm zirconium beads were added. Cells were broken usingFASTPREP (MPBiomedicals) machine with maximum intensity for 30s, repeated 3 times with 3 min pause on ice. Samples were incubated 10min on ice and sonicated by Biorupter XL (Diagenode) for 14 min, high power with on and off cycles 30s. The extracts were centrifuged for 5 min at 12,000 rpm. 10µl supernatants were kept at -20°C as input, while 2µl polyclonal antibody anti-Rad51(PA5-34905 ThermoFischer) were added into the remaining lysates overnight incubation. The next day, 50 µL of magnetic beads protein A (NEB) was added to the extracts / antibody mixture and incubated for 4 h at 4 °C on a rotating wheel. Then, the magnetic beads with the immunoprecipitated material were washed sequentially once with lysis buffer, twice with RIPA buffer (0.1% SDS, 10 mM Tris pH 7.6, 1 mM EDTA pH8, 0.1% sodium deoxycholate, and 1% Triton X-100), twice with RIPA buffer supplemented with 300 mM NaCl, twice in LiCl buffer (250 mM LiCl, 0.5% NP-40, 0.5% sodium

deoxycholate), once with 1× TE 0.2% Triton X-100, and a final was in 1× TE. The beads were then resuspended in 100 µL of elution buffer and placed in an incubator at 65 °C with gentle agitation to elute the immunoprecipitated material from the beads. In the meantime, the inputs were diluted 1/10 with elution buffer. A reversal cross-linking was performed by heating the samples, inputs and IP, overnight at 65 °C. Proteins were digested with Proteinase K (0.4 mg/mL) in the presence of glycogen, and the remaining DNA was purified on QIAquick PCR purification columns. Finally, samples were treated with 29 µg/mL RNase A for 30 min at 37 °C and used for quantitative PCR.

ChIP quantification was performed by quantitative PCR (qPCR) either on the 7900HT Fast Real-Time PCR (Applied Biosystems, Waltham, MA, USA) or on the QuantStudio 5 Real-Time PCR System (Applied Biosystems, Waltham, MA, USA). Sequences of interest were amplified using the SYBR Green PCR Master Mix (Applied Biosystems, Waltham, MA, USA) and the primers listed in Supplementary Table S2 on a dilution of immunoprecipitated DNA at 1/40 and 1/80 for the input DNA. PCR reactions were conducted using the following program: an initial denaturation at 95 °C for 10 min followed by 40 cycles (95 °C for 15 s and 60 °C for 30 s). Each real-time PCR reaction was performed in triplicate. The signal from a given region was normalized to the one from the OGG1 control locus in immunoprecipitated and input DNA samples. Plots represent the mean value obtained for at least three independent experiments and normalized by WT, error bars correspond to the SEM.

Microscopy

Yeast cells were grown in rich medium (YPD) overnight to early log-phase. To induce a single DSB at the I-*Sce*I cut-site, cells were grown overnight in YPA Raf3% medium (yeast extracts, peptone, 3% Raffinose, 0.008 % Adenine HCl) and diluted to OD_{600nm}=0.2 the next morning in the same medium. After 2h, galactose was added directly to the culture to reach a final concentration of 2%. Before microscopy, cells were rinsed with complete synthetic medium (2x final concentration pf CSM, MPBIO-101) and 3% Raffinose and placed on a 1.4% agarose patch for microscopy. For all fluorescent images, images were acquired in 3-dimensions with a z-step of 200nm: images shown are a maximum intensity projection of the z-stack images. Images were acquired on an inverted wide-field microscopy (Nikon TE2000) equipped with a 100x/1.4 NA immersion objective and a C-mos camara. A xenon arc lamp (Sutter Instrument Co. Lambda LS) and a spectra X light engine lamp (Lumenor) were used to illuminate the samples.

Time-lapse microscopy

For time-lapse microscopy, cells were grown overnight in complete synthetic medium (2x final concentration of CSM (yeast nitrogen base; MP Biomedicals) supplemented with 3% Raffinose. Cells were diluted to OD_{600nm}=0.2 the next morning in the same medium. After 2h, galactose was added directly to the culture to reach a final concentration of 2%.

50µl of cells with OD=0.4 (diluted in the original filtered medium) were transferred to the microfluidic yeast plate (CellASIC Onix, using Y04C-02-5PK plates for haploid strains: and Y04D-02-5PK plates for diploid strains). The plates were driven by the Onix microfluidic perfusion system. We loaded the cells into the chamber in 15s = and set the flow pressure at 13.8kPa (2psi) during acquisition.

Time-lapse movies were acquired on a spinning-disk confocal microscopy equipped with a spinning-disk unit (Yokogawa CSU-X1), a Nikon Ti2000 statif, a 100x/1.4NA oil immersion objective and an EM CCD camera (ANDOR iXON DU-8850). The microscope is driven by MetaMorph software, and images were acquired every 2 or 5 minutes in 3-dimensions with z-steps spaces by 300 nm. The images shown in the figures are maximum intensity projections of the z-stacks.

Quantification of filament length

Filaments were cropped to 50x50 pixel size images and deconvolved using the Meinel algorithm in MetaMorph (eight iterations; sigma =0.8; frequency 3; MDS Analytical Technologies). The length quantifications were performed in 3-dimensions using a home-made macro: the segmentation is based on an automatic image thresholding using the Ostu method.

. The intensity of the filaments was calculated after segmentation of the sum-projection images. All programs are available upon request.

Alignment of 2-color images

To align 2-colors images (GFP and RFP), we used a strain harboring the SPB tagged with 2 different proteins (green:SPC110-YFP::HIS3; red:SPC42-mCherry::KanMX) to estimate the shift between the 2 channels. Images from panel 1-H and supplementary figure 3 were aligned using this method.

Quantification through machine learning

2 ilastik (1.3.2 post1) projects were used to quantify the percentages of Rad51 structures, using a pixel and an object classification. At least 10 images were used for training. After segmentation on z-projection images, simple threshold (0.44, with 0.7 and 0.7 smooth) was applied on nuclei to count the total number of nucleus. Hysteresis threshold (core 0.7, final 0.85, smooth 0.5 and 0.5) was done

on nucleus as well as Rad51 signal to classify Rad51 structures. Object features (shape, diameter, length of skeleton and intensity distributions) were used in both projects.
For intensity quantification, 3D filaments stacks (50x50 pixel) were input and possessed by a simple threshold (0.6, with 0.8 and 0.8 smooth). Size in pixels, mean intensity and total intensity were chosen for classification and output.

Models of search

In this section we estimate times of homology search using both simple theory and simulations from Leonid (Mirny et al.2009). We consider the following three mechanisms of search: (1) two compact chromosomal loci search for each other within the nuclear volume; (2) one compact chromosomal locus and a static filament; and (3) one locus and a dynamic filament. In all cases we assume that compact loci are much smaller than the nuclear volume (~50-100nm), and move with the Rouse diffusion, further confined within a spherical nuclear volume. Rouse diffusion $MSD = At^{0.5}$ of chromosomal loci have been now well-established in yeast and multicellular organisms, yielding in yeast $A_{2D} = 0.0055 - 0.01 \approx 0.0065\ \mu m^2/s^{1/2}$ (both before and after DSB) for 2D projections and hence $A = 3/2\ A_{2D} \approx 10^{-2}\mu m^2/s^{1/2}$ that we are using in theory and simulations (see Limitations for discussion of the accelerated movement after DSBs). Use of the Rouse dynamics not confined by other factors (beyond the nuclear volume) is further motivated by the relaxation of confinements after DSB. A simple approach developed here aims at capturing the phenomenon of search facilitation by dynamic filaments, and hence the exact value of effective diffusion coefficient A and prefactors can only affect numerical estimates, but not the main result of significantly facilitated search.

Theory

We base our theory on a widely-used De Genne's argument that the search by compact exploration proceeds through an increase in the volume being explored growing with time, and ends when the whole volume of the systems becomes explored, i.e. when the explored volume equals the volume of the system. For a compact exploration process with $MSD = At^{\alpha}$ $(\alpha < 2/3\ for\ 3D)$, the explored volume is $V_{explored} \sim r^3 \sim MSD^{3/2} \sim t^{3\alpha/2}$, and the search proceeds until the whole volume of the nucleus $V_{nucleus} \sim R^3{}_{nucleus}$ is explored.

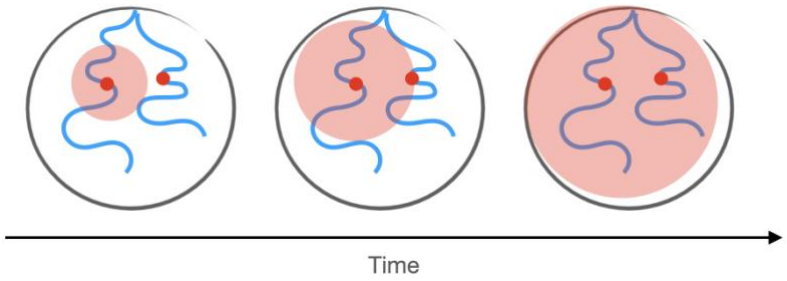

(1) *Two-loci search*. First we estimate the search time for a single Rouse searcher ($MSD = At^{0.5}$) looking for for an immobile target, i.e.

$V_{nucleus} = 4/3\pi R^3{}_{nucleus} = V_{explored} = 4/3\pi \Delta r^3 c = 4/3\pi MSD^{3/2} c = 4/3\pi c A^{3/2} t^{3/4}$,

where a coefficient *c* reflects the fact that starting with a random position within a nucleus the explored volume, if spherical, would cover only a part of the nuclear volume when the volumes equal, and since trajectories reflected from the boundary are likely to cover already explored space, a factor of c larger volume needs to be explored. A sphere centered uniformly randomly within another one of the same radius overlaps by about 0.5 of its volume, suggesting $c \approx 2$. This yields an estimate, $t_{1\,searcher} \approx 2\, R^4_{nucleus}/A^2$, which agrees well with simulations for this case (**median**$(t_{1\,searcher})$=67,000sec, c=1.74). We crudely estimate that the search for two independently moving searchers would be approximately twice faster. Indeed, for each searcher, the other one is akin to an immobile target that can be found anywhere uniformly within the volume. Hence, we can approximate this by just asking what is the minimum of two search times. Since the Rouse search time is distributed approximately exponentially, we take the minimum of the two exponential random numbers (with the same rate) which is an exponential random number with twice the rate, hence we divide the 1-searcher time by half. This agrees with simulations which show that two moving searchers find each other approximately 1.7 times faster than one moving and one immobile.

This argument yield:

$t_{2\,searchers} \approx R^4_{nucleus}/A^2$;

using measured $A \approx 10^{-2}\mu m^2/s^{1/2}$ and $R_{nucleus} \approx 1.4\mu m$

we obtain **the search time**

$$t_{\ 2\,searchers} \approx R^4_{nucleus}/A^2 \approx 38{,}400\ s \approx \textbf{10.7h}$$

This estimate is in very good agreement with Rouse search simulations for two searcher that gives:

Mean **46,000sec** and Median **32,000sec ≈ 8.8h**

(See Supplemental Table 3 for confidence intervals and effects of parameters). Note that this is probably an underestimation of the search time for two compact loci as a number of factors can further constrain the dynamics (see below)

(2) *Search by the stable filament*. In this scenario, one of the loci is extended into a filament, while the other remains a compact locus. In this scenario, we assume that the filament is immobile and only the compact locus is performing a search. We also assume that the search ends once the searching locus touches the filament anywhere along its length, i.e. we assume that the complementarity between the compact locus and the extended filament can be established at any point along the filament. Indeed, rephrasing famous Brouwer fixed-point theorem, if the sequence of the compact locus is complementary to that of the extended filament, no matter where the compact locus touches the filament there is going to be a sequence fragment within the compact one that is complementary to the site of the filament that is being touched.

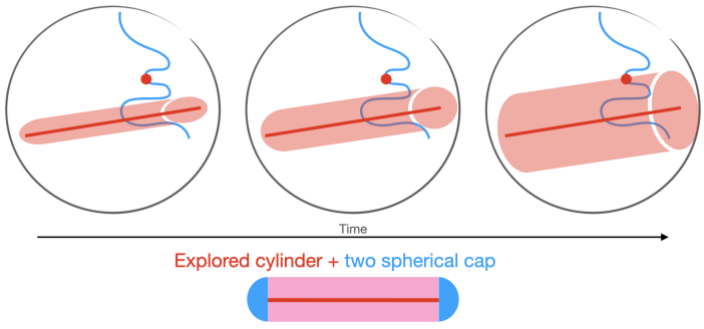

Then one can consider *the explored volume* as the volume *starting from where* the Rouse searcher can reach the filament in time *t.* Since in time t the locus displaces by $\Delta r(t) = MSD^{1/2} = A^{1/2}t^{1/4}$, the *explored volume* will then constitute a cylinder of radius $\Delta r(t)$, capped by semispheres of that radius, around the filament. The semispheres represent volumes around filament tips from where the searcher can travel to touch the tips. The logic stays the same for more complex organization of the filament: circular ones may not have the tips, but have larger L, branched ones would have more

tips. Here for simplicity and due to its experimental prominence, we consider the linear filament. Hence, we obtain the explored volume as

$$V_{explored}(t) = \pi L \Delta r^2(t) + 4/3\pi \Delta r^3(t) = \pi L MSD + 4/3\pi MSD^{3/2}$$
$$= \pi L\, At^{1/2} + 4/3\pi A^{3/2} t^{3/4}.$$

As above, the search ends once the explored volume reaches the nuclear volume ($V_{explored}(t) = V_{nucleus}$) (i.e. a locus that started the search anywhere within the nuclear volume would reach the filament). The search time can be found by solving the cubic equation for variable $y = t^{1/4}$:

$$4/3\pi\, R^3{}_{nucleus} = \pi L\, At^{1/2} + 4/3\pi A^{3/2} t^{3/4};$$
$$R^3{}_{nucleus} \approx LAt^{1/2} + A^{3/2} t^{3/4}$$
$$A^{3/2} y^3 + LAy^2 - R^3{}_{nucleus} = 0$$

For experimentally measured $R_{nucleus} \approx 1.4\mu m$ and taking $L \approx 1.2\mu m$ (at 4h) this approach yield the search time of

$$\boldsymbol{t_{stable\ filament}} \approx \textbf{17,800 sec ≈ 4.5h}$$

which is very close to the results of simulations of such search dynamics:

Mean ≈ 28,000 sec Median ≈ 17,800sec ≈ 4.5h

Note that a static filament provides only about 2-3 fold reduction in the search time compared to the two-loci search. Critical for this facilitated search is the increase on the surface area of the searcher through formation of the filament: the longer filamentous structure the more significant is the acceleration.

(3) *Dynamics filament search*. One can extend the approach developed for the stable filament to a dynamic that experiences cycles of extension and compaction.

Using an approach developed for 3D/1D search of proteins for their sites on DNA, we consider the search process as consistenting from consecutive cycles of search. During each such cycle, the filament is formed for some characteristic period of time τ, after which it compacts and stays in the compact state for τ_0, and then extends again. During each extended phase, the filament is not moving, while each extension starts at a random nuclear location -- together these capture high mobility of the filament we observe in microscopy. If the filament is only accessible for searchers for time τ, searchers from the volume $V_{explored}(\tau)$, defined in the previous section, can reach the filament.

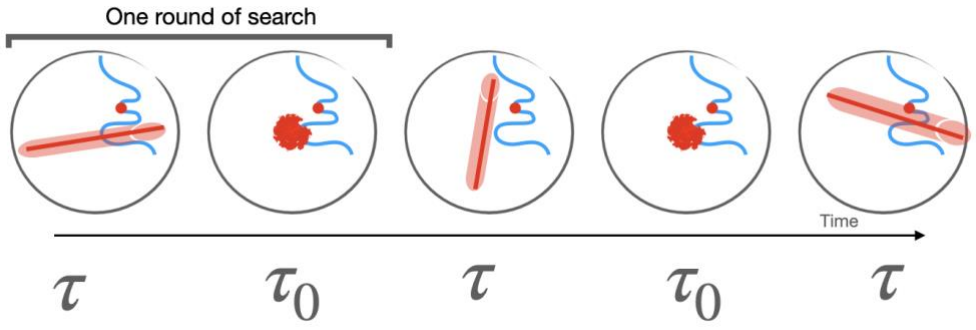

Hence, the probability of having a successful search in a given round is the probability that the searcher is located with the volume explored during this round, i.e. $p_{success} = V_{explored}(\tau)/V_{nucleus}$, assuming that each time an independent volume is explored.

If the probability of success on each round is $p_{success}$, the mean number of rounds required to achieve successful search is then $1/p_{success}$, and using the time each round takes is $\tau + \tau_0$, we obtain the mean search time as

$$t_{dynamic\ filament} = 1/p_{success}(\tau + \tau_0) = V_{nucleus}/V(\tau)_{explored}\ (\tau + \tau_0),$$

where $V_{explored}(t)$ for a linear filament is given above. Since the target is found during the last round of search, only about half of the time of the last round contributes to search, leading to a more accurate expression:

$$t_{dynamic\ filament} = 1/p_{success}(\tau + \tau_0) = [V_{nucleus}/V(\tau)_{explored} - 1/2]\ (\tau + \tau_0),$$

Figure 4 shows a good agreement between the search time computed this way and simulations as a function of τ. One can see that the fastest search can be achieved for $\tau \approx 2\tau_0$, with the coefficient 2 arising due to complex dependence of $V(\tau)_{explored}$ on τ . For experimentally measured $\tau = 1000\ sec; \tau_0 = 100\ sec$ and same geometric parameters as above one gets

$$t_{dynamic\ filament} = 6{,}500 sec \approx \textbf{1.8h}$$

which is remarkably close to the search time seen for this mechanism in simulations.

Mean ≈ 11,700 sec Median≈ 9,360≈2.6h

Moreover, one can estimate the number of rounds needed to find the target as $V_{nucleus}/V_{explored}(\tau)$, yielding **7-8 rounds**.

Interestingly, from both theory and simulations we see that the search time is non-monotonic with τ, allowing to estimate the optimal τ/τ_0 ratio or compute optimal τ numerically. If one were to ignore the semispheres around filament caps and use $V_{explored}(\tau) = \pi L\, A\tau^{1/2}$, then $t_{dynamic\ filament} \sim \tau^{-1/2}(\tau + \tau_0)$, yielding the fastest search as a function of τ. This yields $\tau^{opt} = \tau_0$, i.e. when the filament time is partitioned 50/50 between extended and collapsed states. Using the full expression for $V_{explored}(\tau)$=$\pi L\, A\tau^{1/2} + 4/3\, \pi A^{3/2}\tau^{3/4}$ would give a different value for τ^{opt} that for values of L and A used, gives $\tau^{opt} \approx 1.2\, \tau_0$.

Experimental values deviate more from this optimal time partitioning ($\tau \sim 18min$ $\tau_0 \sim 2min$). However, having $\tau > \tau_0$ leads to only modest and gradual increase in the search time, while, on the contrary, $\tau < \tau_0$ leads to a dramatic increase in the search times, as for small tau the search becomes very inefficient, and many more rounds of search are required. *In vivo* Rad51 filament has the lifetime above the optimal τ, but doesn't

Interestingly, facilitation of search due to dynamics of the filament is very similar to the mechanism of facilitated 3D/1D search by DNA-binding proteins. In both cases compact exploration (1D scanning along DNA or Rouse diffusion in search for a filament) is ineffective, requiring large jumps (3D diffusion or restructuring of the filament). The 3D/1D search time can be written as $t_{3D/1D\ search} = 1/p_{success}(\tau_{1D} + \tau_{3D}) = M/n(\tau_{1D})\ (\tau_{1D} + \tau_{3D})$, where is the total genome length (equivalent to the total volume to search) and $n(\tau_{1D})$ is the number of sites on DNA visited on each round of 1D diffusion that take τ_{1D} , and the time of each 3D flight is τ_{3D}. The optimal search is achieved when τ_{1D}=τ_{3D}. One can see that this expression is identical to the one for dynamic filament. Like for other intermittent search strategies, randomization on every round makes the search much more efficient.

Simulations

The search is simulated as a Rouse diffusion in the spherical nucleus of radius $R_{nucleus}$. The trajectory is modeled as a fractal-Brownian motion (fBm) with 1sec discrete steps, such that $MSD \sim At^{1/2}$. Boundaries of the sphere are considered reflective, as recently introduced for fBms, but with a reflection in random direction, i.e. when a trajectory attempt to leave the sphere, the rest of the trajectory is rotated by a random angle, allowing it to continue inside the sphere (see Limitations,

below). Loci are said to find each other if they approach each other closer than a distance cutoff d_{cutoff}=*50*nm. We tested cutoffs of 25 and 100nm, and, as expected theoretically, found that resulting search time changes by less than by 50%.

For the two-loci search, two fBm trajectories as simulated starting from random initial points within the nuclear volume. For a stable filament, the filament is being placed at a random nuclear position and points in a random direction, conditional on the other end being within the nucleus. For a dynamic filament, the origins and the orientation of the filament are being chosen at random at each round of search, *i.e.* after search for time τ, thus capturing a great deal of filament mobility we observe in microscopy. Each simulation run models the search for $2x10^5$sec, 1000 such simulations are done for each scenario. This allows computing the mean, the median and the distribution of search times, the latter being very close to exponential, as known for Rouse search processes. Obtained values of the search time are given in the Supplemental Table 4.

Limitations and extensions

Our approach to estimate search times has several limitations, opening a possibility of follow-up analysis and simulations.

Dynamics of chromosomal loci were modeled using Rouse dynamics, which is now well-established. Nevertheless, our models assumed otherwise unconstrained Rouse starting from a location uniformly distributed in the nucleus. Specifics of nuclear organization can further slow-down search due to constraints and competition, while other factors can make search faster than estimated.

Factors that could potentially slow-down the search are the following.

(a) **Tethering of centromeres at the spindle pole-body, and telomeres at the nuclear periphery can lead to more constrained movement of loci and slower search.** In fact several studies have suggested some sort of confined diffusion with a radius of confinement of 450-700 nm for an uncut locus. Interestingly, following the DSB, relaxation of this confinement was observed, motivating us to use unconfined Rouse dynamics for our model. In general, we expect the constrained locus dynamics to affect two-loci and static filament scenarios more than the dynamic filament, where the volume is efficiently explored by rounds of filament compaction and expansion.

(b) **Topological and steric interactions between chromosomes could potentially significantly slow down long-term dynamics** turning Rouse diffusion into a much slower process. Note that observations of the Rouse dynamics in yeast were limited to seconds, while topological constraints can become relevant at longer times. Topological constraints may indeed be responsible for observed confined motion of chromosomes before DSB. While tethering to SPB and nuclear periphery effects largely loci close to chromosome ends, topological constraints can have affected all loci.

(c) **Recognition of the locus may take some additional time.** Furthermore, when homology is incomplete, the donor sequence is sequestered by the decoy. This is likely less relevant for filaments as sequestration of any one part of the filament doesn't affect the rest of it allowing other regions to be accessed.

(d) **Sequestration by decoys can potentially prevent recognition on the first encounter**, making search taking longer. The filament provides an advantage by allowing simultaneous probing by multiple decoy donors that do not sterically occlude each other as much as they would for a compact DSB locus. Furthermore, even if occluded by the decoy, the DSB can be recognized by the donor after the decoy dissociates. Due to the compact exploration, recognition of the second or third encounter is likely to immediately follow the first encounter. Also, recognition and rejections of decoy sequences were estimated to take the order of seconds, while the total search time being estimated is in tens of thousands of seconds. So, delay for a few seconds when the searcher arrives wouldn't slow down the global search process.

(e) **Similarly, the compacted states of the locus may require some time for the locus to detect homology**, potentially allowing it to dissociate without detecting it. As explained above, the compact nature of search provides multiple immediate encounters, allowing the searching locus to recognize its target from the second or third attempts.

(f) **Recognition may require a closer than 50nm approach of the locus to the filament.** Supplemental table shows that using 25nm instead of 50nm lead to at about 20-40% increase

in the search time, arguing that this is not a very relevant parameter. Furthermore, 5Kb locus is expected to have the size (end-to-end distance) of ~100nm (ideal chain of 25 nucleosomes, with the persistence length of 5 nucleosomes gives $10nm * \sqrt{25 * 5} \approx$ 100nm). Using parameters from ($60(bp/nm)$ of linear compaction and $80nm$ of the persistence length) we find that 5Kb locus would have the end-to-end distance of $\sqrt{5000bp/60(bp/nm) * 80nm} = 80nm$. Since the radius of gyration is sqrt(6)=2.4 smaller than the end-to-end distance, it yields the radius of gyration of **40nm** and **33nm** for 100nm and 80nm end-to-end distances correspondingly. Together this supports our estimate of 50nm contact distance.

(g) **Variable filament length.** We assumed the filament of a constant 1.2um in length, while experiments show that the average filament length changes from 0.9 at 2h to 1.3um at 4h, both broadly distributed in individual cells (Fig 2a). While shorter filaments make search by a static filament slower, dynamics of the filament is much less affected by this and remains fast 2.5h in simulations for L=0.9um. Moreover, the benefit of the dynamic filament becomes even more pronounced for shorter filaments.

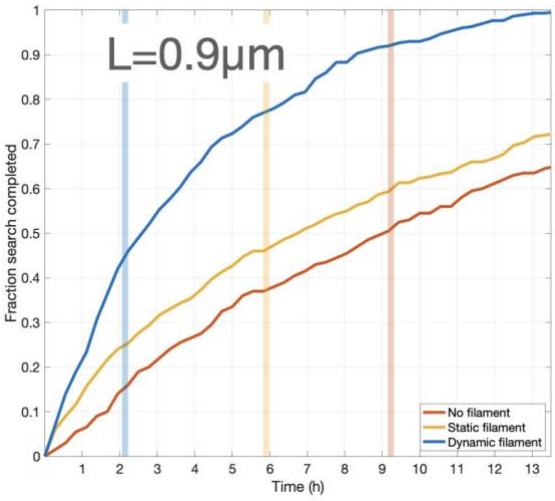

Factors that can potentially make search faster

(a) **Closer relative position of homologous loci that are equidistant from the centromeres**. This factor could potentially reduce the search time for the two-loci case, nevertheless the effect is going to be very modest. In fact, it was shown that the search time scales linearly with the initial distance *d* between loci $t \sim d\ R^3/A^2$. Further moder

Mine-Hattab et al provide extensive measurements of initial distances for *URA3* loci in diploid yeast cells, obtaining the mean approximately 1um. In our simulations the initial distance was random, which is approximately the radius of the sphere (1.4um). Using the linear scaling of the search time with initial distance suggests ~40% reduction in the search time.

(b) **Accelerated dynamics after the break**. An increased mobility after the DSB is hard to capture in a model since it doesn't represent neither a simple increase in A nor a change of α, but some combined and yet to be understood change in the mobility. One possibility is that such increase in mobility is due to the relaxation of some constraints (centromere attachments, linker length etc), but our theory and simulations already consider an unconstrained Rouse mobility. Another possibility is that Rad51-mediated dynamics captured here is the underlying source of increased mobility of a DSB proximal probe and other chromosomes.

(c) Dynamics and structure of the filament can significantly accelerate search. While fluctuations of the filament can increase the explored volume, more complex shapes of the filament can significantly facilitate the search. For example, circular filaments with larger circumference can increase L. Branching ones in turn create more tips further increasing the "surface area" of the target for searchers. Continuously changing shapes can also explore the volume very efficiently.

Taken together these factors suggest that explicit simulations of the full polymer system may provide better estimates of the search time, at a cost of higher computational complexity and many additional parameters of the model. Further understanding the origin of accelerated dynamics after DSB can help take this phenomenon into account.

IV. CONCLUSION and DISCUSSION

During my PhD, I mainly focused on observing and deciphering the dynamics of Rad51 during HR and its regulation in living yeast. We have developed and characterized the first fully functional tagged version of the eukaryotic recombinase Rad51 in yeast.

Monitoring Rad51 upon induction of unique DSB, we show that Rad51 proteins first assemble as a focus that progressively enlarges before elongating as a micrometer long filament able to span across the nucleus. We further show that Rad51 filaments adopt different shapes that are regulated by known regulators of Rad51. Finally, timelapse acquisition revealed a surprisingly dynamic behavior of Rad51 structures during the process of homology search, with filaments undergoing frequent compaction events followed by re-extension. Biophysical modeling of the process of homology search by our collaborator, Leonid Mirny (MIT, USA) demonstrates that these compaction-extension cycles, constitute a robust search strategy, allowing DSB to rapidly explore the nuclear volume and thus enable efficient HR.

1. Rad51 nucleoprotein filaments (NPF) in living yeast

While Rad51 filaments have been extensively studied using different *in vitro* approaches (electronic microscopy, AFM, molecular combing, tweezers …), we observed for the first time Rad51 filaments forming in living yeast. As defined earlier in the manuscript, we call “NPF” a nucleoprotein filament formed by Rad51 proteins bound to ssDNA, while “filament” refers to the fiber observed by FL microscopy: thus a “filament” can be formed by one or several “NPF”.

1.1 Correlation between the formation of filaments and the ability to perform HR:

Several lines of evidence support the significance and function of Rad51 filaments observed *in vivo*. First, we ensured that the formation of Rad51 filaments is not an artefact of the tagged version as they are also observed by immunofluorescence using antibody targeted against the native Rad51. Of note, similar structures were also reported by IF in cdc48 mutant cells upon treatment with the damaging agent zeocin (Bergink et al. 2013). Second the length of Rad51 filament correlate with the extent of Rad51 spreading on DSB flanking sequences as monitored by ChIP (considering 2 kb on ssDNA ~ 1 µm; Convey et al.2004, Ogawa et al.1993). Third, both N-terminal and C-terminal tagged Rad51 cannot form long Rad51 filaments and are sensitive to the DNA damaging agent MMS, suggesting that cells with defects in HR fail to form Rad51 filaments. Furthermore, the different

tagged versions of Rad51 generated in the team show a good correlation between the ability to form filaments and resistance to MMS. Fourth, among the different types of Rad51 structures, filaments are the one that colocalize the most with the donor sequence, suggesting that filaments are the functional structures performing the homology search. Fifth, these structures are transient in the presence of a donor sequence, suggesting that they dismantle once HR is completed.

However, very little is known about the choreography between Rad51 structures and the donor sequence. More movies in strain harboring a labeled donor sequence will help us to better understand dynamics of Rad51 NPF during HR

1.2 Characteristics of Rad51 filaments

The size of Rad51, their kinetic of appearance and disappearance in the presence of a donor sequence are very consistent with the kinetic of DSB end resection and repair reported in previous studies (Mimitou et al.2011, Krejci et al.2012). However, other (less expected) features raise important questions. First, we observed that some Rad51 filaments are non-homogeneous in intensity: interestingly the bright parts are nearly twice brighter as the dim parts. As discussed earlier, up to four NPFs are expected in each cell (corresponding to the two sides of the break on the two sister chromatids), yet most cells show a single Rad51 structure. These structures thus correspond to up to four NPFs, whose precise organization needs to be determined. We hypothesize that the brightest part of a filament may correspond to the overlapping of two or more NPFs. If there are 2 or 4 Rad51 NPFs in the brighter part, the width of structures should also be twice or four times larger than the dim part. However, the resolution of conventional microscopy limited to 300nm for convention optical microscopy), makes it impossible to measure the precise width of Rad51 filaments (a single NPF being 20-30nm from EM (Sheridan et al.2008)). To access the structure of Rad51 filament within cells, super resolution microscopy is required. We propose to use Photo Activable Localization Microscopy PALM and STORM (Stochastic Optical Reconstruction Microscopy) allowing the localization of individual molecules in fixed cells at up to 20 nm resolution (Betzig et al. 2008, Huang et al. 2018). The principle of this technique is to use specific conditions at which we can observe single fluorophores one after another. In PALM, this is achieved by using specific fluorophores which emit light stochastically upon UV and which we bleach extremely rapidly. This process is repeated thousands of times: after localization each molecule with the best possible resolution, a final image can be reconstructed in which each point is a single molecule.

The PALM approach requires specific fluorophores; thus, we constructed several strains expressing fluorophores suitable for PALM (mMaple, mEOS) and we tested their functionality. Results from J. Miné-Hattab and F. Lakhal (M2 internship) show that we can measure filament width down to 40 nm as well as to observe the detailed structure of Rad51 filaments. These preliminary data confirmed that filament width is not homogenous. More detailed and further experiments will be necessary to decipher the precise 3D structures of Rad51 filaments. To complement the PALM/STORM approach, it will also be interesting to investigate the internal dynamics of Rad51 molecules within the filaments. Single Particle Tracking (SPT) is a powerful approach to follow the dynamics of individual molecules in living cells (Manley et al. 2008). Based on the way individual molecules move, SPT allows for i) sorting proteins into subpopulations characterized by their apparent diffusion coefficients, ii) quantifying their motion, iii) estimating residence times on DNA… Using the trains expressing Rad51-mEOS3.2, we could follow individual Rad51 molecules in the presence or in the absence of DSB and estimate the turnover of Rad51 molecules within a filament in different contexts (different shapes, different genetics contexts). It would be interesting to measure the dynamics of Rad51 molecules when a filament compact or re-extend to better understand the mechanism of the compaction/elongation events.

Another interesting question is the persistent length of the Rad51 filament in living cells. *In vitro* studies showed that Rad51 NPF are very stiff with persistence length of 543 nm (Sheridan et al.2008), but how can a stiff rod be so dynamic and forms many different shapes remains to be understood. It will be also very useful to estimate the persistence length of Rad51 filaments in different genetic backgrounds and evaluate the impact of filament stiffness during homology search.

1.3 Biological meaning of different Rad51 filament shapes

The Rad51 filaments are classified into five categories: rod, bent rod, circle, branched structure and others (combinations of the former 4 categories). If it was expected that Rad51 form rods or bent rods, the formation of circles, one-node branched structures, or more complex structures was not anticipated. Combining time lapse microscopy and genetics is extremely useful to better understand how these different shapes form and what are their functions. Using time-lapse microscopy in WT cells, we first observed that the same filament can adopt different shapes through time: we were able to observe a focus transforming into a globular structure, an elongated filament, and more complicated shapes such as circle or “eight” shape”. We performed mainly movies at 2-5 minutes time-intervals lasting around 90 minutes at the maximum: this timescale allowed us to observe and quantify the “compaction events” described in the result section. However, the filaments are very

dynamic, and it is not always possible to catch the transition events happening between frames. Faster time lapse movies will be required to better understand the dynamics of Rad51 structures. We have already acquired several faster time lapse movies with F. Lakhal using super resolution microscopy (live SR module on a spinning disk microscope, resolution 120nm).
Given the length of Rad51 filaments, one can wonder whether their shapes are constrained by the nucleus envelope. We have labelled the nuclear envelope by tagging the nucleoporin, Nup57 with mCherry. Surely, all the Rad51 structures are within the nucleus, but the arcs of bent Rad51 filaments don't follow the nuclear envelope. Yet one cannot rule out that filament bent when they encounter the nuclear envelope before moving away from it keeping this shape due to other constraint such as the mesh of chromatin.

Circular Rad51 filaments. Rad51 filaments forming circles are particularly surprising. We proposed 2 models to explain the formation of such circles: they could be formed by i) long filament bending on themselves or ii) "bubble" emerging from the local separation of two or more NPFs (Figure 1 skeme). Since Rad51 filaments are rigid, a minimum length is necessary to bend them enough and form a circle. Independently of the mechanisms underlying their formation, it is important to understand whether these circles fulfill a specific function.

We found that Rad51 circles are more abundant in *rad54Δ* cells compared to wild type cells. In parallel, we show that *rad54Δ* cells form longer filaments than wildtype cells. Furthermore, we observe that circles form when the filaments are long enough in wildtype cells. These observations are consistent with the first model of circle formation. We also found that in *rad54*□ cells, Rad51 filament do not form branched structures. The increase in circles observed in *rad54*□ cells could be explained by the slow kinetics of circle formation: long filament may engage in branched structures in wildtype cells whereas these structures are not formed in *rad54*□ cells, leaving more time for long filaments to form circles.

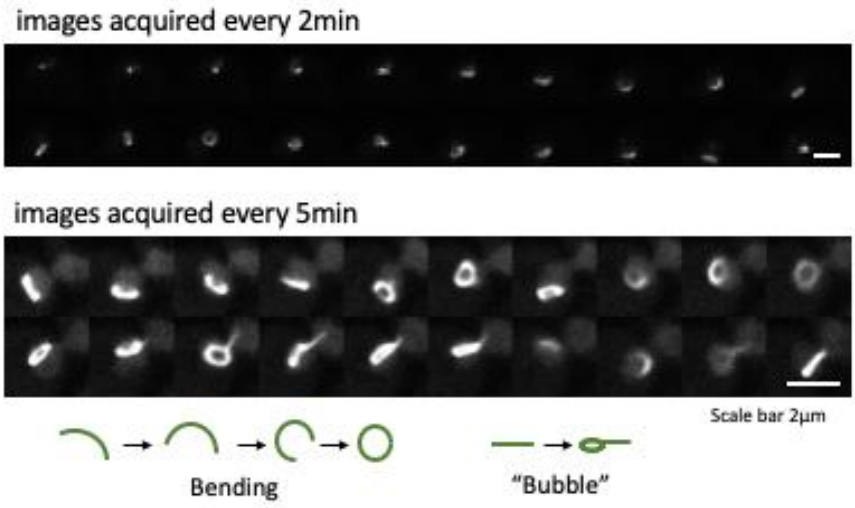

Conclusion_Figure 1 Time lapse images of Rad51-sfGFP and skemes for the formation of ring structrue

DSB induced for 2h30min exhibit the formation of ring-like Rad51 filaments

Rad51 branched structures. Branched structures, could correspond to individual NPFs stretched in different directions. However, how the Rad51 change from rod to branched structure remains unknown, as well as the meaning and function of the branched structures. We assume that individual Rad51 filaments may separately invade dsDNA bearing small tracks of homology and belonging to different parts of the genome, thus separating into branches. The fact that *rad54Δ* strain cannot form branched structures offers indirect evidence to this hypothesis since Rad54 is necessary for the invasion of ds-DNA. In this case, dsDNA invasion would occur at micro-homology since these structures are observed in the absence of a bona fide donor sequence. It is noteworthy that these structures, as well as the more complexed structures belonging to the fifth category of Rad51 filaments (**others**), are rarely observed in the presence of a donor sequence indicating that they might correspond to improper Rad51 structures leading to a dead-end. Note that although these structures represent up to 25 % of the filaments 6 hours after DSB induction in diploid cells, most cells have fixed the DSB at this time as only 25% of the cells still show a filament.

1.4 Rad51 filament dynamics *versus* chromatin mobility

Our results also call for re-interpretation of previous work showing that damaged loci become more mobile in response to DSB (Miné-Hattab et al, 2012; Dion et al, 2012; Miné-Hattab et al, 2017): indeed, such changes in the mobility of the broken locus could be related to the dynamics of the Rad51 filament. So far the dynamics of the dsDNA flanking the DSB was monitored using FROS systems

(LacO:lacI-FP) but the dynamics of the resected ssDNA cover by Rad51 was not accessible. It would be interesting to monitor the dynamics of a lacO array inserted close to the DSB together with the Rad51 filament. Mobility of the rest of the genome has also been shown to increase in cells experiencing a DSB (Mine-Hattab et al. 2012), which could also be a consequence of the dynamics of the Rad51 filaments that set the chromatin in motion.

1.5 Rad51 filament *versus* repair foci

The proper formation and disassembly of repair foci is essential for HR, but how these membrane-less sub-compartments are formed, maintained, and disassembled remain unclear. Recently, several studies proposed that some repair foci are formed *via* the liquid liquid phase separation (LLPS) in different organisms (miné-hattab et al 2021, oshidari et al 2020, altmeyer et al 2015). Rad52 in Sc. yeast for example forms foci and exhibits several hallmarks of LLPS while RPA1 forms foci by binding to the ssDNA (Oshidari et al 2020, Miné-Hattab et al 2021). Although Rad51 form foci with similar appearance than those formed by Rad52, Rad51 foci evolve into elongated structures and filaments which does not seem consistent with a LLPS. It would be interesting to compare the internal dynamics of Rad51 and Rad52 foci using SPT to clarify the physical nature of Rad51 foci. The different behavior of Rad52 and RPA1 already indicate that several kinds of condensates co-exist at damaged sites with different physical nature (Miné-Hattab et al, 2022). One can even imagine that this variety of condensates with different physical nature has a specific function. For example, the existence of a Rad52 droplet may sequester a pool of Rad51 molecules close to the DSB: this organization could help the rapid re-extension a Rad51 filament after a compaction event. In the future, it will be challenging and exciting to dress a comprehensive picture of how the different players organize each other.

1.6 scRad51, hRad51 and RecA filament

As discussed in the introduction of the manuscript, scRad51, hRad51 and RecA filaments share many functional and structural similarities. *In vivo*, RecA-GFP forms bundles, filaments and even branched structures but circular shapes were not reported in *E.Coli* upon DSB induction (Lesterlin et al.2014; Wiktor et al, 2021). One cause might be the geometric constraints imposed by shape of E.Coli cells: RecA structures cannot form round or complex structures in *E. coli* cell due to its thin and long shape. Furthermore, the RecA filaments were not reported to undergo the compaction events that we observed in *S. Cerevisiae*. This difference could reflect the difference in geometry and genome complexity between eukaryotes and prokaryotes. Indeed, *E. coli* cell is an elongated rod whose

genome is made of a unique chromosome, making the search reducible to one dimension. This one-dimension search would not be sufficiently effective in eukaryotic cells where several chromosomes are distributed in a spherical nucleus. Yet, RecA filaments have common features with scRad51, including their heterogeneity. It is noteworthy that most data on RecA were obtained in cells expressing the non-functional RecA-GFP in addition to the endogenous version. It is thus possible that RecA-GFP does not recapitulate all the features of the functional RecA.

In human cells overexpression of the non-functional GFP-Rad51 form filaments independently of DNA damages (Raderschall et al. 2002), while the endogenous protein forms multiple foci in the presence of DSB in mitotic or meiotic cells (Tarsounas et al.2004, Slotman et al.2020). However super resolution microscopy revealed that the hRad51 focalized in clusters before progressively extending into filaments following X-ray irradiation (Hass et al.2018). These filaments are shorter than the one we observe in living yeast possibly reflecting an alteration of these structures by the fixation procedure. Another explanation for these filaments being shorter could be that in this case DSBs are repaired with donor sequences located in proximity of the broken DNA, (*i.e.* the sister chromatid that is unlikely to be damaged at the same locus by X-ray irradiation, or repetitive sequences providing substrate for ectopic HR, or SSA). Interestingly Rad54 was found associated with these filaments in agreement with our observation in yeast living cells.

2. Impact of Rad51 regulators on Rad51 filaments

2.1 Rad52

Rad52 has been regarded as the loader required for Rad51 filament formation for a long time (Mcllwraith et al., 2008), which is consistent with the absence of nuclear Rad51 structures in the absence of Rad52. However, we showed that *rad52srs2Δ* strain form Rad51 filaments (Figure 5, SectionB). This suggests that there should be other proteins loading Rad51 on ssDNA. Alternatively, Rad51 might be able to replace RPA in the absence of Rad52 as shown *in vitro* (Ma et al. 2017). Our results indicate that the main function of Rad52 could be to protect Rad51 filaments against the dismantling activity of Rad52 rather than to load Rad51. Studying the effects of Rad59, the paralog of Rad52, would be interesting, as well its relationship with Rad52 and Srs2 during HR. Several rad52 point mutants that restrict the interaction between Rad51 and Rad52 in varying degrees can contribute to this study.

2.2 Rad55-Rad57

The Rad51 paralogs Rad55 and Rad57 also have dual functions during HR, as they can counteract Srs2 activity but also stabilizes Rad51 filament independently. Former studies (Liu et al.2011, Figure12) suggest that Rad55-Rad57 functions as an obstacle for the Srs2 dismantling activity, but this cannot explain how Rad55-Rad57 impact filament formation in the absence of Srs2 as observed in Figure5 section B. Localizing Rad55 or Rad57 within Rad51 filament could be informative to understand how they protect Rad51 filaments depending on whether they would form a focus like Rad52 or associate along the Rad51 filaments like Rad54.

2.3 Srs2

In contrast to wildtype cells, the *srs2Δ* strain exhibit spontaneous Rad51 filaments in the absence of induced DSB. This is in good agreement with its well-known negative effects on Rad51 filaments *in vitro* (Kerjci *et al.*, 2003). Surprisingly, the number and type of Rad51 structures in this mutant don't show a significant difference with the WT after inducing DSB for 4h.

Interestingly, we noticed that filaments are brighter, but not longer, in this mutant than in the wild-type strain. The current research on the Srs2 helicase shows that it dismantles Rad51 filaments. Our result suggest that Srs2 dismantles the filament at multiple internal sites rather than at one extremity, making the filament dimmer rather than shorter. Although both brighter and longer filaments indicate that more Rad51-GFP molecules are recruited at the broken site they should result from different mechanisms.

2.4 Rad54

Cells deleted for Rad54 also show higher levels of spontaneous Rad51 filaments than wildtype cells. Furthermore, filaments formed upon DSB induction are longer in this mutant compared to the wildtype strain.

This could be related to the known ability of Rad54 to dismantle Rad51 filaments on dsDNA (De Tuillo et al. 2017), which put forward another question. These data are acquired from a haploid strain without donor sequence, so can Rad51 form presynaptic filament on dsDNA? To test whether Rad51 filaments depend on the formation of long stretches of ssDNA in the absence of Rad54 we constructed a *rad54sgs1exo1Δ* strain. In this strain, we observed Rad51 structures (mainly foci) with and without DSB (Figure2), in 45% and 24% of the cells respectively. In both cases, filaments were rarely observed suggesting that the filaments formed in the *absence* of Rad54 depend on the long-range resection by the combined action of Exo1 and Sgs1. The Rad54-mCherry Rad51-sfGFP strain offers another view. Since Rad54 localizes along the Rad51 filaments, it might shorten the length by retracting Rad51 filaments or affecting its persistence length. If Rad54 affects the stiffness of Rad51 filaments, its absence could favor the formation of circular Rad51 filament (see above). Another consequence could be a difference in the dynamics of Rad51 filaments in *rad54Δ* versus WT strains, the mutant showing fewer compaction-extension events. Although these events are observed in the absence of Rad54, more movies and analysis are required to estimate the frequency of these events.

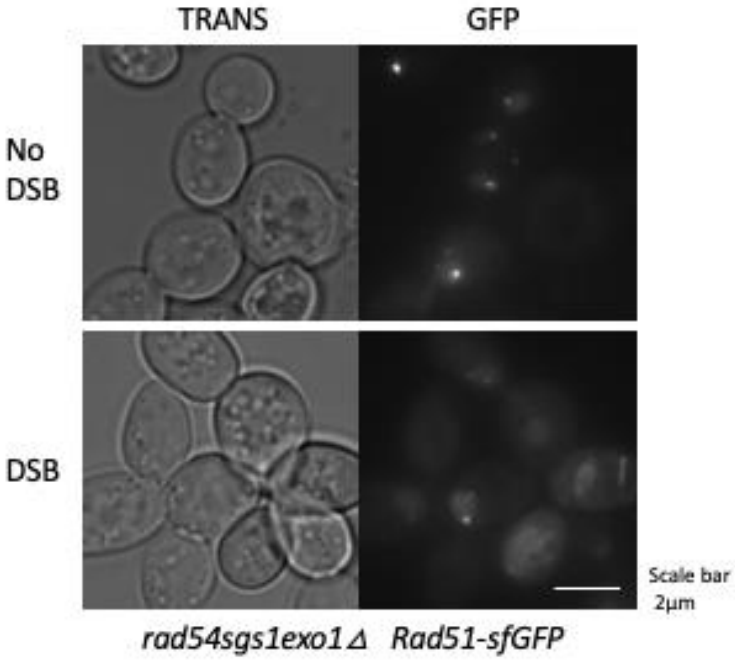

Conclusion_Figure 2 FL and trans images of rad54sgs1exo1Δ strain

2.5 Rdh54

Rdh54 is a negative modulator that catalyzes the Rad51 removal from DNA that origins from DNA replication or transcription (Chi et al. 2006). This is possibly why we observed several spontaneous Rad51 structures in the *rdh54Δ* strain, but cells in either *srs2Δ* or *rad54Δ* strain have zero or one Rad51 structure. However, we do not have direct evidence to show the effects of Rdh54 on Rad51 during HR. Considering that the srs2rad57 or *srs2rad52* strain forms fewer Rad51 filaments than the WT strain, it will be interesting to delete Rdh54 in these two strains to see if there would be more filaments after inducing DSB.

Most of our research concentrates on examining the effects of well-known regulators, such as Srs2, Rad54 and Rad52. We can also consider using our functional Rad51-GFP for screening small molecules inhibiting HR in yeast, for a further understanding on the mechanism of Rad51 filaments regulation.

3. Nucleus wide Homology search model

3.1 Compaction-extension events

It is worthwhile to notice that the median and average length of filaments rise with longer DSB induction time in haploid strain. However, when we focus on a single filament, our work shows that the Rad51 filaments shorten to become a globular structure before the subsequent elongation in haploid and diploid strains rather than continuously elongating. In the former study (Zhu et al.2008), we know the rate of ssDNA generation depends on DNA resection. So is the average growth of Rad51 filament. The abrupt size variation we observed is accompanied by an increase in mean intensity. Therefore, we think that the Rad51 filament length variations are caused by compaction and extension but not by removing Rad51 filament from the ssDNA. These compaction-extension events occur on average every 17 min in haploid strains without donor sequence.

3.2 New homology search model

These unexpected observations led us to propose a new model for homology search. This model shows several benefits over other models, including finding the donor sequence faster and exploring the whole nucleus within 10-12h, before checkpoint adaptation takes place (Pellicioli et al.2001). Interestingly, the fact that gene the conversion rate decreases by 30% between *sgs1Δ* and *sgs1Δ exo1Δ* (Zhu et al.2008*)*, fits very well with the prediction of our simulation as *exo1Δ sgs1Δ* show only foci and could be considered as model 1 which complete search only in 60% of the cells within 12 hours.

The efficiency of our search model is related to the time of the extended state and the compacted state. Though efficient this model is, we have no direct evidence to prove the importance of compaction events for homology search. Therefore, finding the connection between compaction events and homology search will be essential to demonstrate this model.

Regulators of Rad51 with ATPase activity such as Rad54, Sgs1, Srs2 or the ATPase activity of Rad51 itself might be involved in these events. Our preliminary data show that *srs2Δ* and *rad54Δ* strains exhibit compaction-extension events, suggesting that these factors are not individually causing these events. The major concern of using mutants is that we need to consider their effects beyond homology search. Chemical drugs, that could inhibit the compaction events, might be more interpretable than the mutants.

As mentioned above the length of extended Rad51 filaments evolves over time. This length has dual effects on homology search. On the one hand the longer the filament is, the more it can explore the

nucleus within one direction. On the other hand, it also increases the time cost on the compaction and extension. The length of filament is a fixed value in our model, taking the change of filaments length into consideration might reveal more information on homology search.

3.3 Dynamic Rad51 filament

In a mature Rad51 filament, we can observe two kinds of transformations: compaction events, changing the length and size of Rad51 structures; and shapes variations, from rod to circle, or to branched structures. These two types of dynamic events co-exist since filament can adopt different shapes when extended. Combined them together, we think that Rad51 filament bent itself after extension, and the specific shapes also contribute to homology search. As discussed above, the branched structures might be Rad51 in the process of interacting with the dsDNA for homology pairing. Circles and more complex structures remain enigmatic. As circles are observed in a diploid strain that fix a DSB successfully they are potentially functional structures and are thus worthy further investigations. The mechanisms of these two transformations are also unknown. Do they work independently, or do they affect each other? Are they driven both by ATP hydrolyses, microtubes or some other forces? It would be meaningful to have a model combining these two Rad51 activities for uncovering the mist of homology search.

4. Conclusion

During my PhD, I have deciphered the dynamics of Rad51 in living yeast with a functional tagged Rad51-intGFP protein. We observed and quantified for the first times the different structures formed by Rad51 upon DSB induction and studied how Rad51 regulators affect these structures. Most results are consistent with former studies *in vitro* but also bring new insights on the process of homology search within the nucleus and the functions of Rad51 regulators. This Rad51-intGFP strain is a powerful tool to study Rad51 during HR, and lots of experiments are worthwhile to be done in the future. Through super resolution microscopy and single particle tracking, we will be able to have a precise structure of Rad51 NPF and calculate the mobility of Rad51 within and beyond the filaments. Monitoring the Rad51 filaments and the homologous sequence during HR will be helpful to refine our homology search model. More mutants, including separation of function mutants, double-tagged or triple-tagged strains can be used to decipher the mechanisms of Rad51 filament regulators. The fact that we succeeded to tag Rad51 in yeast provides a proof of principle that this protein could be tagged while remaining functional in other organisms opening new avenue to study recombination in different contexts. The future prospect of Rad51 dynamics in living cells is worth expecting.

V. BIBLIOGRAPHY

1.Adzuma, Kenji. "No sliding during homology search by RecA protein." Journal of Biological Chemistry 273.47 (1998): 31565-31573.

2.Agmon, Neta, et al. “Effect of nuclear architecture on the efficiency of double-strand break repair.” Nature cell biology 15.6 (2013): 694-699.

3.Aguilera, Andrés, and Belén Gómez-González. "Genome instability: a mechanistic view of its causes and consequences." Nature Reviews Genetics 9.3 (2008): 204-217.

4.Ahel, Ivan, et al. "The neurodegenerative disease protein aprataxin resolves abortive DNA ligation intermediates." Nature 443.7112 (2006): 713-716

5.Anand, Roopesh, et al. "Phosphorylated CtIP functions as a co-factor of the MRE11-RAD50-NBS1 endonuclease in DNA end resection." *Molecular cell* 64.5 (2016): 940-950.

6.Aparicio, Oscar M. "Location, location, location: It is all in the timing for replication origins." Genes & development 27.2 (2013): 117-128.

7.Aparicio, Tomas, Richard Baer, and Jean Gautier. "DNA double-strand break repair pathway choice and cancer." DNA repair 19 (2014): 169-175.

8.Aravind, L., D. Roland Walker, and Eugene V. Koonin. "Conserved domains in DNA repair proteins and evolution of repair systems." Nucleic acids research 27.5 (1999): 1223-1242.

9.Arcangioli, Benoit. "Fate of mat1 DNA strands during mating-type switching in fission yeast." EMBO reports 1.2 (2000): 145-150.

10.Aten, Jacob A., et al. "Dynamics of DNA double-strand breaks revealed by clustering of damaged chromosome domains." *Science* 303.5654 (2004): 92-95.

11.Aylon, Yael, et al. "Molecular dissection of mitotic recombination in the yeast Saccharomyces cerevisiae." Molecular and cellular biology 23.4 (2003): 1403-1417.

12.Aylon, Yael, and Martin Kupiec. "DSB repair: the yeast paradigm." DNA repair 3.8-9 (2004): 797-815.

13.Bae, Sung-Ho, et al. "RPA governs endonuclease switching during processing of Okazaki fragments in eukaryotes." *Nature* 412.6845 (2001): 456-461.

14.Bae, Sung-Ho, and Yeon-Soo Seo. "Characterization of the enzymatic properties of the yeast dna2 Helicase/endonuclease suggests a new model for Okazaki fragment processing." *Journal of Biological Chemistry* 275.48 (2000): 38022-38031.

15.Ball, Lindsay G., et al. "The yeast Shu complex couples error-free post-replication repair to homologous recombination." Molecular microbiology 73.1 (2009): 89-102.

16.Barnes, Deborah E., et al. "Targeted disruption of the gene encoding DNA ligase IV leads to lethality in embryonic mice." *Current Biology* 8.25 (1998): 1395-1398.

17.Bassing, Craig H., Wojciech Swat, and Frederick W. Alt. "The mechanism and regulation of chromosomal V (D) J recombination." Cell 109.2 (2002): S45-S55.

18.Barzel, Adi, and Martin Kupiec. "Finding a match: how do homologous sequences get together for recombination?." Nature Reviews Genetics 9.1 (2008): 27-37.

19.Batté, Amandine, et al. "Recombination at subtelomeres is regulated by physical distance, double-strand break resection and chromatin status." The EMBO journal 36.17 (2017): 2609-2625.

20.Baudry, Céline, et al. "PiggyMac, a domesticated piggyBac transposase involved in programmed genome rearrangements in the ciliate Paramecium tetraurelia." Genes & development 23.21 (2009): 2478-2483.

21.Baumann, Peter, and Stephen C. West. "Role of the human RAD51 protein in homologous recombination and double-stranded-break repair." Trends in biochemical sciences 23.7 (1998): 247-251.

22.Beagrie, Robert A., et al. "Complex multi-enhancer contacts captured by genome architecture mapping." Nature 543.7646 (2017): 519-524.

23.Bennardo, Nicole, et al. "Alternative-NHEJ is a mechanistically distinct pathway of mammalian

chromosome break repair." PLoS genetics 4.6 (2008): e1000110.
24. Bergink, Steven, et al. "Role of Cdc48/p97 as a SUMO-targeted segregase curbing Rad51–Rad52 interaction." Nature cell biology 15.5 (2013): 526-532.
25. Betzig, Eric, et al. "Imaging intracellular fluorescent proteins at nanometer resolution." *science* 313.5793 (2006): 1642-1645.
26. Bhargava, Ragini, David O. Onyango, and Jeremy M. Stark. "Regulation of single-strand annealing and its role in genome maintenance." *Trends in Genetics* 32.9 (2016): 566-575.
27. Bhowmick, Rahul, Sheroy Minocherhomji, and Ian D. Hickson. "RAD52 facilitates mitotic DNA synthesis following replication stress." Molecular cell 64.6 (2016): 1117-1126.
28. Bishop, Douglas K., et al. "DMC1: a meiosis-specific yeast homolog of E. coli recA required for recombination, synaptonemal complex formation, and cell cycle progression." Cell 69.3 (1992): 439-456.
29. Bizard, Anna H., and Ian D. Hickson. "The dissolution of double Holliday junctions." Cold Spring Harbor perspectives in biology 6.7 (2014): a016477.
30. Bobay, Louis-Marie, and Howard Ochman. "The evolution of bacterial genome architecture." Frontiers in genetics 8 (2017): 72.
31. Boddy, Michael N., et al. "Mus81-Eme1 are essential components of a Holliday junction resolvase." *Cell* 107.4 (2001): 537-548.
32. Bonev, Boyan, and Giacomo Cavalli. "Organization and function of the 3D genome." Nature Reviews Genetics 17, no. 11 (2016): 661-678.
33. Bordelet, Hélène, and Karine Dubrana. "Keep moving and stay in a good shape to find your homologous recombination partner." Current genetics 65.1 (2019): 29-39.
34. Botstein, David, Steven A. Chervitz, and Michael Cherry. "Yeast as a model organism." Science 277.5330 (1997): 1259-1260.
35. Branzei, Dana, and Marco Foiani. "Maintaining genome stability at the replication fork." *Nature reviews Molecular cell biology* 11.3 (2010): 208-219.
36. Bressan, Debra A., Bonnie K. Baxter, and John HJ Petrini. "The Mre11-Rad50-Xrs2 protein complex facilitates homologous recombination-based double-strand break repair in Saccharomyces cerevisiae." *Molecular and cellular biology*19.11 (1999): 7681-7687.
37. Bertucat, Guillaume, Richard Lavery, and Chantal Prèvost. "A model for parallel triple helix formation by Ree A: Single-strand association with a homologous Duple via the minor groove." *Journal of Biomolecular Structure and Dynamics* 16.3 (1998): 535-546.
38. Burma, Sandeep, Benjamin PC Chen, and David J. Chen. "Role of non-homologous end joining (NHEJ) in maintaining genomic integrity." DNA repair 5.9-10 (2006): 1042-1048.
39. Burgess, Rebecca C., et al. "Localization of recombination proteins and Srs2 reveals anti-recombinase function *in vivo*." Journal of Cell Biology 185.6 (2009): 969-981.
40. Bussen, Wendy, et al. "Holliday junction processing activity of the BLM-Topo IIIα-BLAP75 complex." Journal of Biological Chemistry 282.43 (2007): 31484-31492..
41. Caldecott, Keith W. "Single-strand break repair and genetic disease." Nature Reviews Genetics 9.8 (2008): 619-631.
42. Cejka, Petr. "DNA end resection: nucleases team up with the right partners to initiate homologous recombination." Journal of Biological Chemistry 290.38 (2015): 22931-22938.
43. Cejka, Petr, et al. "DNA end resection by Dna2–Sgs1–RPA and its stimulation by Top3–Rmi1 and Mre11–Rad50–Xrs2." *Nature* 467.7311 (2010): 112-116.
44. Chakarov, Stoyan, et al. "DNA damage and mutation. Types of DNA damage." BioDiscovery 11 (2014): e8957.
45. Chen, Clark, Keiko Umezu, and Richard D. Kolodner. "Chromosomal rearrangements occur in S. cerevisiae rfa1 mutator mutants due to mutagenic lesions processed by double-strand-break repair." Molecular cell 2.1 (1998): 9-22.
46. Chen, Jingyang, and JoAnne Stubbe. "Bleomycins: towards better therapeutics." Nature Reviews Cancer 5.2 (2005): 102-112

47. Chen, Xiaoqing, et al. "PCNA promotes processive DNA end resection by Exo1." *Nucleic acids research* 41.20 (2013): 9325-9338.
48. Chen, Ling, et al. "Promotion of Dnl4-catalyzed DNA end-joining by the Rad50/Mre11/Xrs2 and Hdf1/Hdf2 complexes." *Molecular cell* 8.5 (2001): 1105-1115.
49. Chi, Peter, et al. "Yeast recombination factor Rdh54 functionally interacts with the Rad51 recombinase and catalyzes Rad51 removal from DNA." Journal of Biological Chemistry 281.36 (2006): 26268-26279.
50. Chiolo, Irene, et al. "Double-strand breaks in heterochromatin move outside of a dynamic HP1a domain to complete recombinational repair." *Cell* 144.5 (2011): 732-744.
51. Chiruvella, Kishore K., et al. "Saccharomyces cerevisiae DNA ligase IV supports imprecise end joining independently of its catalytic activity." PLoS genetics 9.6 (2013): e1003599.
52. Coïc, Eric, et al. "Mechanisms of Rad52-independent spontaneous and UV-induced mitotic recombination in Saccharomyces cerevisiae." Genetics 179.1 (2008): 199-211.
53. Claussin, Clémence, et al. "Genome-wide mapping of sister chromatid exchange events in single yeast cells using Strand-seq." Elife 6 (2017): e30560.
54. Colleaux, Laurence, et al. "Recognition and cleavage site of the intron-encoded omega transposase." Proceedings of the National Academy of Sciences 85.16 (1988): 6022-6026.
55. Connelly, John C., and David RF Leach. "Tethering on the brink: the evolutionarily conserved Mre11–Rad50 complex." *Trends in biochemical sciences* 27.8 (2002): 410-418.
56. Connelly, John C., et al. "Overexpression, purification, and characterization of the SbcCD protein from Escherichia coli." *Journal of Biological Chemistry* 272.32 (1997): 19819-19826.
57. Conway, Adam B., et al. "Crystal structure of a Rad51 filament." Nature structural & molecular biology 11.8 (2004): 791-796.
58. Costantino, Lorenzo, et al. "Break-induced replication repair of damaged forks induces genomic duplications in human cells." *Science* 343.6166 (2014): 88-91.
59. Crickard, John Brooks. "Discrete roles for Rad54 and Rdh54 during homologous recombination." *Current Opinion in Genetics & Development* 71 (2021): 48-54.
60. D'Angelo, Francesca, et al. "Cellular assays identify barriers impeding iron-sulfur enzyme activity in a non-native prokaryotic host." *Elife* 11 (2022): e70936.
61. D'Amours, Damien, and Stephen P. Jackson. "The yeast Xrs2 complex functions in S phase checkpoint regulation." Genes & Development 15.17 (2001): 2238-2249.
62. Deans, Andrew J., and Stephen C. West. "DNA interstrand crosslink repair and cancer." Nature reviews cancer 11.7 (2011): 467-480.
63. Dekker, Job, and Leonid Mirny. "The 3D genome as moderator of chromosomal communication." *Cell* 164.6 (2016): 1110-1121.
64. de Laat, Wouter. "Long-range DNA contacts: romance in the nucleus?." Current opinion in cell biology 19.3 (2007): 317-320.
65. De Tullio, Luisina, et al. "Yeast Srs2 helicase promotes redistribution of single-stranded DNA-bound RPA and Rad52 in homologous recombination regulation." Cell reports 21.3 (2017): 570-577.
66. Dianov, Grigory L., and Ulrich Hübscher. "Mammalian base excision repair: the forgotten archangel." Nucleic acids research 41.6 (2013): 3483-3490.
67. Dimitrova, Nadya, et al. "53BP1 promotes non-homologous end joining of telomeres by increasing chromatin mobility." *Nature* 456.7221 (2008): 524-528.
68. Dion, Vincent, et al. "Increased mobility of double-strand breaks requires Mec1, Rad9 and the homologous recombination machinery." Nature cell biology 14.5 (2012): 502-509.
69. Dion, Vincent, et al. "Cohesin and the nucleolus constrain the mobility of spontaneous repair foci." *EMBO reports* 14.11 (2013): 984-991.
70. Dixon, Jesse R., et al. "Chromatin architecture reorganization during stem cell differentiation." Nature 518.7539 (2015): 331-336.
71. Dorfman, Kevin D., et al. "Model of RecA-mediated homologous recognition." Physical review letters

93.26 (2004): 268102.
72. Draviam, V. M., Xie, S. & Sorger, P. K. Chromosome segregation and genomic stability. Curr. Opin. Genet. Dev. 14, (2004):120–125.
73. Dubrana, Karine, et al. "The processing of double-strand breaks and binding of single-strand-binding proteins RPA and Rad51 modulate the formation of ATR-kinase foci in yeast." Journal of cell science 120.23 (2007): 4209-4220.
74. Dunham, Melissa A., et al. "Telomere maintenance by recombination in human cells." *Nature genetics* 26.4 (2000): 447-450.
75. Dupaigne, Pauline, et al. "Rad51 polymerization reveals a new chromatin remodeling mechanism." *PLoS One* 3.11 (2008): e3643
76. Dutreix, Marie, Renaud Fulconis, and Jean-Louis Viovy. "The search for homology: a paradigm for molecular interactions?." Complexus 1.2 (2003): 89-99.
77. Espéli, Olivier, and Frédéric Boccard. "Organization of the Escherichia coli chromosome into macrodomains and its possible functional implications." *Journal of structural biology*156.2 (2006): 304-310.
78. Esta, Aline, et al. "Rad52 sumoylation prevents the toxicity of unproductive Rad51 filaments independently of the anti-recombinase Srs2." PLoS genetics 9.10 (2013): e1003833.
79. Fabre, Francis, et al. "Alternate pathways involving Sgs1/Top3, Mus81/Mms4, and Srs2 prevent formation of toxic recombination intermediates from single-stranded gaps created by DNA replication." Proceedings of the National Academy of Sciences 99.26 (2002): 16887-16892.
80. Fernandez, Fabiola Garcia, et al. "Global chromatin mobility induced by a DSB is dictated by chromosomal conformation and defines the outcome of Homologous Recombination." *bioRxiv* (2022).
81. Fishel, Richard, and Jong-Bong Lee. "Mismatch repair." *DNA Replication, Recombination, and Repair* (2016): 305-339.
82. Fogel, S., and D. D. Hurst. "Meiotic gene conversion in yeast tetrads and the theory of recombination." *Genetics* 57.2 (1967): 455.
83. Forget, Anthony L., and Stephen C. Kowalczykowski. "Single-molecule imaging of DNA pairing by RecA reveals a three-dimensional homology search." Nature 482.7385 (2012): 423-427.
84. Frank, Karen M., et al. "Late embryonic lethality and impaired V (D) J recombination in mice lacking DNA ligase IV." *Nature*396.6707 (1998): 173-177.
85. Friedberg, Errol C., et al., eds. DNA repair and mutagenesis. American Society for Microbiology Press, 2005.
86. Friedberg, Errol C. "DNA damage and repair." Nature 421.6921 (2003): 436-440.
87. Friedberg, Errol C. "Suffering in silence: the tolerance of DNA damage." Nature reviews Molecular cell biology 6.12 (2005): 943-953.
88. Fung, Cindy W., et al. "The rad51-K191R ATPase-Defective Mutant Is Impaired for Presynaptic Filament Formation." Molecular and cellular biology 26.24 (2006): 9544-9554.
89. Gaines, William A., et al. "Promotion of presynaptic filament assembly by the ensemble of S. cerevisiae Rad51 paralogues with Rad52." Nature communications 6.1 (2015): 1-7.
90. Game, J. C., and R. K. Mortimer. "A genetic study of X-ray sensitive mutants in yeast." *Mutation Research/Fundamental and Molecular Mechanisms of Mutagenesis* 24.3 (1974): 281-292.
91. Gangloff, Serge, et al. "The yeast type I topoisomerase Top3 interacts with Sgs1, a DNA helicase homolog: a potential eukaryotic reverse gyrase." *Molecular and cellular biology* 14.12 (1994): 8391-8398.
92. Garcia, Valerie, et al. "Bidirectional resection of DNA double-strand breaks by Mre11 and Exo1." Nature 479.7372 (2011): 241-244.
93. García Fernández, Fabiola, and Emmanuelle Fabre. "The Dynamic Behavior of Chromatin in Response to DNA Double-Strand Breaks." *Genes* 13.2 (2022): 215.
94. Gloor, Gregory B., et al. "Targeted gene replacement in Drosophila via P element-induced gap repair." Science 253.5024 (1991): 1110-1117.

95. Gobbini, Elisa, et al. "Functions and regulation of the MRX complex at DNA double-strand breaks." *Microbial Cell* 3.8 (2016): 329.
96. Godin, Stephen, et al. "The Shu complex interacts with Rad51 through the Rad51 paralogues Rad55–Rad57 to mediate error-free recombination." Nucleic acids research 41.8 (2013): 4525-4534.
97. Gonda, David K., and Charles M. Radding. "The mechanism of the search for homology promoted by recA protein. Facilitated diffusion within nucleoprotein networks." Journal of Biological Chemistry 261.28 (1986): 13087-13096.
98. Gorkin, David U., Danny Leung, and Bing Ren. "The 3D genome in transcriptional regulation and pluripotency." Cell stem cell 14.6 (2014): 762-775.
99. Greene, Eric C. "DNA sequence alignment during homologous recombination." Journal of Biological Chemistry 291.22 (2016): 11572-11580.
100. Guidi, Micol, et al. "Spatial reorganization of telomeres in long-lived quiescent cells." Genome biology 16.1 (2015): 1-15.
101. Guirouilh-Barbat, Josée, et al. "Impact of the KU80 pathway on NHEJ-induced genome rearrangements in mammalian cells." Molecular cell 14.5 (2004): 611-623.
102. Groh, Matthias, and Natalia Gromak. "Out of balance: R-loops in human disease." *PLoS genetics* 10.9 (2014): e1004630.
103. Guirouilh-Barbat, Josée, et al. "Is homologous recombination really an error-free process?." *Frontiers in genetics* 5 (2014): 175.
104. Haber, James E. "Mating-type genes and MAT switching in Saccharomyces cerevisiae." Genetics 191.1 (2012): 33-64.
105. Hakem, Razqallah. "DNA-damage repair; the good, the bad, and the ugly." The EMBO journal 27.4 (2008): 589-605.
106. Haas, Kalina T., et al. "Single-molecule localization microscopy reveals molecular transactions during RAD51 filament assembly at cellular DNA damage sites." Nucleic acids research 46.5 (2018): 2398-2416.
107. Hansen, Anders S., et al. "Recent evidence that TADs and chromatin loops are dynamic structures." Nucleus 9.1 (2018): 20-32.
108. Herdman, M. "The evolution of bacterial genomes." The evolution of genome size (1985): 37-68.
109. Heyer, Wolf-Dietrich. "Biochemistry of eukaryotic homologous recombination." Molecular genetics of recombination. Springer, Berlin, Heidelberg, 2007. 95-133.
110. Heyer, Wolf-Dietrich, Kirk T. Ehmsen, and Jachen A. Solinger. "Holliday junctions in the eukaryotic nucleus: resolution in sight?." Trends in biochemical sciences 28.10 (2003): 548-557.
111. Heyer, Wolf-Dietrich, Kirk T. Ehmsen, and Jie Liu. "Regulation of homologous recombination in eukaryotes." Annual review of genetics 44 (2010): 113.
112. Heyer, Wolf-Dietrich, et al. "Rad54: the Swiss Army knife of homologous recombination?" *Nucleic acids research* 34.15 (2006): 4115-4125.
113. Hicks, Wade M., Miyuki Yamaguchi, and James E. Haber. "Real-time analysis of double-strand DNA break repair by homologous recombination." Proceedings of the National Academy of Sciences 108.8 (2011): 3108-3115.
114. Hoeijmakers, Jan HJ. "DNA damage, aging, and cancer." New England Journal of Medicine 361.15 (2009): 1475-1485.
115. Hoffelder, Diane R., et al. "Resolution of anaphase bridges in cancer cells." Chromosoma 112.8 (2004): 389-397.
116. Holligsworth, Nancy M., and Steven J. Brill. "The Mus81 solution to resolution: generating meiotic crossvers without Holliday junctions." *Genes & development* 18.2 (2004): 117-125.
117. Hopfer, Karl-Peter, et al. "The Rad50 zinc-hook is a structure joining Mre11 complexes in DNA recobination and repair." Nature 418.6897 (2002): 562-566.
118. Hozé,Nathanaël, et al. "Spatial telomere organization and clustering in yeast Saccaromyces cerevisiae nucleus is generated by a random dynamic of aggregationdissociation." Molecular biology of the cell 24.11 (2013): 1791-1800.

119. Huang, Bo, et al. "Three-dimensional super-resolution imaging by stochastic optical reconstructionmicroscopy." *Science*319.5864 (2008): 810-813.
120. Hug, C.B. & Vaquerizas, J. M. The birth of the 3Dgenome during early embryonic development. Trends Genet.34, 903–914 (2018).
121. Iftode,Cristina, Yaron Daniely, and James A. Borowiec. "Replication protein A (RPA): the eukaryotic SSB."Critical reviews in biochemistry and molecular biology 34.3 (1999): 141-180.
122. Inbar, Ori, et al. "The relationship between homology length and crossing over during the repair of a broken chromosome." *Journal of Biological Chemistry* 275.40 (2000): 30833-30838.
123. Jakob, B., et al. "Live cell microscopy analysis of radiation-induced DNA double-strand break motion." *Proceedings of the National Academy of Sciences* 106.9 (2009): 3172-3177.
124. Jakob, Burkhard, et al. "DNA double-strand breaks in heterochromatin elicit fast repair protein recruitment, histone H2AX phosphorylation and relocation to euchromatin." *Nucleic acids research* 39.15 (2011): 6489-6499.
125. Janssen, Aniek, et al. "Chromosome segregation errors as a cause of DNA damage and structural chromosome aberrations." Science 333.6051 (2011): 1895-1898.
126. Jilani, Arshad, et al. "Molecular cloning of the human gene, PNKP, encoding a polynucleotide kinase 3'-phosphatase and evidence for its role in repair of DNA strand breaks caused by oxidative damage." Journal of Biological Chemistry 274.34 (1999): 24176-24186.
127. Jiricny, Josef. "The multifaceted mismatch-repair system." Nature reviews Molecular cell biology 7.5 (2006): 335-346.
128. Johzuka, Katsuki, and Hideyuki Ogawa. "Interaction of Mre11 and Rad50: two proteins required for DNA repair and meiosis-specific double-strand break formation in Saccharomyces cerevisiae." Genetics 139.4 (1995): 1521-1532.
129. Joseph, Fraulin, et al. "Temporal coordination between chromosome mobility and homologous recombination." *bioRxiv* (2022).
130. Kapusta, Aurélie, et al. "Highly precise and developmentally programmed genome assembly in Paramecium requires ligase IV–dependent end joining." PLoS genetics 7.4 (2011): e1002049.
131. Kao, Hui-I., Judith L. Campbell, and Robert A. Bambara. "Dna2p helicase/nuclease is a tracking protein, like FEN1, for flap cleavage during Okazaki fragment maturation." Journal of Biological Chemistry 279.49 (2004): 50840-50849.
132. Karran, Peter. "DNA double strand break repair in mammalian cells." Current opinion in genetics & development 10.2 (2000): 144-150.
133. Katou, Yuki, et al. "S-phase checkpoint proteins Tof1 and Mrc1 form a stable replication-pausing complex." *Nature* 424.6952 (2003): 1078-1083.
134. Keyamura, Kenji, Kota Arai, and Takashi Hishida. "Srs2 and Mus81–Mms4 Prevent Accumulation of Toxic Inter-Homolog Recombination Intermediates." *PLoS genetics* 12.7 (2016): e1006136.
135. Kim, Tae Moon, et al. "RAD51 mutants cause replication defects and chromosomal instability." *Molecular and cellular biology* 32.18 (2012): 3663-3680.
136. Kinebuchi, Takashi, et al. "Structural basis for octameric ring formation and DNA interaction of the human homologous-pairing protein Dmc1." *Molecular cell* 14.3 (2004): 363-374.
137. Klar, Amar JS. "Lessons learned from studies of fission yeast mating-type switching and silencing." Annu. Rev. Genet. 41 (2007): 213-236.
138. Klein, Hannah L., et al. "Guidelines for DNA recombination and repair studies: Cellular assays of DNA repair pathways." *Microbial cell* 6.1 (2019): 1.
139. Khadaroo, Basheer, et al. "The DNA damage response at eroded telomeres and tethering to the nuclear pore complex." *Nature cell biology* 11.8 (2009): 980-987.
140. Kobayashi, Takehiko. "Regulation of ribosomal RNA gene copy number and its role in modulating genome integrity and evolutionary adaptability in yeast." *Cellular and Molecular Life Sciences* 68.8 (2011): 1395-1403.
141. Koster, Daniel A., et al. "Antitumour drugs impede DNA uncoiling by topoisomerase I." Nature 448.7150 (2007): 213-217.

142. Krawczyk, P. M., et al. "Chromatin mobility is increased at sites of DNA double-strand breaks." *Journal of cell science* 125.9 (2012): 2127-2133.
143. Krejci, Lumir, et al. "Homologous recombination and its regulation." Nucleic acids research 40.13 (2012): 5795-5818.
144. Krejci, Lumir, et al. "DNA helicase Srs2 disrupts the Rad51 presynaptic filament." Nature 423.6937 (2003): 305-309.
145. Krejci, Lumir, et al. "Interaction with Rad51 is indispensable for recombination mediator function of Rad52." Journal of Biological Chemistry 277.42 (2002): 40132-40141.
146. Krogh, Berit Olsen, and Lorraine S. Symington. "Recombination proteins in yeast." *Annual review of genetics*38.1 (2004): 233-271.
147. Kruhlak, Michael J., et al. "Changes in chromatin structure and mobility in living cells at sites of DNA double-strand breaks." *The Journal of cell biology* 172.6 (2006): 823-834.
148. Kupiec, Martin, and Giora Simchen. "Cloning and mapping of the RAD50 gene of Saccharomyces cerevisiae." *Molecular and General Genetics MGG* 193.3 (1984): 525-531.
149. Lanctôt, Christian, et al. "Dynamic genome architecture in the nuclear space: regulation of gene expression in three dimensions." Nature Reviews Genetics 8.2 (2007): 104-115.
150. Le Breton, Cyrille, et al. "Srs2 removes deadly recombination intermediates independently of its interaction with SUMO-modified PCNA." *Nucleic acids research* 36.15 (2008): 4964-4974.
151. Lee, Cheng-Sheng, et al. "Chromosome position determines the success of double-strand break repair." *Proceedings of the National Academy of Sciences* 113.2 (2016): E146-E154.
152. Léger-Silvestre, Isabelle, et al. "Functional compartmentalization of the nucleus in the budding yeast Saccharomyces cerevisiae." Chromosoma 108.2 (1999): 103-113.
153. Leroy, Christophe, et al. "PP2C phosphatases Ptc2 and Ptc3 are required for DNA checkpoint inactivation after a double-strand break." Molecular cell 11.3 (2003): 827-835.
154. Lesterlin, Christian, et al. "RecA bundles mediate homology pairing between distant sisters during DNA break repair." Nature 506.7487 (2014): 249-253.
155. Li, Jinbao, et al. "Pathways and assays for DNA double-strand break repair by homologous recombination." *Acta biochimica et biophysica Sinica* 51.9 (2019): 879-889.
156. Lioy, Virginia S., et al. "Multiscale structuring of the E. coli chromosome by nucleoid-associated and condensin proteins." *Cell* 172.4 (2018): 771-783.
157. Lisby, Michael, Rodney Rothstein, and Uffe H. Mortensen. "Rad52 forms DNA repair and recombination centers during S phase." *Proceedings of the National Academy of Sciences* 98.15 (2001): 8276-8282.
158. Lisby, Michael, Uffe H. Mortensen, and Rodney Rothstein. "Colocalization of multiple DNA double-strand breaks at a single Rad52 repair centre." Nature cell biology 5.6 (2003): 572-577.
159. Lisby, Michael, et al. "Choreography of the DNA damage response: spatiotemporal relationships among checkpoint and repair proteins." Cell 118.6 (2004): 699-713.
160. Lisby, Michael, and Rodney Rothstein. "DNA damage checkpoint and repair centers." *Current opinion in cell biology* 16.3 (2004): 328-334.
161. Lisby, Michael, and Rodney Rothstein. "DNA repair: keeping it together." *Current biology* 14.23 (2004): R994-R996.
162. Liu, Jie, et al. "Rad51 paralogues Rad55–Rad57 balance the antirecombinase Srs2 in Rad51 filament formation." Nature 479.7372 (2011): 245-248.
163. Liu, Jie, and Wolf-Dietrich Heyer. "Who's who in human recombination: BRCA2 and RAD52." Proceedings of the National Academy of Sciences 108.2 (2011): 441-442.
164. Liu, Jie, et al. "Human BRCA2 protein promotes RAD51 filament formation on RPA-covered single-stranded DNA." *Nature structural & molecular biology* 17.10 (2010): 1260-1262.
165. Liu, Li, Katie K. Maguire, and Eric B. Kmiec. "Genetic re-engineering of Saccharomyces cerevisiae RAD51 leads to a significant increase in the frequency of gene repair *in vivo*." *Nucleic acids research* 32.7 (2004): 2093-2101

166. Liu, Shengqin, et al. "Distinct roles for DNA-PK, ATM and ATR in RPA phosphorylation and checkpoint activation in response to replication stress." *Nucleic acids research* 40.21 (2012): 10780-10794.
167. Lundblad, Victoria. "Telomere maintenance without telomerase." *Oncogene* 21.4 (2002): 522-531.
168. Lupiáñez, Darío G., Malte Spielmann, and Stefan Mundlos. "Breaking TADs: how alterations of chromatin domains result in disease." Trends in Genetics 32.4 (2016): 225-237.
169. Ma, Chu Jian, et al. "Human RAD52 interactions with replication protein A and the RAD51 presynaptic complex." Journal of Biological Chemistry 292.28 (2017): 11702-11713.
170. Ma, Chu Jian, et al. "Protein dynamics of human RPA and RAD51 on ssDNA during assembly and disassembly of the RAD51 filament." *Nucleic acids research* 45.2 (2017): 749-761.
171. Ma, Emilie, et al. "Rad52-Rad51 association is essential to protect Rad51 filaments against Srs2, but facultative for filament formation." Elife 7 (2018): e32744.
172. Ma, Emilie, et al. "Rad52 oligomeric N-terminal domain stabilizes Rad51 nucleoprotein filaments and contributes to their protection against Srs2." Cells 10.06 (2021): 1467.
173. Ma, Wenjian, et al. "Differential effects of poly (ADP-ribose) polymerase inhibition on DNA break repair in human cells are revealed with Epstein–Barr virus." Proceedings of the National Academy of Sciences 109.17 (2012): 6590-6595.
174. Mager, Willem H., and Joris Winderickx. "Yeast as a model for medical and medicinal research." Trends in pharmacological sciences 26.5 (2005): 265-273.
175. Malkova, Anna, Evgeny L. Ivanov, and James E. Haber. "Double-strand break repair in the absence of RAD51 in yeast: a possible role for break-induced DNA replication." Proceedings of the National Academy of Sciences 93.14 (1996): 7131-7136.
176. Maloisel, Laurent, Émilie Ma, and Éric Coïc. "Rad51 filaments assembled in the absence of the complex formed by the Rad51 paralogs Rad55 and Rad57 are outcompeted by translesion DNA polymerases on UV-induced ssDNA gaps." *bioRxiv* (2022): 2021-05.
177. Manley, Suliana, et al. "High-density mapping of single-molecule trajectories with photoactivated localization microscopy." *Nature methods* 5.2 (2008): 155-157.
178. Marchetti, Francesco, and Andrew J. Wyrobek. "Mechanisms and consequences of paternally-transmitted chromosomal abnormalities." Birth Defects Research Part C: Embryo Today: Reviews 75.2 (2005): 112-129
179. Marini, Victoria, and Lumir Krejci. "Srs2: The “odd-job man” in DNA repair." *DNA repair* 9.3 (2010): 268-275
180. Marteijn, Jurgen A., et al. "Understanding nucleotide excision repair and its roles in cancer and ageing." Nature reviews Molecular cell biology 15.7 (2014): 465-481.
181. Martin, Sophie G., et al. "Relocalization of telomeric Ku and SIR proteins in response to DNA strand breaks in yeast." *Cell*97.5 (1999): 621-633.
182. Matos, Dominick A., et al. "ATR protects the genome against R loops through a MUS81-triggered feedback loop." Molecular cell 77.3 (2020): 514-527.
183. McEachern, Michael J., and James E. Haber. "Break-induced replication and recombinational telomere elongation in yeast." *Annual review of biochemistry* 75.1 (2006): 111-135.
184. McIlwraith, Michael J., and Stephen C. West. "DNA repair synthesis facilitates RAD52-mediated second-end capture during DSB repair." Molecular cell 29.4 (2008): 510-516.
185. McMurray, M. A. & Gottschling, D. E. An age-induced switch to a hyper-recombinational state. Science 301, (2003):1908–1911
186. McVey, Mitch, and Sang Eun Lee. "MMEJ repair of double-strand breaks (director’s cut): deleted sequences and alternative endings." Trends in Genetics 24.11 (2008): 529-538
187. Mehta, Anuja, and James E. Haber. "Sources of DNA double-strand breaks and models of recombinational DNA repair." Cold Spring Harbor perspectives in biology 6.9 (2014): a016428.
188. Meir, Aviv, et al. "Rad54 and Rdh54 prevent Srs2-mediated disruption of Rad51 presynaptic filaments." *Proceedings of the National Academy of Sciences* 119.4 (2022): e2113871119.
189. Menetski, Joseph P., David G. Bear, and Stephen C. Kowalczykowski. "Stable DNA heteroduplex formation catalyzed by the Escherichia coli RecA protein in the absence of ATP

hydrolysis." *Proceedings of the National Academy of Sciences* 87.1 (1990): 21-25.
190. Mercier, Romain, et al. "The MatP/matS site-specific system organizes the terminus region of the E. coli chromosome into a macrodomain." *Cell* 135.3 (2008): 475-485.
191. Mewes, HrW, et al. "Overview of the yeast genome." Nature 387.6632 (1997): 7-8.
192. Milligan, Jamie R., et al. "DNA repair by thiols in air shows two radicals make a double-strand break." Radiation research 143.3 (1995): 273-280.
193. Mimitou, Eleni P., and Lorraine S. Symington. "DNA end resection—unraveling the tail." *DNA repair* 10.3 (2011): 344-348.
194. Miné, Judith, et al. "Real-time measurements of the nucleation, growth and dissociation of single Rad51–DNA nucleoprotein filaments." Nucleic acids research 35.21 (2007): 7171-7187.
195. Miné-Hattab, Judith, and Angela Taddei. "Physical principles and functional consequences of nuclear compartmentalization in budding yeast." Current Opinion in Cell Biology 58 (2019): 105-113.
196. Miné-Hattab, Judith, and Rodney Rothstein. "Increased chromosome mobility facilitates homology search during recombination." Nature cell biology 14.5 (2012): 510-517.
197. Miné-Hattab, Judith, et al. "Multi-scale tracking reveals scale-dependent chromatin dynamics after DNA damage." *Molecular biology of the cell* 28.23 (2017): 3323-3332.
198. Miné-Hattab, Judith, and Xavier Darzacq. "Chromatin Dynamics upon DNA Damage." Chromatin and Epigenetics. IntechOpen, 2020.
199. Miné-Hattab, Judith, et al. "Single molecule microscopy reveals key physical features of repair foci in living cells." *Elife* 10 (2021): e60577.
200. Mirny, Leonid, et al. "How a protein searches for its site on DNA: the mechanism of facilitated diffusion." *Journal of Physics A: Mathematical and Theoretical* 42.43 (2009): 434013.
201. Mira, Alex, Howard Ochman, and Nancy A. Moran. "Deletional bias and the evolution of bacterial genomes." Trends in Genetics 17.10 (2001): 589-596.
202. Misteli, Tom, and Evi Soutoglou. "The emerging role of nuclear architecture in DNA repair and genome maintenance." *Nature reviews Molecular cell biology* 10.4 (2009): 243-254.
203. Misteli, Tom. "Where the nucleus comes from." *Trends in Genetics* 17.4 (2001): 190.
204. Misteli, Tom. "Beyond the sequence: cellular organization of genome function." *Cell* 128.4 (2007): 787-800.
205. Mortensen, Uffe H., et al. "DNA strand annealing is promoted by the yeast Rad52 protein." *Proceedings of the National Academy of Sciences* 93.20 (1996): 10729-10734.
206. Moncalian, Gabriel, et al. "The rad50 signature motif: essential to ATP binding and biological function." Journal of molecular biology 335.4 (2004): 937-951.
207. Moustacchi, Ethel. "DNA damage and repair: consequences on dose-responses." Mutation Research/Genetic Toxicology and Environmental Mutagenesis 464.1 (2000): 35-40.
208. Mortensen, Uffe H., Michael Lisby, and Rodney Rothstein. "Rad52." *Current Biology* 19.16 (2009): R676-R677.
209. Muraszko, Jakub, et al. "Rrp1 translocase and ubiquitin ligase activities restrict the genome destabilising effects of Rad51 in fission yeast." Nucleic Acids Research 49.12 (2021): 6832-6848.
210. Myler, Logan R., et al. "Single-molecule imaging reveals how Mre11-Rad50-Nbs1 initiates DNA break repair." *Molecular cell* 67.5 (2017): 891-898.
211. Neumaier, Teresa, et al. "Evidence for formation of DNA repair centers and dose-response nonlinearity in human cells." Proceedings of the National Academy of Sciences 109.2 (2012): 443-448.
212. Nimonkar, Amitabh V., et al. "BLM–DNA2–RPA–MRN and EXO1–BLM–RPA–MRN constitute two DNA end resection machineries for human DNA break repair." *Genes & development* 25.4 (2011): 350-362.
213. Ogawa, Tomoko, et al. "Similarity of the yeast RAD51 filament to the bacterial RecA filament." Science 259.5103 (1993): 1896-1899.
214. Ortiz, Ana María León, et al. "Srs2 overexpression reveals a helicase-independent role at replication forks that requires diverse cell functions." *DNA repair* 10.5 (2011): 506-517.
215. Oshidari, Roxanne, et al. "DNA repair by Rad52 liquid droplets." *Nature communications* 11.1 (2020):

1-8.
216. Ozenberger, BRADLEY A., and G. Shirleen Roeder. "A unique pathway of double-strand break repair operates in tandemly repeated genes." Molecular and cellular biology 11.3 (1991): 1222-1231.
217. Palladino, F., et al. "SIR3 and SIR4 proteins are required for the positioning and integrity of yeast telomeres." *Cell* 75.3 (1993): 543-555.
218. Pannunzio, Nicholas R., Go Watanabe, and Michael R. Lieber. "Nonhomologous DNA end-joining for repair of DNA double-strand breaks." Journal of Biological Chemistry 293.27 (2018): 10512-10523
219. Paulovich, Amanda G., David P. Toczyski, and Leland H. Hartwell. "When checkpoints fail." Cell 88.3 (1997): 315-321.
220. Pellicioli, Achille, et al. "Regulation of Saccharomyces Rad53 checkpoint kinase during adaptation from DNA damage–induced G2/M arrest." Molecular cell 7.2 (2001): 293-300.
221. Prakash, Rohit, et al. "Homologous recombination and human health: the roles of BRCA1, BRCA2, and associated proteins." *Cold Spring Harbor perspectives in biology* 7.4 (2015): a016600.
222. Qi, Zhi, et al. "DNA sequence alignment by microhomology sampling during homologous recombination." *Cell* 160.5 (2015): 856-869.
223. Qiu, Yupeng, et al. "Srs2 prevents Rad51 filament formation by repetitive motion on DNA." Nature communications 4.1 (2013): 1-10.
224. Quevedo, Oliver, et al. "Nondisjunction of a single chromosome leads to breakage and activation of DNA damage checkpoint in G2." PLoS genetics 8.2 (2012): e1002509.
225. Raderschall, Elke, et al. "Formation of higher-order nuclear Rad51 structures is functionally linked to p21 expression and protection from DNA damage-induced apoptosis." *Journal of cell science* 115.1 (2002): 153-164.
226. Rattray, Alison J., and Lorraine S. Symington. "Use of a chromosomal inverted repeat to demonstrate that the RAD51 and RAD52 genes of Saccharomyces cerevisiae have different roles in mitotic recombination." *Genetics* 138.3 (1994): 587-595.
227. Ranatunga, Wasantha, et al. "Human RAD52 exhibits two modes of self-association." *Journal of Biological Chemistry* 276.19 (2001): 15876-15880.
228. Ragunathan, Kaushik, Cheng Liu, and Taekjip Ha. "RecA filament sliding on DNA facilitates homology search." *Elife* 1 (2012): e00067.
229. Renkawitz, Jörg, Claudio A. Lademann, and Stefan Jentsch. "Mechanisms and principles of homology search during recombination." Nature Reviews Molecular Cell Biology 15.6 (2014): 369-383.
230. Rijkers, Tonnie, et al. "Targeted inactivation of mouse RAD52 reduces homologous recombination but not resistance to ionizing radiation." *Molecular and cellular biology* 18.11 (1998): 6423-6429.
231. Roberts, Steven A., et al. "Ku is a 5'-dRP/AP lyase that excises nucleotide damage near broken ends." Nature464.7292 (2010): 1214-1217.
232. Rocha, Eduardo PC. "The organization of the bacterial genome." Annual review of genetics 42 (2008): 211-233.
233. Roman, Herschel. "Studies of gene mutation in Saccharomyces." Cold Spring Harbor symposia on quantitative biology. Vol. 21. Cold Spring Harbor Laboratory Press, 1956.
234. Roy, Upasana, et al. "The Rad51 paralog complex Rad55-Rad57 acts as a molecular chaperone during homologous recombination." Molecular cell 81.5 (2021): 1043-1057.
235. Ruault M et al.: Clustering heterochromatin: Sir3 promotes telomere clustering independently of silencing in yeast. J Cell Biol (2011), 192:417-431.
236. Saad, Hicham, et al. "DNA dynamics during early double-strand break processing revealed by non-intrusive imaging of living cells." PLoS genetics 10.3 (2014): e1004187.
237. Sáez-Vásquez, Julio, and Olivier Gadal. "Genome organization and function: a view from yeast and Arabidopsis." Molecular plant 3.4 (2010): 678-690.
238. Sagi, Dror, Tsvi Tlusty, and Joel Stavans. "High fidelity of RecA-catalyzed recombination: a watchdog of genetic diversity." Nucleic acids research 34.18 (2006): 5021-5031.
239. San Filippo, Joseph, Patrick Sung, and Hannah Klein. "Mechanism of eukaryotic homologous recombination." Annu. Rev. Biochem. 77 (2008): 229-257.

240. Samoshkin, Alexander, et al. "Human condensin function is essential for centromeric chromatin assembly and proper sister kinetochore orientation." PloS one 4.8 (2009): e6831.
241. Santos, Ana L., et al. "Wavelength dependence of biological damage induced by UV radiation on bacteria." Archives of microbiology 195.1 (2013): 63-74.
242. Santos, Teresa de los, et al. "The Mus81/Mms4 endonuclease acts independently of double-Holliday junction resolution to promote a distinct subset of crossovers during meiosis in budding yeast." Genetics 164.1 (2003): 81-94.
243. Sasanuma, Hiroyuki, et al. "A new protein complex promoting the assembly of Rad51 filaments." *Nature communications* 4.1 (2013): 1-13.
244. Sauvageau, Synthia, et al. "Fission yeast rad51 and dmc1, two efficient DNA recombinases forming helical nucleoprotein filaments." *Molecular and cellular biology* 25.11 (2005): 4377-4387.
245. Schatz, David G., and Yanhong Ji. "Recombination centres and the orchestration of V (D) J recombination." Nature Reviews Immunology 11.4 (2011): 251-263.
246. Schwacha, Anthony, and Nancy Kleckner. "Interhomolog bias during meiotic recombination: meiotic functions promote a highly differentiated interhomolog-only pathway." *Cell* 90.6 (1997): 1123-1135.
247. Selmane, Tassadite, et al. "Identification of the subunit–subunit interface of Xenopus Rad51. 1 protein: similarity to RecA." *Journal of molecular biology* 335.4 (2004): 895-904.
248. Shahar, O. D., et al. "Live imaging of induced and controlled DNA double-strand break formation reveals extremely low repair by homologous recombination in human cells." Oncogene 31.30 (2012): 3495-3504.
249. Sheridan, Sean D., et al. "A comparative analysis of Dmc1 and Rad51 nucleoprotein filaments." Nucleic acids research 36.12 (2008): 4057-4066.
250. Shibata, Atsushi, et al. "Factors determining DNA double-strand break repair pathway choice in G2 phase." The EMBO journal 30.6 (2011): 1079-1092
251. Shin, David S., et al. "Full-length archaeal Rad51 structure and mutants: mechanisms for RAD51 assembly and control by BRCA2." *The EMBO journal* 22.17 (2003): 4566-4576.
252. Shinohara, Akira, et al. "Rad52 forms ring structures and co-operates with RPA in single-strand DNA annealing." Genes to Cells 3.3 (1998): 145-156.
253. Shrivastav, Meena, Leyma P. De Haro, and Jac A. Nickoloff. "Regulation of DNA double-strand break repair pathway choice." *Cell research* 18.1 (2008): 134-147.
254. Short, Judith M., et al. "High-resolution structure of the presynaptic RAD51 filament on single-stranded DNA by electron cryo-microscopy." Nucleic acids research 44.19 (2016): 9017-9030.
255. Shou, Wenying, et al. "Exit from mitosis is triggered by Tem1-dependent release of the protein phosphatase Cdc14 from nucleolar RENT complex." *Cell* 97.2 (1999): 233-244.
256. Sinha, Rajeshwar P., and Donat-P. Häder. "UV-induced DNA damage and repair: a review." Photochemical & Photobiological Sciences 1.4 (2002): 225-236.
257. Slotman, Johan A., et al. "Super-resolution imaging of RAD51 and DMC1 in DNA repair foci reveals dynamic distribution patterns in meiotic prophase." PLoS genetics 16.6 (2020): e1008595.
258. Smith, Graeme CM, and Stephen P. Jackson. "The DNA-dependent protein kinase." *Genes & development* 13.8 (1999): 916-934.
259. So, Ayeong, et al. "Genomic rearrangements induced by unscheduled DNA double strand breaks in somatic mammalian cells." *The FEBS journal* 284.15 (2017): 2324-2344.
260. So, Ayeong, et al. "RAD51 protects against nonconservative DNA double-strand break repair through a nonenzymatic function." *Nucleic acids research* 50.5 (2022): 2651-2666.
261. Sonoda, Eiichiro, et al. "Rad51-deficient vertebrate cells accumulate chromosomal breaks prior to cell death." The EMBO journal 17.2 (1998): 598-608.
262. Sobinoff, Alexander P., and Hilda A. Pickett. "Mechanisms that drive telomere maintenance and recombination in human cancers." *Current Opinion in Genetics & Development* 60 (2020): 25-30.
263. Sordet, Olivier, et al. "Ataxia telangiectasia mutated activation by transcription-and topoisomerase I-induced DNA double-strand breaks." *EMBO reports* 10.8 (2009): 887-893.

264. Soulas-Sprauel, Pauline, et al. "V (D) J and immunoglobulin class switch recombinations: a paradigm to study the regulation of DNA end-joining." *Oncogene* 26.56 (2007): 7780-7791.
265. Soutoglou, Evi, et al. "Positional stability of single double-strand breaks in mammalian cells." *Nature cell biology* 9.6 (2007): 675-682.
266. Sotiriou, Sotirios K., et al. "Mammalian RAD52 functions in break-induced replication repair of collapsed DNA replication forks." Molecular cell 64.6 (2016): 1127-1134.
267. Sturzenegger, Andreas, et al. "DNA2 cooperates with the WRN and BLM RecQ helicases to mediate long-range DNA end resection in human cells." *Journal of Biological Chemistry*289.39 (2014): 27314-27326.
268. Sugawara, Neal, Grzegorz Ira, and James E. Haber. "DNA length dependence of the single-strand annealing pathway and the role of Saccharomyces cerevisiae RAD59 in double-strand break repair." *Molecular and cellular biology* 20.14 (2000): 5300-5309.
269. Sugiyama, Tomohiko, and Stephen C. Kowalczykowski. "Rad52 protein associates with replication protein A (RPA)-single-stranded DNA to accelerate Rad51-mediated displacement of RPA and presynaptic complex formation." Journal of Biological Chemistry 277.35 (2002): 31663-31672.
270. Sung, Patrick, and Hannah Klein. "Mechanism of homologous recombination: mediators and helicases take on regulatory functions." *Nature reviews Molecular cell biology* 7.10 (2006): 739-750.
271. Sung, Patrick, and Donald L. Robberson. "DNA strand exchange mediated by a RAD51-ssDNA nucleoprotein filament with polarity opposite to that of RecA." Cell 82.3 (1995): 453-461.
272. Sung, Patrick. "Function of yeast Rad52 protein as a mediator between replication protein A and the Rad51 recombinase." Journal of Biological Chemistry 272.45 (1997): 28194-28197.
273. Sung, Patrick. "Yeast Rad55 and Rad57 proteins form a heterodimer that functions with replication protein A to promote DNA strand exchange by Rad51 recombinase." Genes & development 11.9 (1997): 1111-1121.
274. Sun, Hong, Douglas Treco, and Jack W. Szostak. "Extensive 3'-overhanging, single-stranded DNA associated with the meiosis-specific double-strand breaks at the ARG4 recombination initiation site." Cell 64.6 (1991): 1155-1161.
275. Syeda, Aisha H., Michelle Hawkins, and Peter McGlynn. "Recombination and replication." Cold Spring Harbor perspectives in biology 6.11 (2014): a016550.
276. Symington, Lorraine S. "Mechanism and regulation of DNA end resection in eukaryotes." *Critical reviews in biochemistry and molecular biology* 51.3 (2016): 195-212.
277. Taddei, A, and S M. Gasser. "Structure and function in the budding yeast nucleus." Genetics 192.1 (2012): 107-129.
278. Taddei, A., H. Schober, and S. M. Gasser. "The budding yeast nucleus. Cold Spring Harb Perspect Biol 2: a000612." (2010): 12.
279. Takizawa, Takumi, Karen J. Meaburn, and Tom Misteli. "The meaning of gene positioning." Cell 135.1 (2008): 9-13.
280. Tan, T. L. R., et al. "Mouse Rad54 affects DNA conformation and DNA-damage-induced Rad51 foci formation." Current Biology 9.6 (1999): 325-328.
281. Tarsounas, Madalena, Adelina A. Davies, and Stephen C. West. "RAD51 localization and activation following DNA damage." Philosophical Transactions of the Royal Society of London. Series B: Biological Sciences 359.1441 (2004): 87-93.
282. Tavares, Eliana Moreira, et al. "*In vitro* role of Rad54 in Rad51-ssDNA filament-dependent homology search and synaptic complexes formation." *Nature communications* 10.1 (2019): 1-12.
283. Thompson, Larry H. "Recognition, signaling, and repair of DNA double-strand breaks produced by ionizing radiation in mammalian cells: the molecular choreography." Mutation Research/Reviews in Mutation Research 751.2 (2012): 158-246.
284. Toczyski, David P., David J. Galgoczy, and Leland H. Hartwell. "CDC5 and CKII control adaptation to the yeast DNA damage checkpoint." Cell 90.6 (1997): 1097-1106.
285. Tran, Phuoc T., et al. "Characterization of nuclease-dependent functions of Exo1p in Saccharomyces cerevisiae." *DNA repair* 1.11 (2002): 895-912.

286. Tran, Phuoc T., et al. "A mutation in EXO1 defines separable roles in DNA mismatch repair and post-replication repair." *DNA repair* 6.11 (2007): 1572-1583.
287. Trumtel, Stéphanie, et al. "Assembly and functional organization of the nucleolus: ultrastructural analysis of Saccharomyces cerevisiae mutants." Molecular biology of the cell 11.6 (2000): 2175-2189.
288. Tsabar, Michael, et al. "Caffeine inhibits gene conversion by displacing Rad51 from ssDNA." Nucleic acids research 43.14 (2015): 6902-6918.
289. Tsai, Feng-Ling, and Mihoko Kai. "The checkpoint clamp protein Rad9 facilitates DNA-end resection and prevents alternative non-homologous end joining." *Cell Cycle* 13.21 (2014): 3460-3464.
290. Tsang, Siu Sing, Samson A. Chow, and Charles M. Radding. "Networks of DNA and RecA protein are intermediates in homologous pairing." *Biochemistry* 24.13 (1985): 3226-3232.
291. van Veelen, Lieneke R., et al. "Ionizing radiation-induced foci formation of mammalian Rad51 and Rad54 depends on the Rad51 paralogs, but not on Rad52." Mutation Research/Fundamental and Molecular Mechanisms of Mutagenesis 574.1-2 (2005): 34-49.
292. Veaute, Xavier, et al. "The Srs2 helicase prevents recombination by disrupting Rad51 nucleoprotein filaments." Nature 423.6937 (2003): 309-312.
293. Vijg, Jan, and Yousin Suh. "Genome instability and aging." Annual review of physiology 75 (2013): 645-668.
294. Vilenchik, Michael M., and Alfred G. Knudson. "Endogenous DNA double-strand breaks: production, fidelity of repair, and induction of cancer." Proceedings of the National Academy of Sciences 100.22 (2003): 12871-12876.
295. Ward, J. F. "The complexity of DNA damage: relevance to biological consequences." International journal of radiation biology 66.5 (1994): 427-432.
296. Wassing, Isabel E., and Fumiko Esashi. "RAD51: Beyond the break." Seminars in Cell & Developmental Biology. Vol. 113. Academic Press, 2021.
297. Weinfeld, Michael, and Krista June M. Soderlind. "Phosphorus-32-postlabeling detection of radiation-induced DNA damage: identification and estimation of thymine glycols and phosphoglycolate termini." Biochemistry 30.4 (1991): 1091-1097.
298. Weiffenbach, B. A. R. B. A. R. A., and JAMES E. Haber. "Homothallic mating type switching generates lethal chromosome breaks in rad52 strains of Saccharomyces cerevisiae." *Molecular and Cellular Biology* 1.6 (1981): 522-534.
299. Weinstock, David M., Erika Brunet, and Maria Jasin. "Formation of NHEJ-derived reciprocal chromosomal translocations does not require Ku70." Nature cell biology 9.8 (2007): 978-981.
300. Welcker, Anne J., et al. "Involvement of very short DNA tandem repeats and the influence of the RAD52 gene on the occurrence of deletions in Saccharomyces cerevisiae." *Genetics* 156.2 (2000): 549-557.
301. Wiktor, Jakub. "RecA finds homologous DNA by reduced dimensionality search." Biophysical Journal 121.3 (2022): 446a.
302. Wolfe, Alan, George H. Shimer Jr, and Thomas Meehan. "Polycyclic aromatic hydrocarbons physically intercalate into duplex regions of denatured DNA." Biochemistry 26.20 (1987): 6392-6396.
303. Wong, Ronald P., et al. "Processing of DNA polymerase-blocking lesions during genome replication is spatially and temporally segregated from replication forks." *Molecular cell* 77.1 (2020): 3-16.
304. Wu, Yun, et al. "Rad51 protein controls Rad52-mediated DNA annealing." *Journal of Biological Chemistry* 283.21 (2008): 14883-14892.
305. Wu, Yun, Tomohiko Sugiyama, and Stephen C. Kowalczykowski. "DNA annealing mediated by Rad52 and Rad59 proteins." Journal of Biological Chemistry 281.22 (2006): 15441-15449.
306. Wyatt, Haley DM, and Stephen C. West. "Holliday junction resolvases." Cold Spring Harbor perspectives in biology 6.9 (2014): a023192.
307. Wyrobek, Andrew J., Thomas E. Schmid, and Francesco Marchetti. "Relative susceptibilities of male

germ cells to genetic defects induced by cancer chemotherapies." *JNCI Monographs* 2005.34 (2005): 31-35.
308. Xu, Hong, Charles Boone, and Hannah L. Klein. "Mrc1 is required for sister chromatid cohesion to aid in recombination repair of spontaneous damage." *Molecular and cellular biology* 24.16 (2004): 7082-7090.
309. Yang, Haijuan, et al. "The BRCA2 homologue Brh2 nucleates RAD51 filament formation at a dsDNA–ssDNA junction." *Nature* 433.7026 (2005): 653-657.
310. Yang, Darren, et al. "Integrating multi-scale data on homologous recombination into a new recognition mechanism based on simulations of the RecA-ssDNA/dsDNA structure." *Nucleic acids research* 43.21 (2015): 10251-10263.
311. Yasuhara, Takaaki, and Lee Zou. "Impacts of chromatin dynamics and compartmentalization on DNA repair." *DNA repair* 105 (2021): 103162.
312. Yu, Xin, and Abram Gabriel. "Ku-dependent and Ku-independent end-joining pathways lead to chromosomal rearrangements during double-strand break repair in Saccharomyces cerevisiae." *Genetics* 163.3 (2003): 843-856.
313. Yu, Xiong, et al. "Domain structure and dynamics in the helical filaments formed by RecA and Rad51 on DNA." Proceedings of the National Academy of Sciences 98.15 (2001): 8419-8424.
314. Zheng, Hui, and Wei Xie. "The role of 3D genome organization in development and cell differentiation." Nature Reviews Molecular Cell Biology 20.9 (2019): 535-550.
315. Zhu, Zhu, et al. "Sgs1 helicase and two nucleases Dna2 and Exo1 resect DNA double-strand break ends." Cell 134.6 (2008): 981-994.
316. Zimmer, Christophe, and Emmanuelle Fabre. "Chromatin mobility upon DNA damage: state of the art and remaining questions." Current genetics 65.1 (2019): 1-9.

ANNEX

Table S1. List of strains used in the study

Strain name	Genotype
yAT3392	*MATa ADE2 RAD5+ lys2::ura3-ISceIcutsite(loxP) trp1::Gal-I-SceI-TRP1 ura3Δ::KanMX*
yAT3799	*MATa ADE2 RAD5+ lys2::ura3-ISceIcutsite(loxP) trp1::Gal-I-SceI-TRP1 ura3Δ::KanMX rad51Δ::hph*
W4121-20D	*MATa ADE2 bar1::LEU2 trp1-1 LYS2 RAD5 YFP-RAD51*
yAT3515	*MATa ADE2 RAD5+ lys2::ura3-ISceIcutsite(loxP) trp1::Gal-I-SceI-TRP1 ura3Δ::KanMX RAD51-iGFP1*
yAT3880	*MATa ADE2 RAD5+ lys2::ura3-ISceIcutsite(loxP) trp1::Gal-I-SceI-TRP1 ura3Δ::KanMX RAD51-iGFP2*
yAT3390	*MATa ADE2 RAD5+ lys2::ura3-ISceIcutsite(loxP) trp1::Gal-I-SceI-TRP1*
yAT4041	*MATa ADE2 RAD5+ lys2::ura3-ISceIcutsite(loxP) trp1::Gal-I-SceI-TRP1 Rad51-iGFP2*
yAT3971	*MATa/αADE2/ADE2 RAD5/RAD5 LSY2/lys2::ura3-ISceIcutsite(loxP) TRP1/trp1::Gal-ISCeI-TRP1 URA3/ura3Δ::KanMX RAD51-iGFP2/RAD51-iGFP2*
yAT4284	*MATa/αADE/ADE2 ARS607/ARS607::TRP1::Lacop::LexA ura3::CloNat/ ura3Δ::KanMX RAD5+/rad5 lys2::ura3-ISceIcutsite(loxP) /lys2) trp1::Gal-I-SceI-TRP1 RAD51-iGFP2/RAD51 his3::ADHp-LacIsp-mCherry(HIS) /his3*
yAT4206	*ADE2/ADE2 RAD5+/RAD5+ lys2::ura3-ISceIcutsite(loxP)/ lys2:: LacO (TRP1) trp1::Gal-I-SceI-TRP1/trp1 his/his::LacI mCherry(His) ura3Δ::KanMX/ura3::CloNAT RAD51-iGFP2/RAD51*
yAT3976	*MATa ADE2 RAD5+ lys2::ura3-ISceIcutsite(loxP) trp1::Gal-I-SceI-TRP1 ura3Δ::KanMX RAD51-iGFP2 exo1::hph*
yAT4034	*MATa ADE2 RAD5+ lys2::ura3-ISceIcutsite(loxP) trp1::Gal-I-SceI-TRP1 ura3Δ::KanMX RAD51-iGFP2 sgs1::CloNAT*
yAT4024	*MATa ADE2 RAD5+ lys2::ura3-ISceIcutsite(loxP) trp1::Gal-I-SceI-TRP1 ura3Δ::KanMX RAD51-iGFP2 exo1::hph sgs1::CloNAT*
yAT4032	*MATa ADE2 RAD5+ lys2::ura3-ISceIcutsite(loxP) trp1::Gal-I-SceI-TRP1 ura3Δ::KanMX RAD51-iGFP2 rad52::CloNAT*
yAT3974	*MATa ADE2 RAD5+ lys2::ura3-ISceIcutsite(loxP) trp1::Gal-I-SceI-TRP1 ura3Δ::KanMX RAD51-iGFP2 srs2Δ::HIS*
yAT4023	*MATa* ADE2 RAD5+ *lys2::ura3-ISceIcutsite(loxP) trp1::Gal-I-SceI-TRP1 ura3Δ::KanMX RAD51-iGFP2 rad54::CloNAT*
yAT4354	*MATa ADE2 RAD5+ lys2::ura3-ISceIcutsite(loxP)* trp1::Gal-I-SceI-TRP1 *ura3Δ::KanMX Rad51-GFP(HPH)*
yAT4256	*MATa ADE2 RAD5+ lys2::ura3-ISceIcutsite(loxP) trp1::Gal-I-SceI-TRP1 ura3Δ::KanMX RAD51-iGFP2 exo1::hph sgs1::CloNAT. rad54::CloNAT*
yAT3690	*MATa ADE2 RAD5+ lys2::ura3-ISceIcutsite(loxP) trp1::Gal-ISCeI-TRP1 ura3Δ::KanMX RAD51-iGFP1 Nup57::NUP57-mCherry(HpH)*
yAT2604	*MATa ade2-1::ADE2 DDC1-CFP SPC42::SPC42-mcherry(KanMX) SPC110-YFP::HIS*

Table S2. List of primers used in this study

Primers for plasmid construction	
	Sequence
Guide Rad51	am2449 ATCTGGCGGATTGCAGGAGCAAG am2450 AACCTTGCTCCTGCAATCCGCCA
dDNA Rad51-iGFP2	am558 CATTCCCTGAGCATTCCAAC am2401 CCTGAATTCACCGAAAAGCTCA
dDNA Rad51-iGFP1	am2334 GCAACGGTAGCAGCGAAGATATTGAGGCCACCAACGGCTCCGGCGATGGTGGAGG TGCTGGATCTGCTGGTGGTGCAGGTGGATCTAAAGGTGAAGAATTATT am2335 AGGCAGCTTCATCGTATGCTTCATCCTCCATTTCACCTTGCGCTTCTGCTTGCTCCTGC AATCCGCCACCACCAGCACCACCAGCAGAACCAGCACCACCTTTGTACAATTCATCCA TAC
Primers for ChIP	
Name	Sequence
OGG1	F CAATGGTGTAGGCCCCAAAG R ACGATGCCATCCATGTGAAGT
-200bp	F AAGGAACGTGCTGCTACTC R ACATCCAATGAAGCACACAAG
-600bp	F CGTCAGGGCCAAGGATGA R AGTACCATAGGTGATACCTGCCTTTT
-800bp	F TGATTTACCATTGGGCACAATTT R AATTTCCGCGGCAAAGG
-1.4kb	F TCGCAAAAATGCCGACAAT R GCTTGTCAAATCTTGGGACCAT
-5kb	F GCTCTGGCAACAAGAAAGAC R ACCGATCAATTCAGGCAAAAC
-8kb	F CTTTTCCCAACCCTTGTACC R GTTCCATTCGTCCCAATCTC
-12kb	F TCGAAGAAGTTTTGGAAGCTC R TAGCAGCGGCATTAGCATC
-18kb	F TCATCAAGCTCAACAAGCTC R GAAAACCGGACCAGGAATAG

Table S3. Filament lengths and intensities

Filament Median lengths in haploid and diploid strain (N>180, μm)

	2h	4h	6h	P 2h *vs* 4h	P 2h *vs* 6h	P 4h *vs* 6h
Haploid	0.91	1.30	1.69	1.08e-07 ***	2.70e-18 ***	7.92e-08 ***
Diploid	1.30	1.69	1.43	1.32e-04 ***	7.01e-02 ns	1.08e-02 *

Filament Median lengths in WT, *srs2Δ* and *rad54Δ* strain (N>230, μm)

	WT	*srs2Δ*	*rad54Δ*	P (WT *vs srs2Δ*)	P (WT *vs rad54Δ*)	P (*srs2Δ vs rad54Δ*)
4h	1.36	1.45	1.56	6.92e-01 ns	5.35e-05 ***	5.23e-05 ***
6h	1.75	1.82	2.40	8.41e-01 ns	3.60e-11 ***	1.97e-09 ***

Filament Median intensities in WT, *srs2Δ* and *rad54Δ* strain (N>230, a.u)

	WT	*srs2Δ*	*rad54Δ*	P (WT *vs srs2Δ*)	P (WT *vs rad54Δ*)	P (*srs2Δ vs rad54Δ*)
4h	1210	1400	1280	5.88e-16 ***	35.61e-03 ***	3.02e-06 ***

RÉSUMÉ

L'ADN est le principal vecteur d'information génétique dans les cellules procaryotes et eucaryotes et son intégrité est vitale pour la survie des cellules. Malgré son importance. L'ADN est sous la pression des dommages causés par des facteurs exogènes et endogènes. La rupture double brin (DSB) est l'un des dommages à l'ADN les plus toxiques et même un DSB non réparé est mortel pour les cellules. Les cellules ont développé plusieurs voies pour réparer les DSB, y compris la jonction d'extrémités non homologues (NHEJ) et la recombinaison homologue (HR). HR est une voie de réparation sans erreur qui utilise une séquence homologue intacte comme modèle pour réparer les dommages. Il s'agit d'identifier la séquence homologue parmi les méga-bases du génome et dans le volume nucléaire des cellules eucaryotes. Au niveau moléculaire, l'échantillonnage de l'ADN et l'invasion des brins de l'ADNdb homologue sont réalisés par un filament de nucléoprotéine (NPF), formé par la recombinase, RecA chez les bactéries et Rad51 chez les eucaryotes, enrobant l'ADNss. Ce mécanisme a été largement étudié in vitro et in vivo par des approches moléculaires au niveau des populations cellulaires. Cependant, pour être identifié comme homologue à la séquence endommagée, un locus donné doit être suffisamment proche du NPF. Comment cette recherche d'homologie à l'échelle du noyau est-elle effectuée reste une question ouverte. Un verrou méthodologique pour répondre à cette question a été le manque d'outils expérimentaux pour visualiser le NPF dans les cellules vivantes. En effet, les tentatives passées de marquer Rad51 par fluorescence ont donné une protéine non fonctionnelle formant des foyers discrets dans les cellules.

Compte tenu de l'importance de Rad51 au cours de la RH, il a été intensivement étudié in vitro ou sur de grandes populations de cellules in vivo, par des tests génétiques ou moléculaires, mais le manque d'étude sur des cellules vivantes individuelles comme l'absence d'étiquette fonctionnelle sur Rad51.

Grâce aux connaissances structurelles de notre collaborateur Raphael Guerois (I2BC, CEA), nous avons développé et caractérisé une version fonctionnelle et étiquetée en interne de S.cerevisiae Rad51. Suite à l'induction de DSB unique, nous observons pour la première fois dans des cellules vivantes, Rad51 formant des filaments micrométriques longs s'étendant sur tout le noyau et en contact avec la séquence donneuse. Il est important de noter que la longueur de ces filaments coïncide avec l'étendue de la formation d'ADNsb et de la propagation de Rad51 sur l'ADN. Comme prédit à partir de données génétiques et in vitro, leur formation nécessite le chargeur de recombinase Rad52 et la formation d'un long tronçon d'ADNsb. De plus, les filaments émergents adoptent une variété de formes, non rapportées in vitro et modulées par des facteurs auxiliaires Rad51, apportant un nouvel éclairage sur la fonction de ces facteurs dans les cellules vivantes.

Contrairement à ce qui a été rapporté pour les filaments RecA chez les bactéries, les filaments Rad51 montrent un comportement étonnamment dynamique : avec des événements de compactage fréquent suivis d'une réextension offrant des opportunités pour le NPF d'être projeté dans une zone nucléaire différente, et ainsi d'explorer de nouvelles régions génomiques. La modélisation biophysique du processus de recherche d'homologie par notre collaborateur Leonid Mirny (MIT, USA) révèle que ces cycles de compaction/extension constituent une stratégie très robuste pour qu'une identité unique trouve sa cible dans l'espace nucléaire. De manière constante, la capacité des versions étiquetées Rad51 à former un filament étendu est en corrélation avec leur capacité à maintenir une recombinaison homologue efficace.

En résumé, ce travail révèle des mécanismes radicalement différents pour la recherche d'homologie à l'échelle du génome et du noyau que les modèles dominants d'extrémités brisées recherchant la séquence homologue comme un foyer compact. Au lieu de cela, nous montrons que des unités d'échantillonnage d'homologie s'étendent dynamiquement à travers le noyau et subissent des cycles de compactage/extension permettant une exploration rapide et robuste du volume nucléaire.

Compte tenu de l'importance de la recombinaison homologue pour la stabilité du génome et de la conservation de ce mécanisme à travers l'évolution, nos résultats ont de larges implications pour la maintenance du génome chez d'autres espèces.

Enfin, la capacité de surveiller la dynamique de Rad51 dans les cellules vivantes ouvre de nouvelles voies pour cribler les facteurs génétiques et les petites molécules ayant un impact sur la régulation HR avec de fortes implications à la fois pour notre compréhension de la régulation HR dans les cellules vivantes et le développement de nouvelles interventions à valeur thérapeutique.

MOTS CLÉS

Rupture double brin ; Recombinaison homologue ; Rad51

ABSTRACT

DNA is the major carrier of genetic information in prokaryotic and eukaryotic cells and its integrity is vital for the survival of cells. Despite its importance. DNA is under pressure of damages caused by both exogenous and endogenous factors. Double strand break (DSB) is one of the most toxic DNA damages and even one unrepaired DSB is lethal to cells. Cells have evolved several pathways to repair DSBs, including non-homologous end joining (NHEJ), and homologous recombination (HR). HR is an error free repair pathway that uses an intact homologous sequence as a template to repair the damage. This involves identifying the homologous sequence among the mega bases of the genome and in the nuclear volume of eukaryotic cells. At the molecular level, DNA sampling and strand invasion of the homologous dsDNA is achieved by a nucleoprotein filament (NPF), formed by the recombinase, RecA in bacteria and Rad51 in eukaryotes, coating ssDNA. This mechanism has been extensively studied *in vitro* and *in vivo* through molecular approaches at the level of cell populations. However, to be identified as homologous to the damaged sequence a given locus has to be in sufficient proximity to the NPF. How is this nucleus wide homology search performed remains an open question. One methodological lock to address this question has been the lack of experimental tools to visualize the NPF in living cells. Indeed, past attempts to fluorescently tag Rad51 yielded a non-functional protein forming discrete foci in cells.
Considering the importance of Rad51 during HR, it has been intensively studied *in vitro* or on large cells population *in vivo*, by genetic or molecular assays but lack of study on single live cells as the lack of functional tag on Rad51. Thanks to structural insights from our collaborator Raphael Guerois (I2BC, CEA), we developed and characterized a functional, internally tagged version of S.cerevisiae Rad51. Following the induction of unique DSB, we observe for the first time in living cells, Rad51 forming micrometer long filaments spanning across the whole nucleus and contacting the donor sequence. Importantly, the length of these filaments coincides with the extent of ssDNA formation and Rad51 spreading on DNA. As predicted from genetic and *in vitro* data, their formation requires the recombinase loader Rad52 and the formation of long stretch of ssDNA. Furthermore, emerging filaments adopt a variety of shapes, not reported *in vitro* and modulated by Rad51 ancillary factors, shedding new light on the function of these factors in living cells.
In contrast to what has been reported for RecA filaments in bacteria, Rad51 filaments show a surprisingly dynamic behavior: with frequent compaction events followed by re-extension providing opportunities for the NPF to be projected into a different nuclear area, and thus explore new genomic regions. Biophysical modeling of the homology search process by our collaborator Leonid Mirny (MIT, USA) reveals that these cycles of compaction/extension constitute a very robust strategy for a unique identity to find its target in the nuclear space. Consistently, the capacity of Rad51 tagged versions to form extended filament correlates with their ability to sustain efficient homologous recombination.
In summary, **this work reveals a radically different mechanisms for genome- and nucleus-wide homology search than the prevailing models** of broken ends seeking the homologous sequence as a compact focus. Instead, we show that of homology sampling units dynamically stretch across the nucleus and undergo cycles of compaction/extension allowing a rapid and robust exploration of the nuclear volume.
Given the importance of Homologous recombination for genome stability, and the conservation of this mechanism across evolution, our findings bear broad implications for genome maintenance in other species
Finally, the capacity to monitor the dynamics of Rad51 in living cells opens new avenues to screen genetic factors and small molecules impacting on HR regulation with strong implications for both our understanding of HR regulation in living cells and the development of new intervention of therapeutic value.

KEYWORDS

Double strand break ; Homologous recombination ; Rad51